Studies on Molecular Design and Mechanical Properties of Supramolecular Soft Materials with Polymer Network via Non-covalent Bonding Interactions

Mikihiro HAYASHI

Studies on Molecular Design and Mechanical Properties of Supramolecular Soft Materials with Polymer Network via Non-covalent Bonding Interactions

非共有結合性高分子網目を有する超分子ソフト材料の設計とその力学特性に関する研究

Table of contents

Chapter 1

General Introduction

Polymers are one of the three major materials in modern society along with metals and ceramics. There are two main classifications of polymers; one is “natural polymers” which exist in nature and the other is “synthetic polymers” which are artificially synthesized by chemical reactions.[1] Cellulose and protein are examples of formers, which have been used in human society as clothing or foods since ancient times, while Bakelite and celluloid belong to the class of latters. Although some kinds of synthetic polymers had already been industrialized in the 1800s, the people of this age did not even recognize that these materials were made of “giant molecules”. It was in the 1920s that H. Staudinger proposed the “macromolecular hypothesis”, where the hypothesis indicated that macromolecules maintain long chain structures composed of repeating molecular units linked by covalent bonds.[2,3] In light of the argument toward his proposal, a new class of science, “polymer chemistry,” has risen. Polymer chemistry has been developed due to the advancement of synthesis technology or theory, and the polymer industry has also been expanded due to the great efforts of chemists in synthesis field, such as W. H. Carothers. Nowadays, various functional polymeric materials with good processability, lightness, adiabaticity or conductivity have been studied in combination with the development of science and technology. Especially in recent years, polymeric materials to deal with environmental issues have attained great attention.[4]

Polymer gels[5-8] and elastomers[9-15] are some of the most well known polymeric materials, as are plastics and synthetic fibers. In some cases, they are referred to as soft materials because they have unique mechanical features, such as flexibility and stretchability, unlike other

polymeric materials. Such unique mechanical properties are attributed to the characteristic molecular structure which consists of several elements, including bridging strands of "melt" polymers, crosslink points (or junctions), dangling ends, loops, etc.[16] The main difference between gels and elastomers consists in the manner in which the flexibility of the network strands is achieved. In general, gels contain a large amount of solvent; in other words, solvents are conceived to be necessary to achieve the flexibility of chains in gel, whereas elastomers use melt polymers, which have a lower glass transition temperature (T_g) than room temperature, as the component polymers of the network strands.

The history of cross-linking reactions in elastomers is fairly old. It says that it started with vulcanization of natural rubbers, invented by C. Goodyear in the 1800s.[17] Although it has been believed that the discovery of vulcanization happened by fortuity, very interestingly, the discovery can be considered the biggest event in the history of the rubber industry. In the same period, T. Hancock studied the vulcanization reaction at the molecular level in more detail, which led to the establishment of vulcanization in the industrial field. The two major ingredients of rubber are raw rubber latices and cross-linkers. In the time of C. Goodyear and T. Hancock, natural rubbers, which can be extracted from rubber trees, were used as raw rubber. In the beginning of the 20th century, the automobile industry had developed drastically, which caused the supply of natural rubber to no longer be able to match the demand. This situation also led to the invention of synthetic rubbers such as poly(isoprene) rubber and poly(butadiene) rubber, and now synthetic rubbers are widely used as alternatives for natural rubbers.

The history of gels started in the mid-1900s. Researchers have paid particular attention to the unique feature of gels; they can contain a large amount of solvents. In our daily lives, various kinds of gel materials, such as super absorbent polymers and contact lenses, are utilizing this feature. Although fragility due to solvent content has been regarded as a defect of gel materials,

new class of gels with great mechanical strength have been reported by several research groups in recent years with materials known as tetra-PEG gels,[18] slide-ring gels, [19] double network gels,[20] and nanocomposite (NC) gels.[21]

One of the defects for conventional soft materials, including gels and elastomers, is the difficulty in processing. In conventional network materials, the cross-link points are composed of covalent bonds, which are strong but irreversible. Therefore, gels and elastomers are normally insoluble in solvents, and they are not reactive against external-stimuli. In addition, since the cross-linking reaction tends to proceed explosively once it has started, another problem arises in the control of cross-linking reactions. Thus, disordered networks with inhomogeneous cross-link points are easily formed, and the investigation of gelation behavior is also difficult due to the insoluble nature.

Recently, network materials with precisely designed network structures formed via non-covalent cross-links, which are referred to as "supramolecular soft materials,"[22] including supramolecular polymers,[23,24] supramolecular (polymer) gels,[25-27] supramolecular rubbers or supramolecular elastomers,[28,29] have been studied to overcome the defects of conventional soft materials explained above. The term "supramolecuar" is associated with "supramolecular chemistry" proposed by J-M. Lehn in the 1970s,[30-32] and supramolecular soft materials express the soft materials composed of supramolecular associations. Unlike conventional materials, supramolcular soft materials show stimuli-responsiveness, such as thermo-,[33,34] and pH-responsiveness,[35,36] due to the weak association strength of the cross-link points. Therefore, macroscopic transition between semi-solid state (or gel state) and liquid state can be achieved.

Meijer et al. have reported the supramolecular polymers formed by self-complementary quadruple hydrogen-bonding units based on 2-ureido-4-[1H]-pyrimidone (UPy) (Figure 1-1a).[37,38] The materials obtained are able to melt at high temperatures due to the dissociation of

hydrogen bonded cross-links. Leibler's groups have reported the preparation of supramolecular rubbers composed of hydrogen bonded small molecules (Figure 1-1b),[39] where self-healing ability[40-45] was generated due to the re-association of dissociated functional groups near the fractured surfaces. Various kinds of supramolecular soft materials formed via non-covalent bonds, e.g. hydrogen bonds,[46-52] ionic interaction,[53-60] metal-ligand coordination,[61-70] or inclusion complexation,[71-75] have been reported in recent days. On the other hand, there are not many reports which demonstrated the effects of stoichiometric valance on the physical properties of supramolecular soft materials in detail.

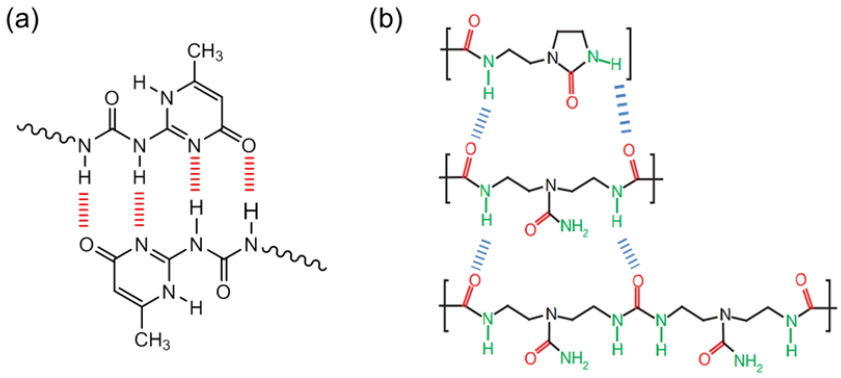

Figure 1-1. (a) Formation of quadruple hydrogen bonding between 2-ureido-4-[1H]-pyrimidone (UPy) units reported by Meijer et al. (see reference #37 and #38). (b) Components and hydrogen bonds used in the supramolecular rubbers reported by Leibler et al. (see reference #39).

Studies on thermoplastic elastomers (TPEs) have also been explored to overcome the difficulty in material processing of elastomers.[76-80] ABA triblock copolymers, such as polystyrene-*b*-polybutadiene-*b*-polystyrene and polystyrene-*b*-polyisoprene-*b*-polystyrene,[81-85] are used in some typical TPEs, where polymer species with a T_g higher than room temperature are used as the A end blocks and polymer species with a T_g lower than room temperature are used as the B middle block. The glassy A blocks form pseudo cross-link domain[86-88] due to the segregation from the soft middle blocks, while the soft B middle block serves as a network

strand bridging the cross-link domains. TPEs are able to melt at higher temperatures than the T_g of component polymers, which enables re-shaping after processing.[87-95] The use of precisely synthesized ABA triblock copolymers[96-100] has another advantage for preparing elastomers because the bridge-type conformation can directly contribute to enhance the macroscopic physical properties of the materials.[101-108]

In addition, the studies of network materials composed of an ABA triblock copolymer and a cross-linker polymer having a non-covalent interaction to the A end blocks have been developing,[109-113] e.g. by Noro and Lodge et al. (some examples are represented in Figure 1-2).[114-118] For further improvement of mechanical properties of ABA triblock copolymer-based elastomers, modification of the soft middle block could be effective. If transient weak cross-links of non-covalent bonding are incorporated into the soft middle blocks, such cross-links would improve the stiffness due to an increase in the cross-link density. Furthermore, the transient cross-links[22] incorporated in the middle block can repeat dissociation and re-association during stress application due to the dynamic nature, which could work to prevent local stress concentration in the network. In other words, incorporating transient cross-links into the soft middle block enables enhancement of the mechanical properties of elastomers.

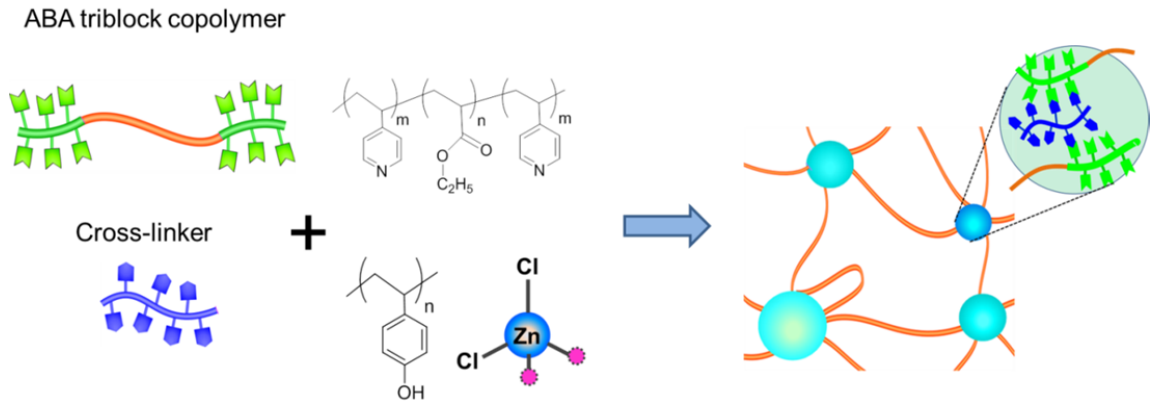

Figure 1-2. Schematic illustration of the molecular design on the basis of blend of ABA triblock copolymer chains and cross-linker molecules. See references #114-118.

The dynamics of supramolecular soft materials with transient cross-links have also been developing as a basic study, which are mainly conducted through rheological measurements.[119-129] Feldman et al. have reported the viscoelasticity of the materials formed by random copolymers of *n*-butyl acrylate units and hydrogen bonding units based on UPy.[130] Theoretical studies on the materials of associative polymers have also been explored on the basis of scaling laws by several researchers.[131-137] In other words, investigation of the dynamics of supramolecular network is important to understand the macroscopic physical properties of supramolecular soft materials.

In chapter 2 of this thesis, syntheses of component polymers and methods of blend preparation were described. Details of experimental conditions for physical property investigations were also explained, where some basics of rheological measurements were demonstrated.

In chapter 3, carboxyl-terminated telechelic poly(ethyl acrylate) (PEA-$(COOH)_2$) was prepared, and was blended with polyethyleneimine (PEI) possessing multiple amines in a chain. The use of telechelic-type polymer could be effective to form relatively homogeneous network. In addition, these component polymers have opposite solubility nature, that is, PEA is hydrophobic while PEI is hydrophilic, which could work to form self-assembled network even with component polymers having small molecular weights. The supramolecular network was formed via ionic hydrogen bonding[138-140] between carboxylic acids on PEA-$(COOH)_2$ and amines on PEI, where PEA-$(COOH)_2$ and PEI serve as a network strand and a cross-linker, respectively, as schematically shown in Figure 1-3.[141] Note that both polymers have lower T_gs than room temperature, and hence solvents were not needed to attain the softness of materials,

which can remove the complication of solvent evaporation during measurements at high temperatures. The importance of stoichiometric valance between functional groups in optimization of supramolecular networks was studied through rheological measurements, while the effects of the molecular weight of component polymers on the mechanical properties were investigated.[22]

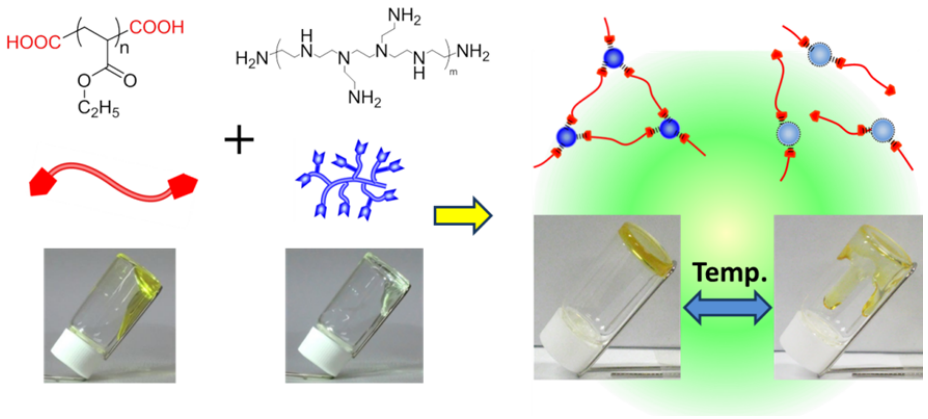

Figure 1-3. Molecular design and schematic illustration of the component polymers and network structure. See reference #22.

In chapter 4, a novel strategy to enhance material properties by incorporating hydrogen bonds on the soft middle block of ABA triblock-based elastomers was proposed.[142] To realize this objective, an ABA triblock-type copolymer, poly(4-vinylpyridine)-*b*-[(poly(butyl acrylate)-*co*-polyacrylamide]-*b*-poly(4-vinylpyridine) (P-Ba-P), was prepared. In the molecular design, the end blocks of poly(4-vinylpyridine) were aimed to form pseudo cross-link domains due to segregation from the soft middle block, while acrylamide units were introduced to form self-complementary hydrogen bonds on the middle block, serving as transient cross-links (Figure 1-4). The mechanical properties of the elastomers were investigated by dynamic mechanical measurements and tensile tests. In addition, the effects of the hydrogen bonds in the middle block on the dynamics of triblock copolymers were discussed in detail in terms of the sticky Rouse-type relaxation of the middle block of P-Ba-P.

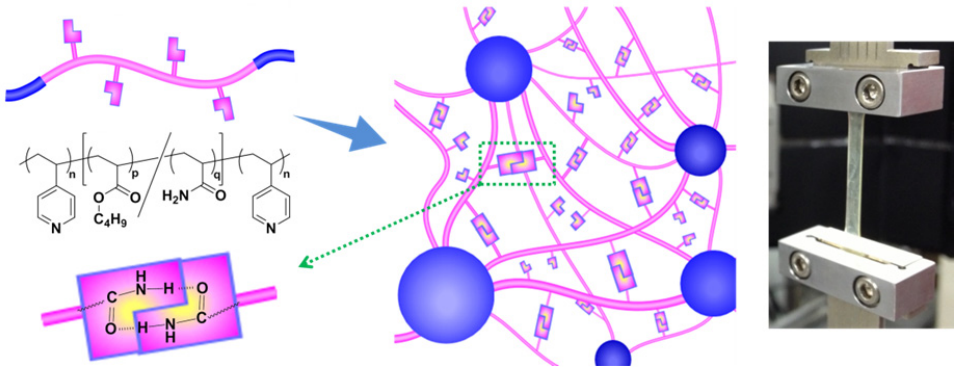

Figure 1-4. Chemical structure of P-Ba-P and schematic illustration of P-Ba-P based network structure. The elastomer sample during elongation is also shown. See reference #142.

In chapter 5, further enhancement in physical properties was attained by preparing ABA triblock copolymer-based elastomers cross-linked via coordination and hydrogen bonds. The above mentioned P-Ba-P was used as a component polymer, which was blended with metal salt, $ZnCl_2$. The pyridine units can serve as the ligand site to form metal-ligand coordination,[143-148] and thus, coordination bonds can be formed in the cross-link domains of P blocks by blending with $ZnCl_2$. Simultaneously, self-complementary hydrogen bonds form between acrylamide units on the middle block. The effects of simultaneous cross-links in the middle blocks and in the end blocks on the physical properties were investigated by morphological observations and mechanical measurements.

Finally, please note that the Figures, Schemes, and Tables and even many technical terms, phrases and sentences adopted in this thesis referred to previous papers written by the authors including myself to make clear the expression concerning experimental procedures, results and discussion.

References

[1] *A Primer of Polymeric Materials for Engineers (Kogaku Gijyutsusya no Kobunshi Zairyo Nyumon)*. Ogawa, T., Kyoritu Shuppan, **1993**.

[2] *Polymer Science 5th ed (Kobunshi Kagaku 5th ed.)*. Kabachi, K., Murahashi, S., Norisue, N., Kodaka, T., Kyoritu Shuppan, **2007**.

[3] *Polymer Science (II) – Physical Properties (Kobunshi Kagaku (II) – Bussei)*. Matsushita, Y., Maruzen Shuppan, **1996**.

[4] *Polymer Industry and Chemistry (Kobunsi Kogyo Kagaku)*. Yamaoka, A., Asakura Syoten, **2003**.

[5] Flory, P. J. *J. Am. Chem. Soc.* **1941,** 63, 3083-3090.

[6] Osada, Y.; Gong, J. P. *Adv. Mater.* **1998,** 10, 827-837.

[7] Lee, K. Y.; Mooney, D. J. *Chem. Rev.* **2001,** 101, 1869-1879.

[8] Qiu, Y.; Park, K. *Adv. Drug Deliv. Rev.* **2001,** 53, 321-339.

[9] Lendlein, A.; Langer, R. *Science* **2002,** 296, 1673-1676.

[10] Wang, Y. D.; Ameer, G. A.; Sheppard, B. J.; Langer, R. *Nat. Biotechnol.* **2002**, 20, 602-606.

[11] Davis, D. A.; Hamilton, A.; Yang, J.; Cremar, L. D.; Van Gough, D.; Potisek, S. L.; Ong, M. T.; Braun, P. V.; Martinez, T. J.; White, S. R.; Moore, J. S.; Sottos, N. R. *Nature* **2009,** 459, 68-72.

[12] Kupfer, J.; Finkelmann, H. *Makromole.Chem. Rapid Commun.***1991,** 12, 717-726.

[13] Gheneim, R.; Perez-Berumen, C.; Gandini, A. *Macromolecules* **2002,** 35, 7246-7253.

[14] Yamazaki, H.; Takeda, M.; Kohno, Y.; Ando, H.; Urayama, K.; Takigawa, T. *Macromolecules* **2011**, 44, 8829-8834.

[15] Urayama, K.; Miki, T.; Takigawa, T.; Kobjiya, S. *Chem. Mater.* **2004**, 16, 173-178.

[16] *Polymer Chemistry 2nd ed*. Himenz, P. C.; Lodge, T. P. CRC Press, **2007**.

[17] *Why rubbers have elasticity? (Gomu wa Naze Nobiru?)*. Ito, M., Omu Sha, **2007**.

[18] Sakai, T.; Matsunaga, T.; Yamamoto, Y.; Ito, C.; Yoshida, R.; Suzuki, S.; Sasaki, N.; Shibayama, M.; Chung, U.-i. *Macromolecules* **2008,** 41, 5379-5384.

[19] Okumura, Y.; Ito, K. *Adv. Mater.* **2001,** 13, 485-487.

[20] Gong, J. P.; Katsuyama, Y.; Kurokawa, T.; Osada, Y. *Adv. Mater.* **2003,** 15, 1155-1158.

[21] Haraguchi, K.; Takehisa, T. *Adv*. *Mater*. **2002**, 14, 1120-1124.

[22] Hayashi, M.; Noro, A.; Matsushita, Y. *J. Polym. Sci., Part B: Polym. Phys.* **2014**, 52, 755-764.

[23] Nair, K. P.; Breedveld, V.; Weck, M. *Macromolecules* **2008,** 41, 3429-3438.

[24] Seiffert, S.; Sprakel, J. *Chem. Soc. Rev.* **2012,** 41, 909-930.

[25] Noro, A. ; Hayashi, M.; Matsushita, Y. *Soft Matter*, **2012**, 8, 2416-2429

[26] Yan, X.; Xu, D.; Chen, J.; Zhang, M.; Hu, B.; Yu, Y.; Huang, F. *Polym. Chem,* **2013,** 4, 3312-3322.

[27] Weng, W.; Fang, X.; Zhang, H.; Peng, H.; Lin, Y.; Chen, Y. *Eur. Polym. J.* **2013,** 49, 4062-4071.

[28] Zhang, A.; Yang, L.; Lin, Y.; Yan, L.; Lu, H.; Wang, L. *J. Appl. Polym. Sci.* **2013,** 129, 2435-2442.

[29] Montarnal, D.; Cordier, P.; Soulie-Ziakovic, C.; Tournilhac, F.; Leibler, L. *J. Polym. Sci., Part A: Polym. Chem.* **2008,** 46, 7925-7936.

[30] Lehn, J. M., *Angew. Chem. Int. Ed.* **1988**, 27, 89-112.

[31] Lehn, J. M., *Angew. Chem. Int. Ed.* **1990**, 29, 1304-1319.

[32] *Lehn Supramolecular Chemistry (Lehn Chobunshi Kagaku)*, Lehn, J. M, Takauchi, K (translation), Kagaku Dojin, **1997**.

[33] Weng, W.; Beck, J. B.; Jamieson, A. M.; Rowan, S. J. *J. Am. Chem. Soc* .**2006,** 128, 11663-11672.

[34] Wojtecki, R. J.; Meador, M. A.; Rowan, S. J. *Nature Mater*. **2011**, 10, 14-27.

[35] Ge, Z. S.; Hu, J. M.; Huang, F. H.; Liu, S. Y. *Angew. Chem., Int. Ed.* **2009,** 48, 1798-1802.

[36] Yan, X.; Xu, D.; Chi, X.; Chen, J.; Dong, S.; Ding, X.; Yu, Y.; Huang, F. *Adv. Mater.* **2012**, 24, 362-369.

[37] Folmer, B. J. B.; Sijbesma, R. P.; Versteegen, R. M.; van der Rijt, J. A. J.; Meijer, E. W. *Adv. Mater.* **2000,** 12, 874-878.

[38] Lange, R. F. M.; Van Gurp, M.; Meijer, E. W. *J. Polym. Sci., Part A: Polym. Chem.* **1999,** 37, 3657-3670.

[39] Cordier, P.; Tournilhac, F.; Soulie-Ziakovic, C.; Leibler, L. *Nature* **2008**, 451, 977-980.

[40] Maes, F.; Montarnal, D.; Cantournet, S.; Tournilhac, F.; Corte,L.; Leibler, L. *Soft Matter* **2012**, 8, 1681−1687.

[41] Stukalin, E. B.; Cai, L.-H.; Kumar, N. A.; Leibler, L.; Rubinstein, M. *Macromolecules* **2013,** 46, 7525-7541.

[42] Michal, B. T.; Jaye, C. A.; Spencer, E. J.; Rowan, S. J. *Acs Macro Lett.* **2013,** 2, 694-699.

[43] Hong, G.; Zhang, H.; Lin, Y.; Chen, Y.; Xu, Y.; Weng, W.; Xia, H. *Macromolecules* **2013,** 46, 8649-8656.

[44] Herbst, F.; Doehler, D.; Michael, P.; Binder, W. H. *Macromol. Rapid Commun.* **2013,** 34, 203-220.

[45] Chen, Y.; Kushner, A. M.; Williams, G. A.; Guan, Z. *Nature Chem.* **2012,** 4, 467-472.

[46] Montarnal D.; Tournilhac, F.; Hidalgo, M.; Leibler, L. *J. Polym. Sci., Part A: Polym. Chem.* **2010**, 48, 1133-1141.

[47] Courtois, J.; Baroudi, I.;Nouvel, N.; Degrandi, E.; Pensec, S.; Ducouret, G.; Chaneac, C.; Bouteiller, L.; Creton, C. *Adv. Funct. Mater.* **2010**, 20, 1803-1811.

[48] Binder, W. H.; Petraru, L.; Roth, T.; Groh, P. W.; Palfi, V.; Keki, S.; Ivan, B. *Adv. Funct. Mater.*, **2007**, 17, 1317-1326.

[49] Guo, M.; Pitet, L. M.; Wyss, H. M.; Vos, M.; Dankers, P. Y. W.; Meijer, E. W. *J. Am. Chem. Soc.* **2014,** 136, 6969-77.

[50] Tamesue, S.; Ohtani, M.; Yamada, K.; Ishida, Y.; Spruell, J. M.; Lynd, N. A.; Hawker, C. J.; Aida, T. *J. Am. Chem. Soc.* **2013,** 135, 15650-15655.

[51] Khor, S. P.; Varley, R. J.; Shen, S. Z.; Yuan, Q. *J. Appl. Polym. Sci.* **2013,** 128, 3743-3750.

[52] Hofmeier, H.; Hoogenboom, R.; Wouters, M. E. L.; Schubert, U. S. *J. Am. Chem. Soc.* **2005,** 127, 2913-2921.

[53] Sun, T. L.; Kurokawa, T.; Kuroda, S.; Ihsan, A. B.; Akasaki, T.; Sato, K.; Haque, M. A.; Nakajima, T.; Gong, J. P. *Nature Mater.* **2013,** 12, 932-937.

[54] Hunt, J. N.; Feldman, K. E.; Lynd, N. A.; Deek, J.; Campos, L. M.; Spruell, J. M.; Hernandez, B. M.; Kramer, E. J.; Hawker, C. J. *Adv. Mater.*, **2011**, 23, 2327.

[55] Wang, Q.; Mynar, J. L.; Yoshida, M.; Lee, E.; Lee, M.; Okuro, K.; Kinbara, K.; Aida, T. *Nature* **2010**, 463, 339-343.

[56] Shibata, M.; Kimura, Y.; Yaginuma, D. *Polymer* **2004**, 45, 7571-7577.

[57] Kulikovska, O.; Goldenberg, L. M.; Kulikovsky, L.; Stumpe, J. *Chem. Mater.*, **2008**, 20, 3528-3534.

[58] Wathier, M.; Grinstaff, M. W. *Macromolecules* **2010**, 43, 9529-9533.

[59] Banerjee, S.; Das, R. K.; Maitra, U. *J. Mater. Chem.* **2009,** 19, 6649-6687.

[60] Furusho, Y.; Endo, T. *J. Polym. Sci., Part A: Polym. Chem.* **2014,** 52, 1815-1824.

[61] Zhao, Y. Q.; Beck, J. B.; Rowan, S. J. Jamieson, A. M. *Macromolecules* **2004**, 37, 3529-3531.

[62] Sivakova, S.; Bohnsack, D. A.; Mackay, M. E.; Suwanmala P.; Rowan, S. J. *J. Am. Chem. Soc.*, **2005**, 127, 18202-18211.

[63] Weng, W.; Beck, J. B.; Jamieson A. M.; Rowan, S. J. *J. Am. Chem. Soc.*, **2006**, 128, 11663-11672.

[64] Weng, W.; Li, Z.; Jamieson, A. M.; Rowan, S. J. *Soft Matter* **2009**, 5, 4647-4657.

[65] Weng, W.; Li, Z.; Jamieson, A. M.; Rowan, S. J. *Macromolecules* **2009**, 42, 236-246.

[66] Kumpfer, J. R.; Jin, J.; Rowan, S. J. *J. Mater. Chem.* **2010,** 20, 145-151.

[67] Burnworth, M.; Tang, L.; Kumpfer, J. R.; Duncan, A. J.; Beyer, F. L.; Fiore, G. L.; Rowan, S. J.; Weder, C. *Nature* **2011,** 472, 334-337.

[68] Yount, W. C.; Juwarker, H.; Craig, S. L. *J. Am. Chem. Soc.* **2003,** 125, 15302-15303.

[69] Harris, R. D.; Auletta, J. T.; Motlagh, S. A. M.; Lawless, M. J.; Perri, N. M.; Saxena, S.; Weiland, L. M.; Waldeck, D. H.; Clark, W. W.; Meyer, T. Y. *Acs Macro Lett.* **2013,** 2, 1095-1099.

[70] Jackson, A. C.; Beyer, F. L.; Price, S. C.; Rinderspacher, B. C.; Lambeth, R. H. *Macromolecules* **2013,** 46, 5416-5422.

[71] Oku, T.; Furusho, Y.; Takata, T. *Angew. Chem., Int. Ed.* **2004,** 43, 966-969.

[72] Ogawa, M; Kawasaki, A.; Koyama, A.; Takata, T. *Polym. J.* **2011**, 43, 909-915.

73 Huh, K. M.; Ooya, T.; Lee, W. K.; Sasaki, S.; Kwon, I. C.; Jeong, S. Y.; Yui, N. *Macromolecules* **2001**, 34, 8657-8662.

[74] Huh, K. M.; Cho, Y. W.; Chung, H.; Kwon, I. C.; Jeong, S. Y.; Ooya, T.; Lee, W. K.; Sasaki, S.; Yui, N. *Macromol. Biosci.* **2004,** 4, 92-99.

[75] Takata, T.; Kohsaka, Y.; Konishi, G.-i. *Chem. Lett.*, **2007**, 36, 292-293.

[76] Bailey, J. T.; Bishop, E. T.; Hendrick.Wr; Holden, G.; Legge, N. R. *Rubber Age* **1966,** 98, 69.

[77] Holden, G.; Bishop, E. T.; Legge, N. R. *J. Polym. Sci., Part C: Polym. Symp.* **1969,** 37.

[78] Koerner, H.; Price, G.; Pearce, N. A.; Alexander, M.; Vaia, R. A. *Nature Mater.* **2004,** 3, 115-120.

[79] Krol, P. *Prog. Mater. Sci.* **2007,** 52, 915-1015.

[80] Kylma, J.; Seppala, J. V. *Macromolecules* **1997,** 30, 2876-2882.

[81] Fong, H.; Reneker, D. H. *J. Polym. Sci., Part B: Polym. Phys.* **1999,** 37, 3488-3493.

[82] Goosen, M. F. A.; Sefton, M. V. *J. Biomed. Mater. Res.* **1979,** 13, 347-364.

[83] Takano, A.; Kamaya, I.; Takahashi, Y.; Matsushita, Y. *Macromolecules* **2005,** 38, 9718-9723.

[84] Matsumiya, Y.; Watanabe, H.; Takano, A.; Takahashi, Y. *Macromolecules* **2013,** 46, 2681-2695.

[85] Takahashi, Y.; Yahata, S.; Takano, A.; Matsushita, Y. *Nihon Reoroji Gakk.* **2006,** 34, 177-180.

[86] Furukawa, J.*Polym. Bull.* **1982**, 7, 23-30.

[87] Furukawa, J.*Polym. Bull.* **1982**, 7, 31-37.

[88] Furukawa, J.*Polym. Bull.* **1983**, 10, 336-342.

[89] Eceiza, A.; Martin, M. D.; de la Caba, K.; Kortaberria, G.; Gabilondo, N.; Corcuera, M. A.; Mondragon, I. *Polym. Eng. Sci.* **2008,** 48, 297-306.

[90] Hosono, N.; Pitet, L. M.; Palmans, A. R. A.; Meijer, E. W. *Polym. Chem.* **2014,** 5, 1463-1470.

[91] Seiffert, S.; Sprakel, J. *Chem. Soc. Rev.* **2012,** 41, 909-930.

[92] Versteegen, R. M.; Kleppinger, R.; Sijbesma, R. P.; Meijer, E. W. *Macromolecules* **2006**, 39, 772-783.

[93] Shi, W.; Lynd, N. A.; Montarnal, D.; Luo, Y.; Fredrickson, G. H.; Kramer, E. J.; Ntaras, C.; Avgeropoulos, A.; Hexemer, A. *Macromolecules* **2014,** 47, 2037-2043.

[94] Han, C. D.; Kim, J.; Kim, J. K.; Chu, S. G. *Macromolecules* **1989**, 22, 3443−3451.

[95] Appleby, T.; Cser, F.; Moad, G.; Rizzardo, E.; Stavropoulos, C. *Polym. Bull.* **1994**, 32, 479-485.

[96] Matsushita, Y. *J. Polym. Sci., Part B: Polym. Phys.* **2000,** 38, 1645-1655.

[97] Matsen, M. W.; Thompson, R. B. *J. Chem. Phys.* **1999,** 111, 7139-7146.

[98] Lynd, N. A.; Meuler, A. J.; Hillmyer, M. A. *Prog. Poly. Sci.* **2008,** 33, 875-893.

[99] Bates, F. S.; Fredrickson, G. H. *Phys. Today* **1999,** 52, 32-38.

[100] Martin-Gomis, L.; Fernandez-Garcia, M.; de la Fuente, J. L.; Madruga, E. L.; Cerrada, M. L. *Macromol. Chem. Phys.* **2003,** 204, 2007-2016.

[101] Brinkmann-Rengel, S.; Abetz, V.; Stadler, R.; Thomas, E. L. *Kautsch. Gummi Kunstst.* **1999,** 52, 806-813.

[102] Watanabe, H.; Kuwahara, S.; Kotaka, T. *J. Rheol.* **1984**, 28, 393-409.

[103] Yamaguchi, D.; Cloitre, M.; Panine, P.; Leibler, L. *Macromolecules*, **2005**, 38, 7798-7806.

[104] Wang, S.; Kesava, S. V.; Gomez, E. D.; Robertson, M. L. *Macromolecules* **2013,** 46, 7202-7212.

[105] Henderson, K. J.; Zhou, T. C.; Otim, K. J.; Shull, K. R. *Macromolecules* **2010,** 43, 6193-6201.

[106] Corte, L.; Yamauchi, K.; Court, F.; Cloitre, M.; Hashimoto, T.; Leibler, L. *Macromolecules* **2003,** 36, 7695-7706.

[107] Zhang, Y.; Chung, I. S.; Huang, J. Y.; Matyjaszewski, K.; Pakula, T. *Macromol. Chem. Phys.* **2005,** 206, 33-42.

[108] Rosati, D.; Van Loon, B.; Navard, P. *Polymer* **2000,** 41, 367-375.

[109] Jackson, N. R.; Wilder, E. A.; White, S. A.; Bukovnik, R.; Spontak, R. J. *J. Polym. Sci., Part B: Polym. Phys.* **1999,** 37, 1863-1872.

[110] Walker, T. A.; Semler, J. J.; Leonard, D. N.; van Maanen, G. J.; Bukovnik, R. R.; Spontak, R. J. *Langmuir* **2002,** 18, 8266-8270.

[111] Hunt, J. N.; Feldman, K. E.; Lynd, N. A.; Deek, J.; Campos, L.M.; Spruell, J. M.; Hernandez, B. M.; Kramer, E. J.; Hawker, C. J. *Adv. Mater*. **2011**, 23, 2327−2331.

[112] Mather, B. D.; Baker, M. B.; Beyer, F. L.; Green, M. D.; Berg, M.A. G.; Long, T. E. *Macromolecules* **2007**, 40, 4396−4398.

[113] Chen, Y.; Guan, Z. *Chem. Commun.* **2014,** 50, 10868-10870.

[114] Noro, A.; Matsushita, Y.; Lodge, T. P. *Macromolecules* **2008**, 41, 5839-5844.

[115] Noro, A.; Matsushita, Y.; Lodge, T. P. *Macromolecules* **2009**, 42, 5802-5810.

[116] Lei, Y.; Lodge, T. P. *Soft Matter* **2012**, 8, 2110-2120.

[117] Matsushima, S.; Hayashi, M.; Yamagishi, H.; Noro, A.; Matsushita, Y. *Nihon Reoloji Gakk.* **2014**, 42, 135-141.

[118] Noro, A.; Matsushima, S.; He, X.; Hayashi, M.; Matsushita, Y. *Macromolecules* **2013**, 46, 8304-8310.

[119] Yang, J.; Han, C.-R.; Zhang, X.-M.; Xu, F.; Sun, R.-G. *Macromolecules* **2014,** 47, 4077-4086.

[120] Stavrouli, N.; Aubry, T.; Tsitsilianis, C. *Polymer* **2008,** 49, 1249-1256.

[121] Agrawal, S. K.; Sanabria-DeLong, N.; Tew, G. N.; Bhatia, S. R. *Langmuir* **2008,** 24, 13148-13154.

[122] Xu, D.; Craig, S. L. *Macromolecules* **2011,** 44, 5465-5472.

[123] Brassinne, J.; Gohy, J.-F.; Fustin, C.-A. *Macromolecules* **2014,** 47, 4514-4524.

[124] Ali Aboudzadeh, M.; Eugenia Munoz, M.; Santamaria, A.; Jose Fernandez-Berridi, M.; Irusta, L.; Mecerreyes, D. *Macromolecules* **2012,** 45, 7599-7606.

[125] Chen, Q.; Liang, S.; Shiau, H.-s.; Colby, R. H. *Acs Macro Lett.* **2013,** 2, 970-974.

[126] Spruijt, E.; Stuart, M. A. C.; van der Gucht, J. *Macromolecules* **2013,** 46, 1633-1641.

[127] Lewis, C. L.; Stewart, K.; Anthamatten, M. *Macromolecules* **2014,** 47, 729-740.

[128] Kumpfer, J. R.; Wie, J. J.; Swanson, J. P.; Beyer, F. L.; Mackay, M. E.; Rowan, S. J. *Macromolecules* **2012,** 45, 473-480.

[129] Yan, T.; Schroeter, K.; Herbst, F.; Binder, W. H.; Thurn-Albrecht, T. *Macromolecules* **2014,** 47, 2122-2130.

[130] Feldman, K. E.; Kade, M. J.; Meijer, E. W.; Hawker, C. J.; Kramer, E. J. *Macromolecules* **2009**, 42, 9072-9081.

[131] Indei, T.; Takimoto, J. *J. Chem. Phys*. **2010**, 133, 194902.

[132] Leibler, L.; Rubinstein, M.; Colby, R. H. *Macromolecules* **1991**, 24, 4701-4707.

[133] Tanaka, F.; Edwards, S. F. *Macromolecules* **1992,** 25, 1516-1523.

[134] Semenov, A. N.; Rubinstein, M. *Macromolecules* **1998**, 31, 1373-1385.

[135] Rubinstein, M.; Semenov, A. N. *Macromolecules* **1998**, 31, 1386-1397.

[136] Rubinstein, M.; Semenov, A. N. *Macromolecules* **2001**, 34, 1058-1068.

[137] Rubinstein, M.; Dobrynin, A. V. *Curr.Opin. Colloid Interface Sci.* **1999**, 4, 83-87.

[138] Krygowski, T. M.; Wozniak, K.; Anulewicz, R.; Pawlak, D.; Kolodziejski, W.; Grech, E.; Szady, A. *J. Phys. Chem. A* **1997,** 101, 9399-9404.

[139] Mazik, M.; Cavga, H. *J. Org. Chem.* **2006,** 71, 2957-2963.

[140] Yashima, E.;Matsushima , T.; Okamoto, Y. *J. Am. Chem. Soc.*, **1997**, 119, 6345-6359.

[141] Noro, A. ; Hayashi, M.; Ohshika, A.; Matsushita, Y. *Soft Matter* **2011**, 7, 1167-1670

[142] Hayashi, M.; Matsushima, S.; Noro, A.; Matsushita, Y. *Macromolecules,* in press.

[143] Noro, A.; Sageshima, Y.; Arai, S.; Matsushita, Y. *Macromolecules* **2010**, 43, 5358-5364.

[144] Sageshima, Y.; Noro, A.; Matsushita, Y. *J. Polym. Sci., Part B: Polym. Phys.* **2014**, 52, 377-386.

[145] Ruokolainen, J.; Saariaho, M.; Ikkala, O.; ten Brinke, G.; Thomas, E. L.; Torkkeli, M.; Serimaa, R. *Macromolecules* **1999,** 32, 1152-1158.

[146] Lee, D. H.; Kim, H. Y.; Kim, J. K.; Huh, J.; Ryu, D. Y. *Macromolecules* **2006,** 39, 2027-2030.

[147] Lee, D. H.; Han, S. H.; Joo, W.; Kim, J. K.; Huh, J. *Macromolecules* **2008,** 41, 2577-2583.

[148] Sageshima, Y.; Arai, S.; Noro, A.; Matsushita, Y. *Langmuir* **2012,** 28, 17524-17529.

Chapter 2

Experiment and Analytical Procedures

2-1. Synthesis and characterization of polymers used in the 3rd chapter.

The synthetic procedure and characterization of three PEA-$(COOH)_2$ and PEA used in the 3rd chapter are explained below. The method for preparing blends of PEA-$(COOH)_2$ and PEI is also described.

2-1-1. Synthesis of PEA-$(COOH)_2$ and PEA.

Ethyl acrylate monomer was purchased from TCI, and was purified by passing them through an aluminum oxide column before polymerizations.

Carboxyl-terminated telechelic poly(ethyl acrylate**)** (**PEA-$(COOH)_2$**) was synthesized via reversible addition-fragmentation chain transfer (RAFT) polymerization by using a difunctional chain transfer agent with two carboxylic acids, *S,S'*-bis(α,α'-dimethyl-α"-acetic acid) trithiocarbonate as a chain transfer agent (CTA) and 2,2'-azobis(isobutyronitrile) (AIBN) as an initiator (Scheme 2-1).[1] Firstly, CTA and AIBN were added to a 200 mL Schlenk flask, and the atmosphere was substituted by argon gas. After injecting ethyl acrylate monomer into the flask, it was bubbled with nitrogen for 15 min. The polymerization was conducted in an oil bath at 75 ºC for 45 min. The progress of polymerization was confirmed by monitoring the viscosity, and the polymerization was terminated by immersing the flask in liquid nitrogen. The polymer obtained was purified by repeating reprecipitation two times with THF as a good solvent and hexane as a poor solvent. The molecular weight of PEA-$(COOH)_2$ was tuned by the feed ratio of the CTA and the monomer. To investigate the effects of the molecular weight of PEA-$(COOH)_2$

on the physical properties, three PEA-$(COOH)_2$ with different molecular weights were synthesized. In addition, a control sample, non-functionalized poly(ethyl acrylate**)** (PEA), was also synthesized via RAFT polymerization by using 2-Cyano-2-propyldodecyl trithiocarbonate as a CTA and AIBN as an initiator (Scheme 2-2). The synthetic procedure was similar to that for PEA-$(COOH)_2$ as explained above. PEA was purified in the similar way to the case of PEA-$(COOH)_2$.

Scheme 2-1. Synthesis of PEA-$(COOH)_2$

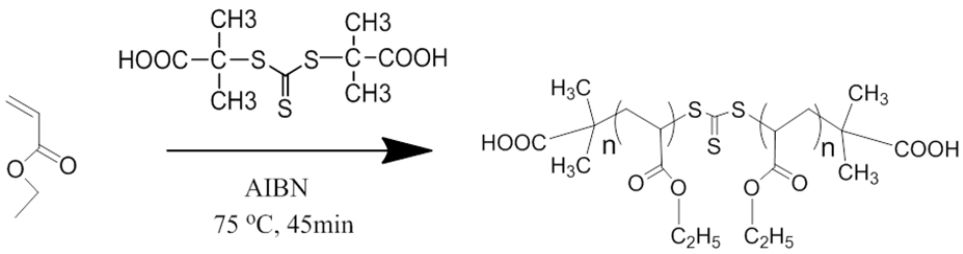

Scheme 2-2. Synthesis of PEA

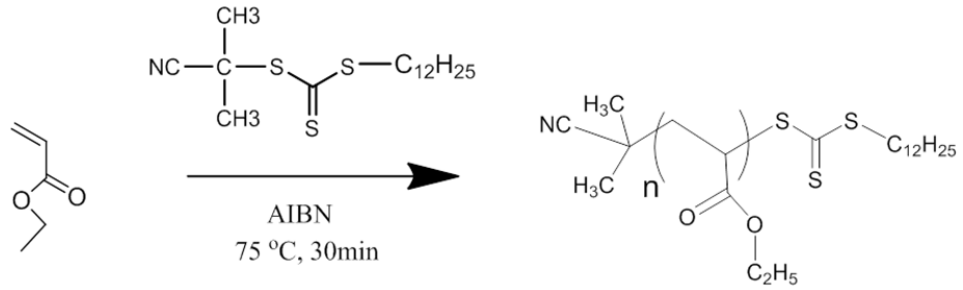

2-1-2. Characterization.

NMR spectroscopy. The degree of polymerization (*N*) and number average molecular weight (M_n) of three PEA-$(COOH)_2$ were determined by proton nuclear magnetic resonance (^{1}H-NMR) by using dDMSO, and the NMR spectra for three PEA-$(COOH)_2$ are shown in Figure 2-1. The *N* value was estimated by comparing the integral of peaks at 4.7 ppm from two protons adjacent to the CTA residue (S-C(=S)-S) with the integral of the peaks at around 4.0 ppm from two protons of methylene on the side chain of PEA-$(COOH)_2$. The *N* value of PEA was also estimated by the same way (Figure 2-2). Since the PEI used has a branched structure, ^{13}C-NMR was performed for PEI by using D_2O to estimate the fraction of primary, secondary, tertiary amines in a chain. The ^{13}C-NMR spectrum is shown in Figure 2-3, revealing that the ratio of primary, secondary, and tertiary amines was approximately 0.4, 0.4, and 0.2, respectively.

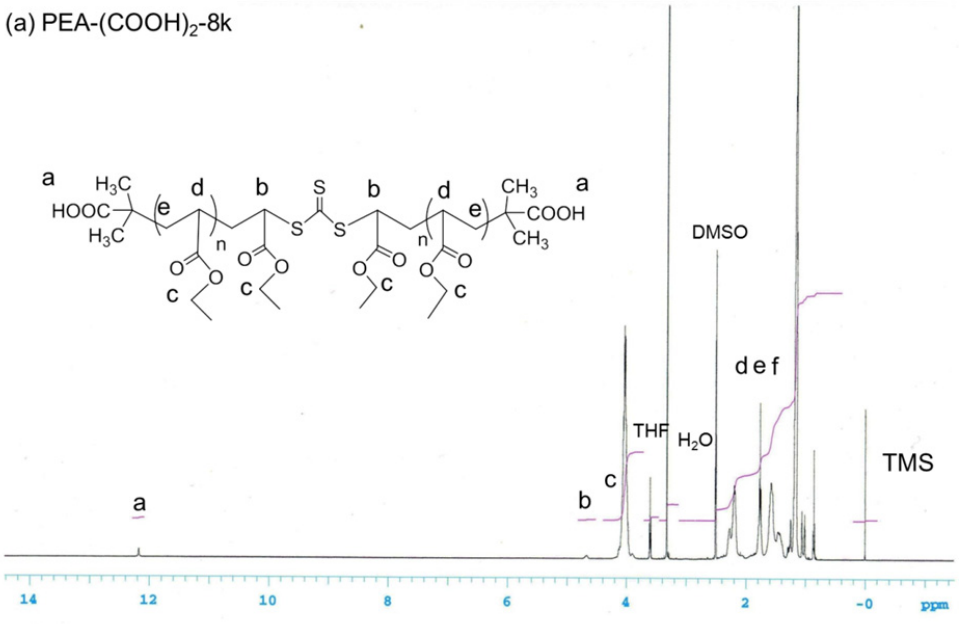

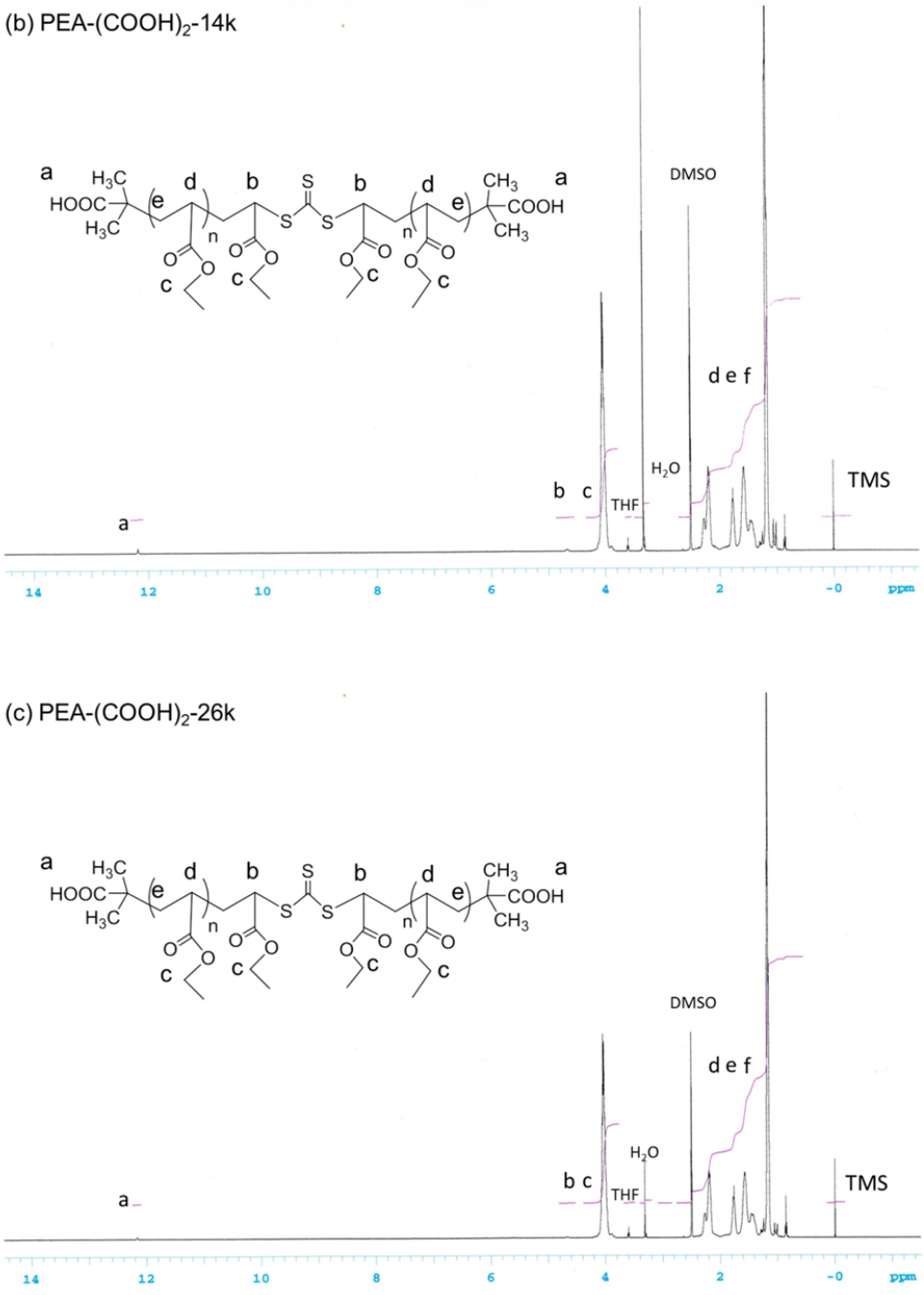

Figure 2-1. ^{1}H-NMR spectra of (a) PEA-$(COOH)_2$-8k, (b) PEA-$(COOH)_2$-14k, and (c) PEA-$(COOH)_2$-26k.

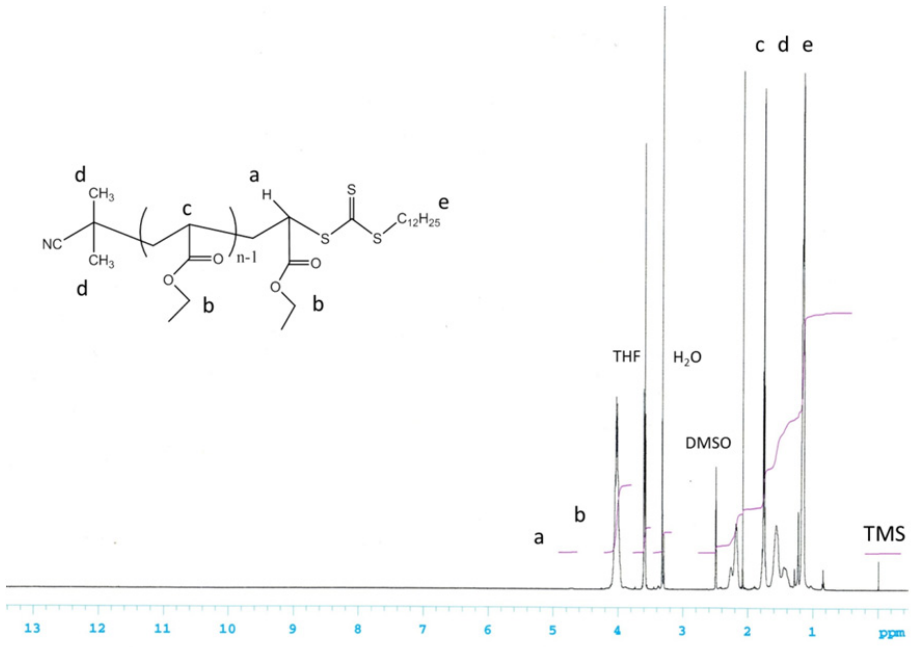

Figure 2-2. ^{1}H-NMR spectrum of PEA.

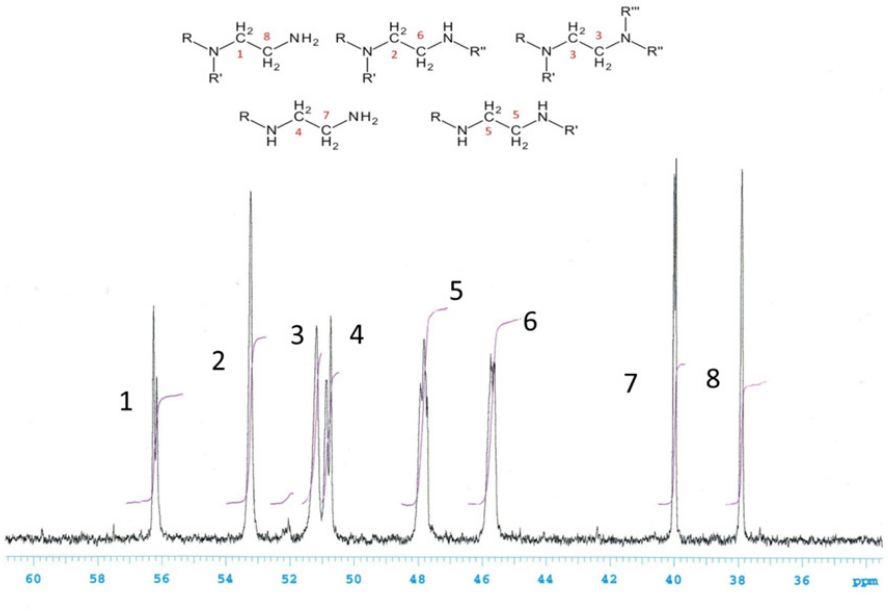

Figure 2-3. ^{13}C-NMR of PEI.

SEC measurements. Polydispersity indices (PDIs) of three PEA-$(COOH)_2$ and PEA were determined by size exclusion chromatography (SEC), using three TSK gel columns (two $G3000H_{HR}$ and one $G4000H_{HR}$ Tosoh Corp.), combined with an HPLC pump and a refractive index detector (Tosoh Corp.). THF was used as an eluent, and the flow rate was 1 ml/min. Calibration was done with polystyrene standards. The SEC spectra for three PEA-$(COOH)_2$ and PEA are shown in Figure 2-4.

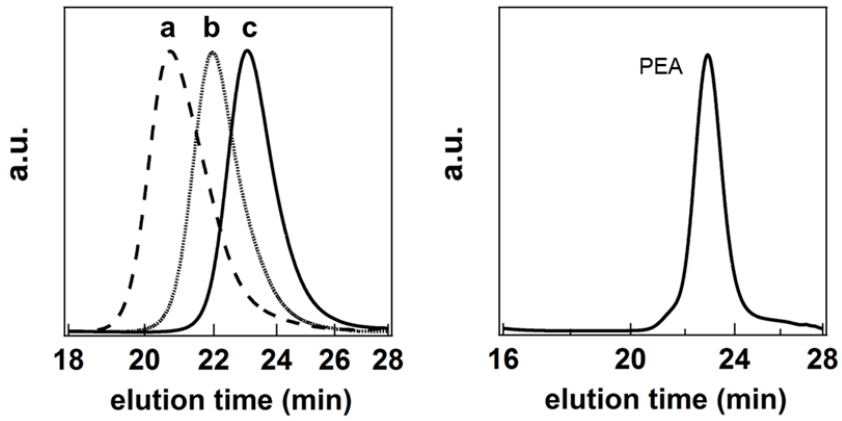

Figure 2-4. SEC spectra of; (a) PEA-$(COOH)_2$-8k, (b) PEA-$(COOH)_2$-14k, and (c) PEA-$(COOH)_2$-26k (left), and PEA (right). Please refer to the section below for the explanation of the molecular codes.

Molecular characteristics and codes. Three PEA-$(COOH)_2$ were coded as PEA-$(COOH)_2$-X, where *X* represents M_n of each PEA-$(COOH)_2$ in the unit of kg/mol. Note that the critical molecular weight (M_c) of PEA related to the entanglement molecular weight (M_e~12 kg/mol) is approximately 24 kg/mol at room temperature.[2] Molecular characteristics of three PEA-$(COOH)_2$ are summarized in Table 2-1, together with those of PEA and PEI.

Table 2-1. Molecular characteristics of polymers

Sample code	M_n[a]	PDI[b]	n_{func}[c]
PEA-$(COOH)_2$-8k	8,000	1.13	2
PEA-$(COOH)_2$-14k	14,000	1.16	2
PEA-$(COOH)_2$-26k	26,000	1.15	2
PEA	11,000	1.14	-
PEI	1,200	1.11[d]	28[e]

[a]Number average molecular weight determined by ^{1}H-NMR. [b]Polydispersity index measured by SEC. [c]Average number of functional groups per chain (carboxylic acids or amines). [d]PDI for PEI was calculated from the sample information obtained from Aldrich (M_n ~ 1200, M_w ~ 1300). [e]n_{func} of PEI was calculated by dividing the number average molecular weight (1200 g/mol) by that of a monomer unit of (-CH_2-CH_2-NH-, 43 g/mol).

2-1-3. Blend preparation. An aqueous solution of polyethyleneimine (**PEI**, M_n ~ 1200, M_w ~ 1300) was purchased from Aldrich. Neat PEI polymer for blend experiments was prepared by drying the PEI solution *in vacuo*. For preparation of the blends, PEA-$(COOH)_2$ and PEI were firstly dissolved in a mixture solvent of THF and MeOH (1: 1 vol%) separately. After mixing the solutions in a metal mold, the solvents were evaporated on a heater at 40 ºC for 48 h, followed by drying *in vacuo* at 40 ºC for 24 h. To investigate the effects of the blend weight ratio and the molecular weight of PEA-$(COOH)_2$ on the physical properties, three series of blends were prepared by varying the weight ratio of PEA-$(COOH)_2$: PEI as 10 : *Y*. Blend samples were coded as AI-Xk-Y, where *X* is a molecular weight of PEA-$(COOH)_2$ and *Y* represents the value in the weight ratio of 10 : *Y*. The information for the blend samples are summarized in Table 2-2.

Table 2-2. Blend samples

code	$w_{PEA\text{-}(COOH)2}$: w_{PEI} [a]	n_{COOH}: n_{amine} [b]
AI-8k-0.4	10 : 0.4	1 : 3.9
AI-8k-0.6	10 : 0.6	1 : 5.8
AI-8k-0.8	10 : 0.8	1 : 7.7
AI-8k-1	10 : 1.0	1 : 9.7
AI-8k-1.2	10 : 1.2	1 : 12
AI-14k-0.3	10 : 0.3	1 : 4.8
AI-14k-0.4	10 : 0.4	1: 6.4
AI-14k-0.5	10 : 0.5	1 : 8.0
AI-14k-0.6	10 : 0.6	1 : 9.5
AI-14k-0.7	10 : 0.7	1: 11
AI-26k-0.1	10 : 0.1	1: 3.0
AI-26k-0.2	10 : 0.2	1 : 6.0
AI-26k-0.3	10 : 0.3	1 : 8.9
AI-26k-0.35	10 : 0.35	1 : 10.4
AI-26k-0.4	10 : 0.4	1 : 12.0

[a]Weight ratio of PEA-$(COOH)_2$: PEI. [b] Mole ratio of carboxylic acids on PEA-$(COOH)_2$ to amines on PEI, where n_{amine} includes primary and tertiary amines as well as secondary amine.

2-2. Synthesis and characterization of polymers used in the 4th and 5th chapter.

Here in this section, the synthesis and characterization of P-Ba-P, P-B-P, Ba, and B, which are used for the chapter 4 and 5, are explained below.

2-2-1. Synthesis.

Synthesis of triblock copolymers. All monomers, including 4-vinylpyridine, butyl acrylate, and acrylamide, were purchased from TCI. The monomers were purified by passing them through an aluminum oxide column before polymerizations.

The component polymers were synthesized via RAFT polymerization. Firstly, 4-vinylpyridine (8.0 g, 76 mmol) was polymerized via RAFT polymerization by using a difunctional chain transfer agent (CTA), *S,S'*-bis(α,α'-dimethyl-α"-acetic acid) trithiocarbonate CTA (0.33 g, 1.15 mmol) and 2,2'-azobis(isobutyronitrile) (AIBN, 60 mg, 0.35 mmol) as an initiator in 1,1,2,2-tetrachroloethane (12 ml) at 80 °C for 2 h. After purification by repeating reprecipitations, butyl acrylate (3.5 g, 27 mmol) and acrylamide (0.4 g. 5.6 mmol) were *co*-polymerized from the precursor poly(4-vinylpiridine) (P, 0.62 g, 0.11 mmol) as a macro-CTA with AIBN (7 mg) in DMF (3 ml) at 80 °C for 45 min. The triblock-type copolymer was purified by reprecipitation procedures, followed by removing unreacted precursor P with a selective solvent. The scheme for P-Ba-P synthesis is shown in Scheme 2-3.

Scheme 2-3. Syntheses of P-Ba-P and P-B-P

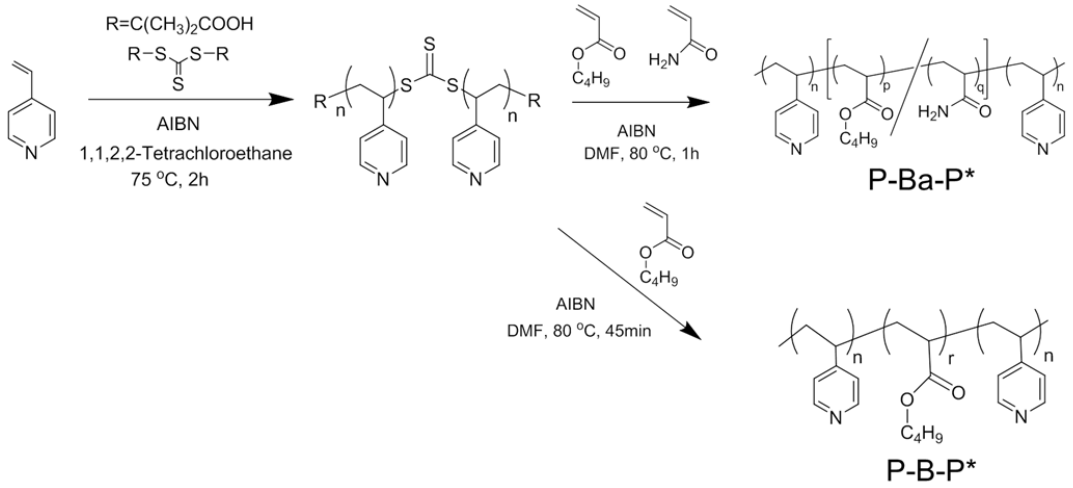

*RAFT agent residue was omitted in their chemical structures for simplification

As a control sample, P-B-P was prepared in the similar way to P-Ba-P synthesis. Unlike the P-Ba-P synthesis, only butyl acrylate monomer (2.5 g, 20 mmol) was polymerized from the precursor P (0.41 g, 0.075 mmol) as a macro CTA. Purification and removal of unreacted P precursor were conducted in the same way to P-Ba-P synthesis. The scheme for P-B-P synthesis is also shown in Scheme 2-3.

Synthesis of Ba and B.

As reference samples in physical property investigations, two homopolymers, i.e., poly(butyl acrylate)-*co*-polyacrylamide (Ba) and poly(butyl acrylate) (B), were individually synthesized via RAFT polymerization by using 2-Cyano-2-propyldodecyl trithiocarbonate as a CTA with AIBN in DMF at 80 °C for 45 min. Schemes for Ba and B synthesis are shown in Scheme 2-4.

Scheme 2-4. Syntheses of Ba and B

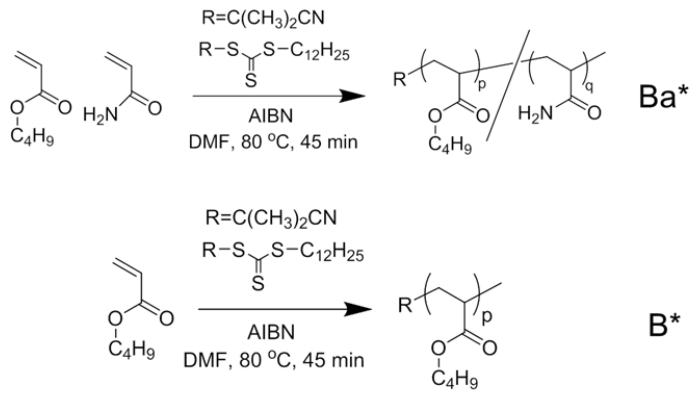

*RAFT agent residue was omitted in their chemical structures for simplification

2-2-2. Characterization.

NMR spectroscopy. The degree of polymerization (N) and the number-average molecular weight (M_n) of polymers were estimated by ^{1}H-NMR (see Figures 2-5 to 2-9). The degree of polymerization of 4-vinylpyridine of the precursor P (N_P) was firstly estimated by end-group analysis. The value of N_P was determined by comparing integral of peaks at 4.7 ppm from two protons adjacent to the CTA residue (S-C(=S)-S) with the integral of peaks at around 8.2 ppm from two protons on the side chain of pyridine rings of P block. The N values of butyl acrylate (N_B) and acrylamide (N_a) in P-Ba-P were then estimated by comparing the integral of peaks originating from pyridine rings of P block with the integral of peaks at 4 ppm and at 6 – 7 ppm from protons on the side chain of butyl acrylate and acrylamide, respectively, after subtracting the integral of peaks originating from pyridine rings. The value of N_B in P-B-P was estimated by the similar way to the case of P-Ba-P. The value of N_B and N_a in Ba or B was estimated by comparing the integral of of peaks at 4.7 ppm from one proton adjacent to the CTA residue (S-C(=S)-S) with the integral of peaks at 4 ppm and at 6 – 7 ppm from protons on the side chain of butyl acrylate and acrylamide, respectively.

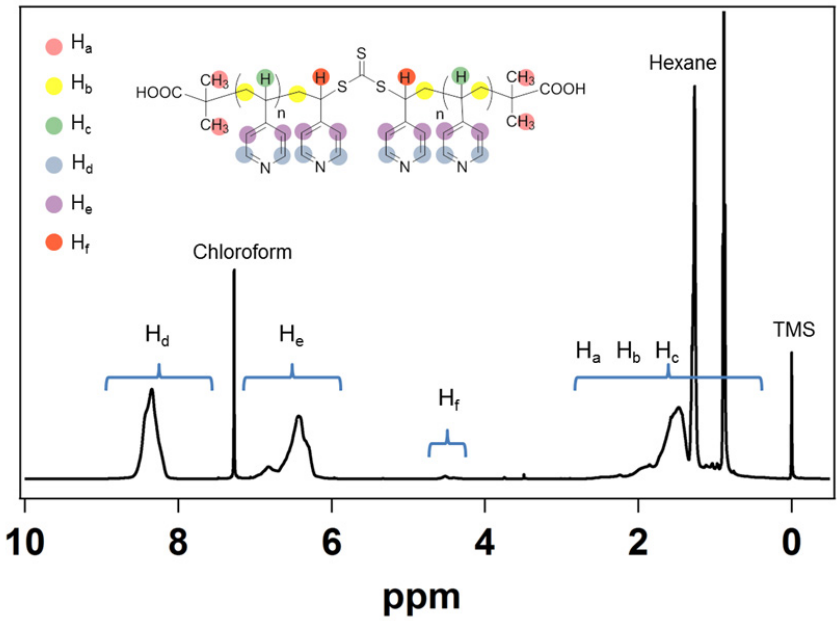

Figure 2-5. ^{1}H-NMR spectrum of P.

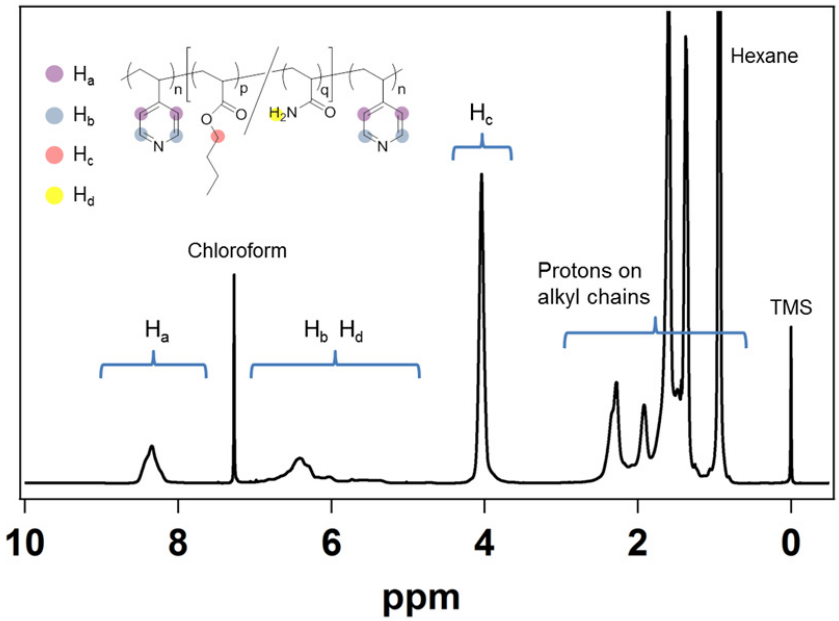

Figure 2-6. ^{1}H-NMR spectrum for P-Ba-P.

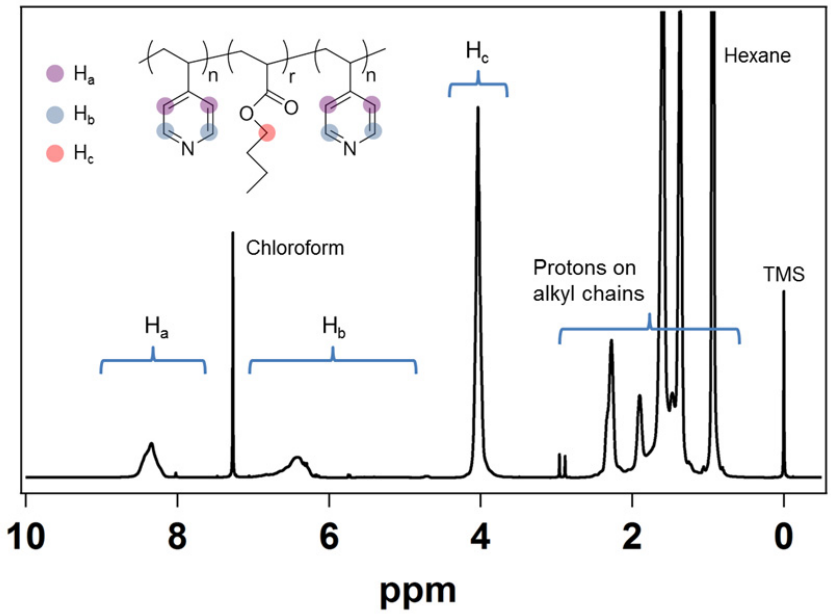

Figure 2-7. ^{1}H-NMR spectrum of P-B-P.

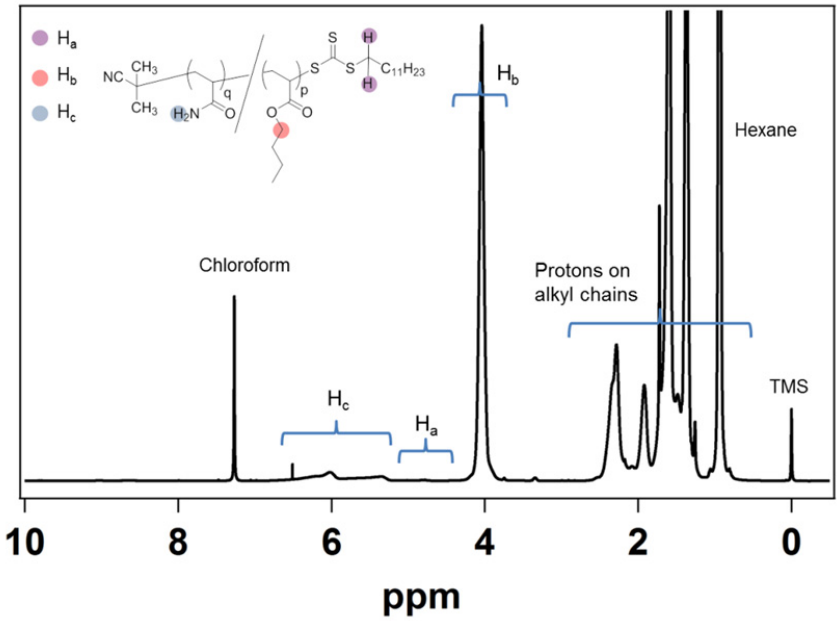

Figure 2-8. ^{1}H-NMR spectrum of Ba.

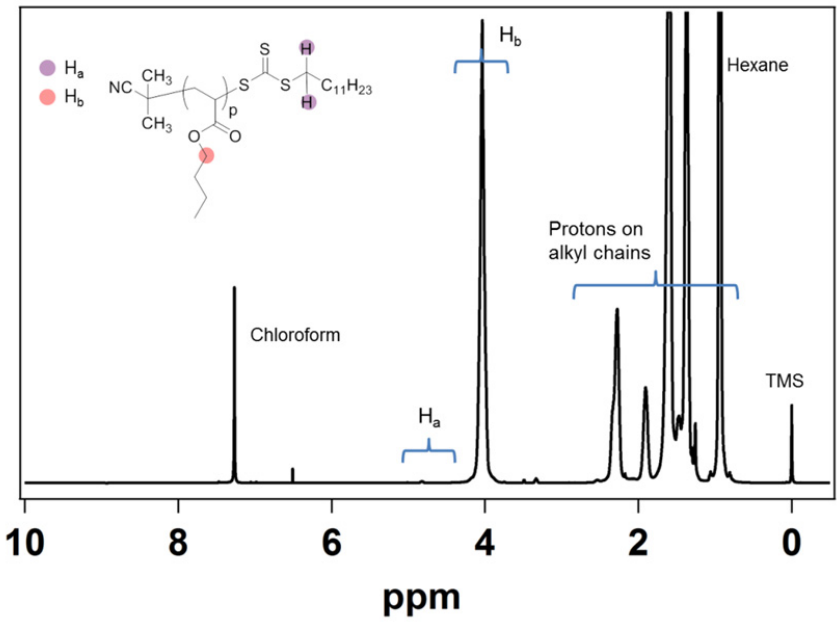

Figure 2-9. ^{1}H-NMR spectrum for B.

SEC measurements. PDIs of the polymers were determined by SEC measurements, using three TSK gel columns (two G3000H_{HR} and one G4000H_{HR}), combined with an HPLC pump and a refractive index detector (Tosoh Corp.). Dimethylformamide (DMF) was used as an eluent, and the flow rate was 1 ml/min. The elution volumes were calibrated with polystyrene standards. SEC chromatograms of the polymers are shown in Figure 2-10, revealing that the precursor P for synthesizing P-Ba-P (or P-B-P) was completely removed by purification and that polymers with relatively low PDIs were synthesized (Figure 2-10a).

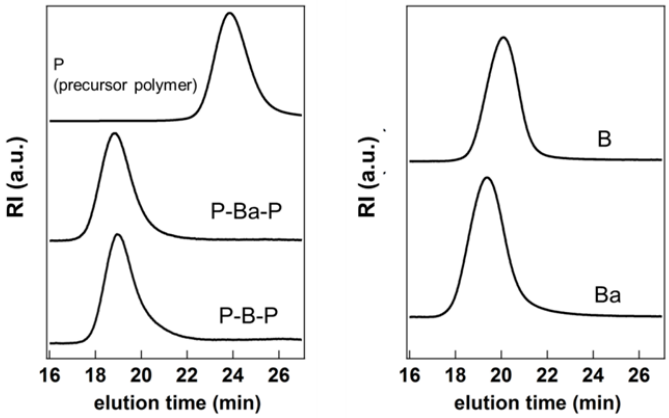

Figure 2-10. SEC spectra for P, P-Ba-P, and P-B-P (left side), and B and Ba (right side)

Molecular characteristics and codes. Molecular characteristics of B, Ba, P-B-P and P-Ba-P are summarized in Table 2-3. Since the entanglement molecular weight (M_e) of poly(butyl acrylate) is approximately 30,000 g/mol,[3] the molecular weights of B, Ba, and the middle blocks in P-B-P and P-Ba-P are all lower than M_e of poly(butyl acrylate), meaning entanglements are rarely generated. It should be also noted that the molecular weights of the middle blocks (M_{middle}) in the triblock copolymers, and those of two homopolymers, B and Ba, are nearly the same.

Table 2-3. Codes and molecular characteristics of polymers

Sample code	N_P[a]	N_B[a]	N_a[a]	f_a[b]	M_{middle}[c]	M_{total}[c]	PDI[d]
B	-	194	-	-	-	25,000	1.05
Ba	-	195	30	0.13	-	27,000	1.10
P-B-P	48	196	-		25,000	30,000	1.22
P-Ba-P	48	178	30	0.15	25,000	30,000	1.17

[a]Average number of monomeric units of 4-vinylpyridine (N_P), butyl acrylate (N_B), and acrylamide (N_a) in a polymer chain determined by ^{1}H-NMR. [b]Mole fraction of acrylamide units in a random copolymer chain, which was calculated from $N_a/(N_B+N_a)$. [c]Number average molecular weight of the middle block (M_{middle}) and the triblock copolymer (M_{total}), which was calculated from the number of monomeric units and the mass of each monomeric unit. [d]Polydispersity indices measured by SEC.

In addition, various P-Ba-P polymers with different f_a were prepared to investigate the effects of f_a on the elongation properties. They are coded as P-Ba-P-*X*, where *X* represents f_a. The molecular characteristics of various P-Ba-P synthesized are summarized in Table 2-4.

Table 2-4. Molecular characteristics of three P-Ba-P

Sample code	N_P[a]	N_B[a]	N_a[a]	f_a[b]	M_{middle}[c]	M_{whole}[d]	PDI[e]
P-Ba-P-15	48	178	30	15	25,000	30,000	1.17
P-Ba-P-8	48	236	21	8	32,000	37,000	1.10
P-Ba-P-4	48	210	10	4	28,000	33,000	1.22

[a]Average number of monomeric units of 4-vinylpyridine (N_P), butyl acrylate (N_B), and acrylamide (N_a) in a polymer chain determined by ^{1}H-NMR. [b]Mole fraction of acrylamide units in the middle block, which was calculated from $N_a/(N_B+N_a)$. [c]Number average molecular weight of the middle block (M_{middle}) and the triblock copolymer (M_{total}), which was calculated from the number of molecular units and the mass of each monomeric unit. [d]Polydispersity index measured by SEC.

Randomness of butyl acrylate and acrylamide.

Note that copolymerization of butyl acrylate and acrylamide should proceed in a nearly random sequence, considering their reactivity ratio, where the reactivity ratio of acrylamide to butyl acrylate and that of butyl acrylate to acrylamide are 0.72 and 1.26,[4,5] respectively. The randomness was also evaluated by performing DSC measurements for various poly(butyl acrylate)-*co*-polyacrylamide with changing the fraction of acrylamide units (f_a). These are coded as Ba-*X*, where *X* represents f_a. The characteristics of random polymers synthesized are summarized in Table 2-5. A single endothermic peak originating from the T_g was observed (see Figure 2-11), and the peak was gradually shifted to a higher temperature with an increase in f_a. This suggests that the copolymerization of butyl acrylate and acrylamide via RAFT polymerization proceeds in a random way.

Table 2-5. Molecular characteristics of various poly(butyl acrylate)-*co*-polyacrylamide

Sample code	M_n[a]	N_B[b]	N_a[b]	f_a[c]	PDI[d]	T_g[e] (°C)
B	25,000	194	-	0	1.05	-50
Ba-7	27,000	204	16	7	1.10	-39
Ba-15	27,000	195	30	15	1.11	-26
Ba-22	24,000	166	37	22	1.13	-6

[a]The number average molecular weight determined by ^{1}H-NMR. [b,c]The average number of monomeric units of butyl acrylate (N_B) and acrylamide (N_a) determined by ^{1}H-NMR. [c]Mole fraction of acrylamide units in a polymer chain. [d]Polydispersity indices determined by SEC. [e]The glass transition temperature determined by DSC measurements.

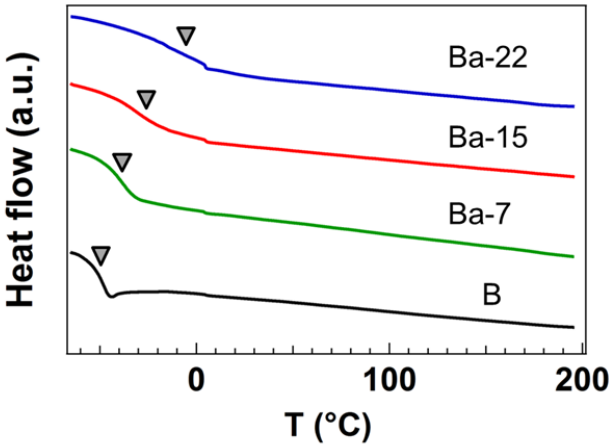

Figure 2-11. DSC thermograms of various poly(butyl acrylate)-*co*-polyacrylamide with different f_a, where that of B is also shown.

2-2-3. Preparation of bulk films. Preparation of bulk films used in the 4th chapter was carried out as follows. P-Ba-P or P-B-P was dissolved in a mixed solvent of pyridine / water (9 / 1 by volume), which was poured into a Teflon-made mold (W × 25 mm, D × 10 mm, H × 10 mm). The solvent was evaporated slowly during solvent casting at 40 °C for 3 days and dried *in*

vacuo at 40 °C for one day. The mass of the polymers used was fixed at 250 mg to prepare films with the same thickness.

Preparation of blends used in the 5th chapter was carried out as follows. First, P-Ba-P (or P-B-P) and zinc (II) chloride $ZnCl_2$ were dissolved in a mixed solvent of pyridine / water (9 / 1 by volume) separately. The use of the solvent mixture was to prevent rapid aggregation between P-Ba-P (or P-B-P) and $ZnCl_2$. Then, both solutions were mixed in a Teflon-made mold, and the solvent was evaporated slowly in the same way as explained above. P-Ba-P (or P-B-P) and $ZnCl_2$ was mixed with the mole ratio of $ZnCl_2$ / pyridine units = 0.5. Since $ZnCl_2$ possesses two available coordination sites,[6] the mole ratio between available coordination sites and ligands attains the stoichiometric equivalence at the mole ratio. The total mass of the polymers and $ZnCl_2$ was fixed at 250 mg to prepare the films with the same thickness. Blends of P-Ba-P (or P-B-P) and $ZnCl_2$ were coded as P-Ba-P/$ZnCl_2$ (or P-B-P/$ZnCl_2$).

2-3. Experimental conditions for structure determination and rheological properties.

FT-IR measurements. In the 3rd chapter, Fourier-transform infrared spectroscopy (FT-IR) measurements will be performed for AI-8k-Y series to identify the interaction between PEA-$(COOH)_2$ and PEI with FT-IR 6100 (Jasco, Japan). Each measurement was conducted at room temperature under the reduced pressure.

In the 4th and 5th chapter, FT-IR measurements will be performed to identify the hydrogen bonds between acrylamide units and metal-ligand coordination between 4-vinylpyridine units and $ZnCl_2$. The instrument was an IR Prestige-21 spectrometer combined with an AIM 8800 attachment (SHIMADZU) for microscopic sample positioning.

DSC measurements. In the 4th and 5th chapter, differential scanning calorimetry (DSC)

measurements will be performed to investigate the T_gs. The instrument was a Q2000 calorimeter (TA Instruments). The temperature range was from -60 °C to 200 °C, and the temperature increase rate was 10 °C/min.

SAXS measurements. Small angle X-ray scattering (SAXS) measurements were conducted to obtain the morphological information at a nanometer scale. The instrument was Rigaku Nano Viewer, where an X-ray generator was operated at the voltage of 45 kV and the current of 60 mA. The wavelength of the incident X-rays and the camera length were 0.154 nm and 735 mm, respectively. For the polymers and the blends in the chapter 3, samples were held between polyimide films, which were exposed to the incident beam for 2 h at 10 °C. For the polymers and the blends in the chapter 4 and 5, the bulk films of samples were directly exposed to the incident beam for 2 h at room temperature. Imaging plates were used as detectors.

TEM observations. The TEM observations were conducted for P-Ba-P, P-Ba-P/$ZnCl_2$ and P-B-P/$ZnCl_2$ to investigate the assembly states at a nanometer scale. The instrument was JEM 1400 (JEOL) at an accelerating voltage of 120 kV. Ultrathin films with a 50 nm thickness were prepared with a microtome (Reica ultracut FUS) in a wet condition. The films were stained with I_2 vapor to observe TEM images with clearer contrast.

Rheology. Rheological measurements were performed for the samples to investigate the dynamic properties of the supramolecular networks (in chapter 3). Oscillatory shear measurements were conducted on an ARES-G2 rheometer (TA Instruments) with 25 mm parallel plates in a N_2 atmosphere. Dynamic temperature ramp tests were performed from 40 °C to 0 °C at a ramp rate of 1 °C/min with a strain of 0.5% (or 1%) and a frequency of 0.3 rad/s. The tests

are equivalent to the measurement of stress in nearly 3 seconds after application of shear strain of 0.5% (or 1%) at each temperature. Dynamic frequency sweeps were acquired at ten degree intervals from 70 °C to 0 °C. Dynamic strain sweeps were also performed to estimate the linear viscoelastic regime in advance, and all above dynamic tests were conducted in the linear regime. Creep-recovery tests were performed for AI-8k-1, AI-14k-0.6, and AI-26k-0.35 with the same experimental set up as explained above, where the tests were conducted by applying a constant shear stress of 4000 Pa for 300 sec. After removal of the stress, sample recovery was measured for an additional period of 3000 sec.

Rheological measurements for the triblock copolymers and the blends were performed with an uniaxial rheometer RSA-G2 (TA Instruments) by using strip-shaped samples (in chapter 4 and 5). The measurements for B and Ba were performed with a shear rheometer of ARES-G2 (TA Instruments) with 25 mm parallel plates. The dynamic temperature ramp tests with the uniaxial rheometer were conducted from -60 °C to 130 °C (or till a temperature of sample deformation) for the triblock copolymers and the blends with a heating rate of 3 °C/min under 0.1% strain at a frequency of 1 Hz. The tests with shear rheometer were also conducted from -40 °C to 0 °C for B and from -10 °C to 40 °C for Ba with a heating rate of 3 °C/min under 1% strain at a frequency of 1 rad/sec. Dynamic frequency sweep tests for the triblock copolymers were carried out at ten degree intervals from -50 °C to 130 °C (or till a temperature of sample deformation) in the frequency range from 100 to 0.3 Hz. The tests were also conducted from -30 °C to 30 °C for B and from 0 °C to 60 °C for Ba in the frequency range from 100 to 0.1 rad/sec. All dynamic tests were performed in a linear regime in a N_2 gas atmosphere. It should be noted that the degradation by heating of the polymers synthesized via RAFT polymerization can be negligible in an inert gas atmosphere under 130 °C.[7]

The mechanism to obtain the information of storage modulus (*G'* or *E'*) and the loss

modulus (*G"* or *E"*) in rheological measurements and an important concept for the analysis of rheological data, that is, the time-temperature superposition principle will be explained in the later section as well as the longest relaxation time, rubbery plateau, plateau modulus, and flow activation energy.

Tensile tests. Tensile tests for the triblock copolymers and the blends were performed with an ARES-G2 rheometer (TA Instruments) by using dogbone-shaped samples prepared by a cutting die (detailed sample shape is shown in Figure 2-12). The tests were carried out with an elongation rate of 10 mm/min at room temperature (in chapter 4 and 5).

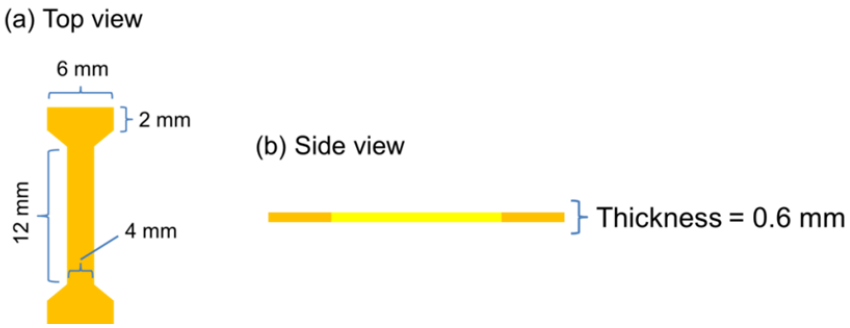

Figure 2-12. Sample shape of a dogbone sample for tensile tests.

2-4. Linear Viscoelasticity

Viscoelasticity is one of the most distinctive properties of polymers. Polymers represent solid-like behavior and liquid-like behavior depending on the time (or frequency), which is associated with the relaxation of polymer chains. The stress relaxation is also observed in supramolecular soft materials composed of non-covalent bonded cross-links, where the relaxation originates from the dissociation (and re-association) of the non-covalent bonded

cross-links. Therefore, investigation of the viscoelasticity of supramolecular networks is important to understand their macroscopic physical properties.

2-4-1. Storage modulus and loss modulus.

Maxwell model.

Basically, the storage modulus *G'* and the loss modulus *G"* indicate the elastic and viscous aspects of the materials, respectively. Here in this section, the mechanism to detect *G'* and *G"* in rheological measurements is explained.

Firstly, the stress relaxation on the basis of the simple Maxwell model, which is composed of a Hooken spring with spring constant *G* and a Newtonian dash pot with viscosity η (illustrated in Figure 2-13), is described below.

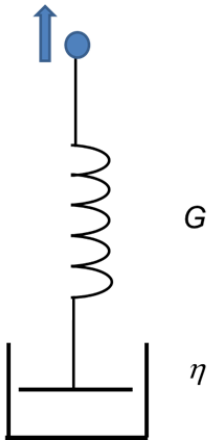

Figure 2-13. Illustration of the Maxwell element.

In the spring element, the relationship between stress σ and strain γ is written by eq (2-1).

$$\sigma = G\gamma \qquad (2\text{-}1)$$

The relationship in the dashpot is written by eq (2-2),

$$\sigma = \eta\dot{\gamma} \qquad (2\text{-}2)$$

When the stresss is applied to the model at t = 0, the stress is preferentially transmitted to the spring, where the deformation of the spring is not very drastic because it is connected with the viscous dashpot. After the deformation of the spring reached some level, the stress can be also transmitted to the dashpot element. The total deformation, $\gamma_{0,}$ should be composed of two elements, i.e., the strain from the spring (γ_{spring}) and dashpot ($\gamma_{dashpot}$), and hence γ_0 is described by eq (2-3).

$$\gamma_0 = \gamma_{spring} + \gamma_{dashpot} \qquad (2\text{-}3)$$

The strain is constant for t > 0, and so force the deformation rate $d\gamma_0/dt$ can be written as eq (2-4).

$$\frac{d\gamma_0}{dt} = 0 = \dot{\gamma}_{spring} + \dot{\gamma}_{dashpot} = \frac{d}{dt}\frac{\sigma(t)}{G} + \frac{\sigma(t)}{\eta} \qquad (2\text{-}4)$$

Since the relaxation time τ is defined as $\tau = \eta/G$, eq (2-4) can be transformed to eq (2-5),

$$\dot{\sigma} + \frac{1}{\tau}\sigma = 0 \qquad (2\text{-}5)$$

Dynamic response.

The most common experimental approach to detect *G'* and *G"* is applying sinusoidally time-varying strain, i.e., $\gamma(t) = \gamma_0 \sin\omega t$. The advantage of this procedure is that both viscous character (*G'*) and elastic character (*G"*) can be extracted in the same measurements.

The response of the Maxwell element against the stress can be written by,

$$\gamma_0 \frac{d}{dt}\sin\omega t = \gamma_0 \omega \cos\omega t = \frac{1}{G}\dot{\sigma} + \frac{1}{\eta}\sigma \qquad (2\text{-}6)$$

$$\dot{\sigma} + \frac{1}{\tau}\sigma = G\gamma_0 \omega \cos\omega t \qquad (2\text{-}7)$$

Eq (2-7) is the transformed from (2-6).

To solve the first-order differential equation for $\gamma(t)$, the following equation (2-8) is set.

$$\sigma(t) = A\sin\omega t + B\cos\omega t = A_0 \sin(\omega t + \varphi) \qquad (2\text{-}8)$$

By substituting the eq (2-8) into (2-7), one can obtain eq (2-9),

$$A\omega\cos\omega t - B\omega\sin\omega t + \frac{1}{\tau}A\sin\omega t + \frac{1}{\tau}B\cos\omega t = G\gamma_0\omega\cos\omega t \qquad (2\text{-}9)$$

By focusing on the sine and cosine part individually in eq (2-9), two equations (2-10) and (2-11) can be obtained to give *A* and *B*.

$$-B\omega + \frac{1}{\tau}A = 0 \quad \text{from the sine part} \qquad (2\text{-}10)$$

$$A\omega + \frac{1}{\tau}B = G\gamma_0\omega \quad \text{from the cosine part} \qquad (2\text{-}11)$$

Then, *A* and *B* are found to be,

$$A = G\gamma_0\frac{\omega^2\tau^2}{1+\omega^2\tau^2}, \quad B = G\gamma_0\frac{\omega\tau}{1+\omega^2\tau^2}$$

Therefore, the whole equation can be written as

$$\frac{\sigma(t)}{\gamma_0} = G\frac{\omega^2\tau^2}{1+\omega^2\tau^2}\sin\omega t + G\frac{\omega\tau}{1+\omega^2\tau^2}\cos\omega t = G'\sin\omega t + G''\cos\omega t \qquad (2\text{-}12)$$

, where one notices *A* and *B* can be replaced with *G'* and *G"*, and those are defined as

$$G' = G\gamma_0\frac{\omega^2\tau^2}{1+\omega^2\tau^2}, \quad G'' = G\gamma_0\frac{\omega\tau}{1+\omega^2\tau^2}.$$

From the above derivation, it is found that *G'* has no phase-shift from the stress of $\sin\omega t$, while *G"* has phase-shift by 90º from the stress. When *G'* >> *G"*, the material is solid-like (or gel-like), and when *G"* >> *G'*, the materials is liquid-like.

2-4-2 Time-Temperature Superposition.

For melt polymers or polymer solutions, some rheological data attained at an arbitrary

temperature can be treated as the data attained at a reference temperature T_{ref} by applying the "time-temperature superposition (TTS)." Note that there is a strict limitation for the application of TTS; the TTS can be available only in the condition that the origin of the relaxation is the same within the temperature range for the superposition. For example, TTS cannot be applied to the polymer showing phase transition, such as crystalline polymers, since the motion of polymer chains against temperatures is completely different before and after the transition.

Figure 2-14 describes the operation of TTS for a linear polystyrene with $M_w \sim 40{,}000$ (synthesized by anionic polymerization) as an example to create a master curve. The rheological measurements with dynamic frequency sweep modes were conducted at the temperature range from 120 °C to 180 °C. Each spectrum obtained at different temperatures was shifted to create a smooth curve with T_{ref} = 160 °C, i.e., the spectrum at 160 °C was used as a standard spectrum without any frequency shifts. The frequency shift required to create the master curve is called "shift factor a_T." Note that a_T has a relational equation with τ_1 and η as written by eq (2-13) under the condition that temperature dependency of the polymer density is negligible.[8]

$$a_T \equiv \frac{\tau_1(T)}{\tau_1(T_{ref})} = \frac{\eta(T)}{\eta(T_{ref})} \qquad (2\text{-}13)$$

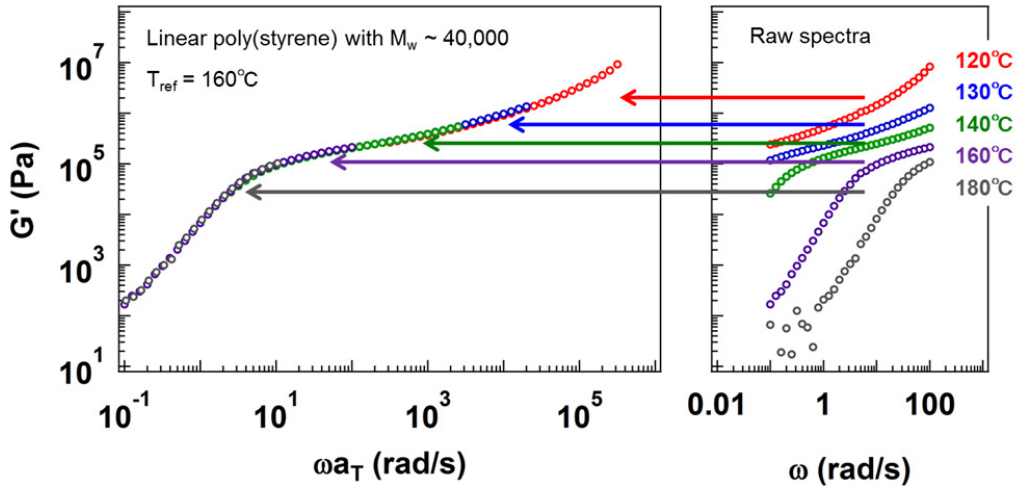

Figure 2-14. The operation of time-temperature superposition. The master curve (left side) was created by shifting the raw spectra (right) with a standard spectrum obtained at 160 °C (i.e. T_{ref} = 160 °C).

2-4-3. The longest relaxation time and Rubbery plateau

The longest relaxation time, τ_1, is one of the most important rheological parameter, which represents the time required for the relaxation of a material against the applied stress. The value of τ_1 can be evaluated by *G'* and *G'* data obtained by frequency sweep tests. The value of τ_1 is estimated by the crossover frequency (ω_{cross}) of extended lines of *G'* and *G"* in the terminal region with $G' \sim \omega^2$ and $G'' \sim \omega$, where the τ_1 has a relationship with ω_{cross} as $\tau_1 = 1/\omega_{cross}$. Figure 2-15 compares the master curves of various linear poly(styrene) (PS) with different molecular weights created at the same T_{ref} of 160 °C, where the *X*k in the sample codes represent the molecular weight with a unit of kg/mol. The crossover frequency of *G'* and *G"* is shifted to a lower frequency with an increase in the molecular weight (see yellow circles in Figure 2-15), meaning that τ_1 increases with an increase in the molecular weight. Experimentally or theoretically, τ_1 is known to has a relationship with *M* as $\tau_1 \sim M^{3.4}$ for linear polymer chains.

Note that distinctive plateau region, which is called "rubbery plateau" is seen in PS-250k, while that is not clear in PS-40k. The appearance of the rubbery plateau indicates

existence of distinctive network structure originating from the intermolecular entanglement.

The modulus of rubbery plateau, so called plateau modulus G_P, is associated with the molecular weight between cross-links (M_x) and the cross-link density (ν_e) as described in eq (2-14),[7]

$$G_P = kT\frac{\nu_e}{V} = \frac{\rho RT}{M_X} \qquad (2\text{-}14)$$

, where k, T, V, ρ, R represent the Boltzmann's constant, an absolute temperature, the volume, the density, and the gas constant, respectively. For melt polymers, the value of G_P is not governed by the molecular weight, since the molecular weight between entanglements, that is, entanglement molecular weight (M_e), is uniquely determined by the kind of polymers. On the other hand, for gels and elastomers, the cross-link density can be influenced by various parameters, such as concentration of cross-linkers or the number of functional groups; therefore, the value of G_P is often used to determine the cross-link density and the average molecular weight between cross-links.

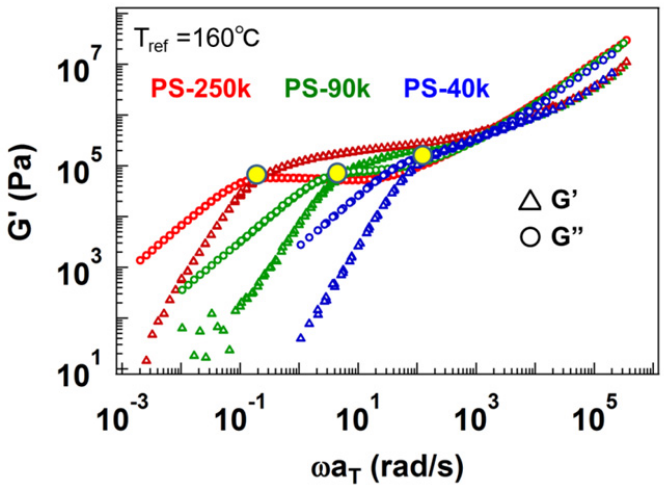

Figure 2-15. Comparison of master curves of various linear polystyrene (PS). The polymers are coded as PS-Xk, where Xk represents M_w with a unit of kg/mol. The color of the codes corresponds to the spectrum

with the same color. The yellow circles represent the crossover point of *G'* and *G"*.

2-4-4. Flow activation energy

Although the value of τ_1 should be used to evaluate the stableness of supramolecular networks, the discussion based on τ_1 only should not be absolute. It is because the value of τ_1 has the reference temperature dependence. To evaluate the stableness, estimation of the flow activation energy E_a, which does not depend on the reference temperature, could be more reliable.

The E_a value can be estimated by the relationship between a_T for creating master curves and the inverse temperature. The blue curve in Figure 2-16 represents typical behavior of a_T with a logarithmic scale as a function of inverse temperatures. It is known that the relationship between a_T and inverse temperature follows Arrhenius-type equation (2-15) at temperatures sufficiently higher than the glass transition temperature ($T > T_g$+50 °C).[7]

$$a_T \propto \exp(\frac{E_a}{RT}) \qquad (2\text{-}15)$$

$$\ln a_T = A + \frac{E_a}{RT} \qquad (2\text{-}16)$$

The eq (2-16) is the logarithmic form of (2-15), where A is a constant. The slope of the black straight line in Figure 2-16 represents the E_a / R, which gives E_a. The E_a value could be regarded as the energy required for the material flow, and thus, E_a could be associated with the stableness of supramolecular networks.

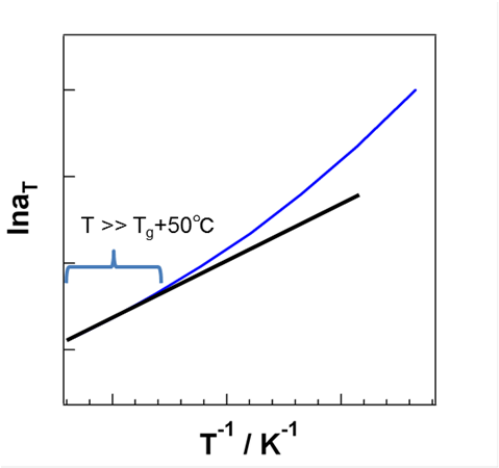

Figure 2-16. Typical a_T variation against inverse temperature (blue curve), where black straight line at $T >> T_g$+50 °C can be used to estimate E_a.

References

[1] Lai, J. T.; Filla, D.; Shea, R. *Macromolecules* **2002,** 35, 6754-6756.

[2] Andreozzi, L.; Castelvetro, V.; Faetti, M.; Giordano, M.; Zulli, F. *Macromolecules* **2006**, 39, 1880-1889.

[3] Yamazaki, H.; Takeda, M.; Kohno, Y.; Ando, H.; Urayama, K.; Takigawa, T. *Macromolecules* **2011**, 44, 8829-8834.

[4] Brar, A. S.; Mukherjee, M.; Chatterjee, S. K. *Polym. J.* **1998,** 30, 664-670.

[5] Abraham, A. A.; Sen, A. K. *J. Appl. Polym. Sci.* **2010**, 117, 2795-2802.

[6] Noro, A.; Matsushima, S.; He, X.; Hayashi, M.; Matsushita, Y. *Macromolecules* **2013**, 46, 8304-8310.

[7] Altintas, O.; Riazi, K.; Lee, R.; Lin, C. Y.; Coote, M. L.; Wilhelm, M.; Barner-Kowollik, C. *Macromolecules* **2013,** 46, 8079-8091.

[8] *Polymer Chemistry 2nd ed*. Himenz, P. C.; Lodge, T. P. CRC Press, **2007**.

Chapter 3

Preparation and Viscoelastic Properties of Supramolecular Soft Materials with Transient Polymer Network via Hydrogen bonding

Abstract: Preparation of supramolecular soft materials according to a simple molecular design in a bulk state was demonstrated by blending carboxy-terminated telechlic poly(ethyl acrylate) (PEA-$(COOH)_2$) and polyethyleneimine (PEI) with multiple amines. Supramolecular polymer networks were evidently formed via ionic hydrogen bonds between carboxylic acids on PEA-$(COOH)_2$ and amines on PEI. Both the effects of molecular weight of PEA-$(COOH)_2$ (M_{PEA}) and the blend ratios on the viscoelastic properties were investigated by rheological measurements. The highest temperature of a storage modulus - loss modulus crossover and the highest flow activation energy were both attained at a certain stoichiometric carboxylic acids / amines ratio, irrelevant to M_{PEA}, suggesting that the ratio plays the key factor on the formation of supramolecular polymer networks. In addition, it has been found the plateau modulus was inversely proportional to M_{PEA} at the optimized blend ratio, probably because PEA-$(COOH)_2$ served as a network strand in the supramolecular network.

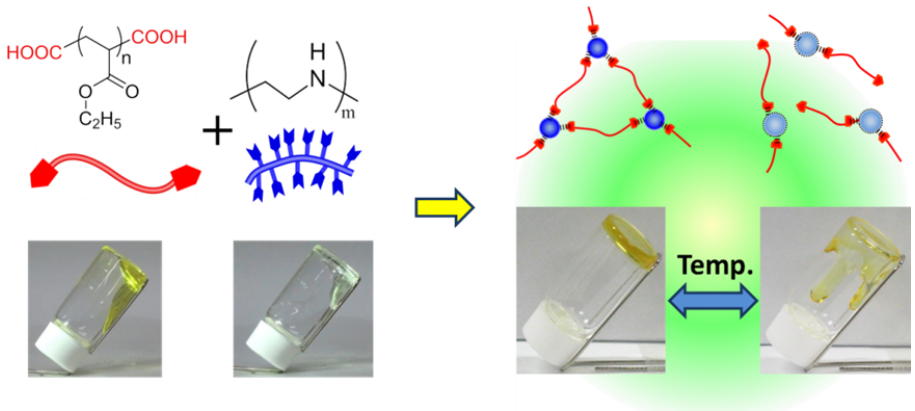

Introduction Polymer gels reveal unique material properties,[1-3] such as flexibility and swellability, and hence they have been widely used in our daily lives as contact lenses, artificial muscles, vibration-proof materials, and other applications. Such polymer gels together with elastomers or rubbers with flexible nature are typical examples of "soft materials." The flexibility of soft materials is attributed to the characteristic molecular structures, that is, 3D network structures from cross-linked polymers.[4]

Supramolecular soft materials with transient polymer networks, including polymers,[5-7] gels,[8-11] rubbers or elastomers,[12-14] have been extensively studied in recent years, where the term "transient" implies that the networks are formed by the reversible non-covalent bonded cross-links with finite lifetimes.[15] Unlike the conventional gels with "permanent" networks formed by covalent bonded cross-links, the materials with transient polymer networks present reversible nature against stimuli such as thermo-[16,17] and pH-responsiveness,[18,19] due to dissociation and re-association of the non-covalent bonded cross-links.

In addition, studies on the viscoelasticity of such supramolecular soft materials composed of associated polymers have also been explored to understand macroscopic physical properties.[20-22] The distinctive viscoelastic properties of them are derived from dynamic nature of the non-covalent bonded cross-links. Although a lot of research groups have reported their preparation, few reports have demonstrated the importance of stoichiometric valance of the functional groups on the physical properties. Therefore, fundamental studies on supramolecular soft materials are required to extend their potential for the applications. To investigate the viscoelastic properties in detail, the rheological measurements covering a wide temperature range is necessary. Noro et al. have reported the gelation mechanism of supramolecular polymer gels containing an ionic liquid as a solvent, where the useful nature of an ionic liquid with non-volatility and high thermal stability enabled quantitative investigation of

thermoresponsibility up to a high temperature (~180°C).[23-26] On the other hand, the design of gel-like materials free from solvents are also preferable because solvent evaporation effects on the dynamic properties during measurements need not be taking into account. This condition was also achieved by preparing the materials composed of melt polymers with T_gs lower than room temperature as reported by Feldman et al,[27] where there are no solvent effects on the interaction strength of the noncovalent bonded cross-links in such bulk system.

On the basis of this background, supramolecular soft materials were prepared by blending two liquid polymers, that is, poly(ethyl acrylate) with two carboxylic acids on its chain ends (PEA-$(COOH)_2$) and polyethyleneimine (PEI) possessing multiple amines, where they can be formed via ionic hydrogen bonds between carboxylic acids and amines (Figure 3-1).[28,29] In the present system, there are no needs to care the solvent evaporation during physical property investigation at high temperatures. The use of telechelic-type polymer should be effective to prepare the soft materials with controllable distance between cross-links. In addition, PEA and PEI show quite deferent solubility nature, that is, PEA is hydrophobic and PEI is hydrophilic. This could work to form self-assembled networks even with component polymers with small molecular weights only if attractive interactions between functional groups are large enough to prevent macrophase separation. In this work, three kinds of PEA-$(COOH)_2$ with different molecular weights were synthesized via reversible addition-fragmentation chain transfer (RAFT) polymerization and PEA-$(COOH)_2$ / PEI blends were prepared at various blend ratios. Small angle X-ray scattering (SAXS) and rheological measurements were conducted for these blends to investigate the effects of mole ratio between functional groups on the physical properties.

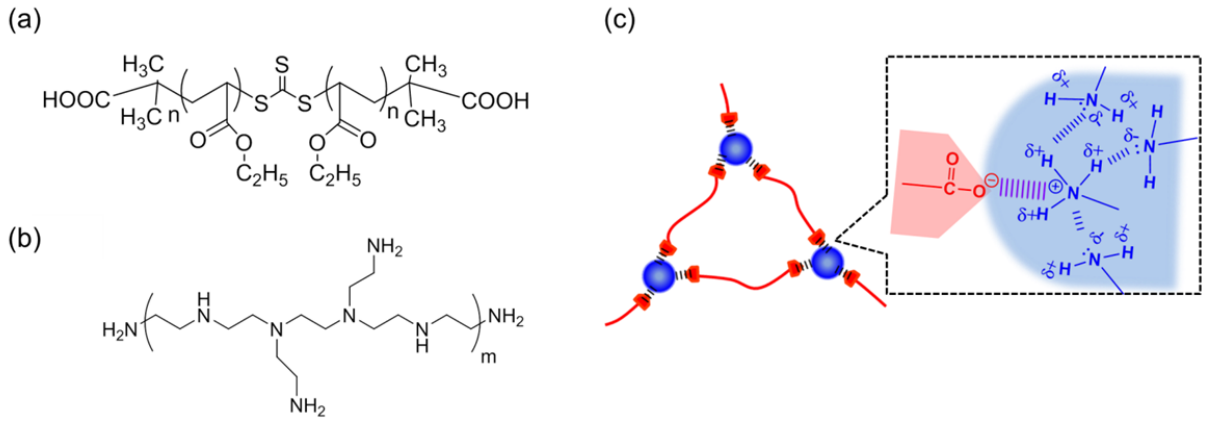

Figure 3-1. Chemical structures of (a) PEA-$(COOH)_2$ and (b) PEI. (c) Schematic illustration of a supramolecular network, where red chains represent PEA-$(COOH)_2$ as network strands and blue clusters express the assemblies of PEI molecules as cross-linkers. See reference #28, Figure 1.

Characteristics and codes of component polymers.

Table 3-1. Molecular characteristics of parent polymers

Sample code	M_n[a]	PDI[b]	n_{func}[c]
PEA-$(COOH)_2$-8k	8000	1.13	2
PEA-$(COOH)_2$-14k	14000	1.16	2
PEA-$(COOH)_2$-26k	26000	1.15	2
PEI	1200	1.11[d]	28[e]

[a]Number average molecular weight determined by ^{1}H-NMR. [b]Polydispersity index measured by SEC. [c]Average number of functional groups per chain (carboxylic acids or amines). [d]PDI for PEI was calculated from the sample information obtained from Aldrich (M_n~1200, M_w~1300). [e]n_{func} of PEI was estimated by simply dividing the number average molecular weight (1200 g/mol) by that of a monomer unit of (-CH_2-CH_2-NH-, 43 g/mol). See synthesis procedures in the chapter 2.

Characteristics and codes of blends.

Table 3-2. Characteristics of blend samples

code	$w_{PEA\text{-}(COOH)2}$: w_{PEI} [a]	n_{COOH}: n_{amine} [b]	T_{cross} [c]/ °C	E_a [d]/ (kJ/mol)
AI-8k-0.4	10 : 0.4	1 : 3.9	13	122
AI-8k-0.6	10 : 0.6	1 : 5.8	15	125
AI-8k-0.8	10 : 0.8	1 : 7.7	17	133
AI-8k-1	10 : 1.0	1 : 9.7	21	134
AI-8k-1.2	10 : 1.2	1 : 12	11	128
AI-14k-0.3	10 : 0.3	1 : 4.8	10	110
AI-14k-0.4	10 : 0.4	1: 6.4	14	117
AI-14k-0.5	10 : 0.5	1 : 8.0	18	126
AI-14k-0.6	10 : 0.6	1 : 9.5	19	129
AI-14k-0.7	10 : 0.7	1: 11	17	125
AI-26k-0.1	10 : 0.1	1: 3.0	1	90
AI-26k-0.2	10 : 0.2	1 : 6.0	10	105
AI-26k-0.3	10 : 0.3	1 : 8.9	15	112
AI-26k-0.35	10 : 0.35	1 : 10.4	17	117
AI-26k-0.4	10 : 0.4	1 : 12.0	17	115

[a]Weight ratio of PEA-$(COOH)_2$:PEI. [b] Mole ratio of carboxylic acids on PEA-$(COOH)_2$ to amines on PEI, where n_{amine} includes primary and tertiary amines as well as secondary amine. [c]Temperature at tanδ = 1 (i.e., *G'-G"* crossover), which was determined by the data in Figure 3-4. [d]Flow activation energy estimated from the slope of plots of $\ln a_T$ versus inverse temperature in Figure 3-14. See the blend preparation method in the chapter 2.

Results

Blend experiment. Before investigating the physical properties, various blends at different blend weight ratio were prepared by using PEA-$(COOH)_2$-8k. Figure 3-2a represents the macroscopic appearance of the blend samples, where the blend weight ratio of PEA-$(COOH)_2$-8k : PEI were 10 : 0.5, 0.75, 1, 2, and 3, respectively. Note that these blend samples are different from those summarized in Table 3-2. The viscosity increased with an increase of PEI content, and the transparent sample without fluidity was obtained at 10 : 1. Further increase in PEI content generated the samples with turbidity, suggesting the occurrence of macrophase separation. In contrast, macrophase separation was observed in the blends of PEA (with no functional groups on the chain ends, see Table 2-1) as a control sample and PEI even at small content of PEI (Figure 3-2c) unlike PEA-$(COOH)_2$-8k : PEI = 10 : 1 (Figure 3-2b), meaning that the segregation power between PEA chains and PEI chains is inherently large. This result also indicates that the attractive interaction between carboxylic acids on PEA-$(COOH)_2$ and amines on PEI enables the formation of homogeneous blends.

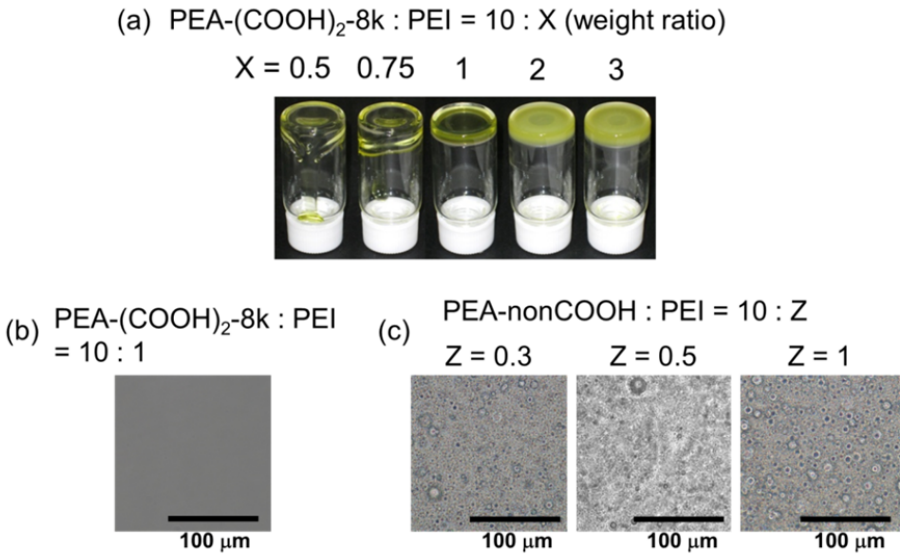

Figure 3-2. (a) Macroscopic appearance of blend samples of PEA-$(COOH)_2$-8k and PEI. Images obtained by optical microscopic observations. (b) PEA-$(COOH)_2$-8k : PEI = 10 : 1. (c) PEA-nonCOOH / PEI blends with

weight ratios of 10 : Z (Z = 0.3, 0.5, 1). The images are displayed in order of the Z value from left to right. Scale bars represent 100 μm in all images. The Optical microscopic observations were performed by using OLYMPUS BX51 (Olympus co.) at room temperature under nitrogen atmosphere. Sample preparation for observations was carried out as follows. First, the blend was dissolved in a mixed solvent of THF / MeOH (5 : 5 by volume). Then, 10 μm of the solution was dropped to a cover glass and the solvent was evaporated under the atomospheric pressure. The solvent wasfurther evaporated by drying *in vacuo* before measurements. See reference #28, Figure S19.

FT-IR measurements. Figure 3-3 compares FT-IR spectra of blends with those of component polymers, i.e., neat PEA-$(COOH)_2$-8k and PEI. An absorption peak originating from carboxylate anions (O=C-O^-) gradually appeared at 1657 cm^{-1} with an increase in Y,[30] while another absorption peak also appeared at 1550 cm^{-1} with an increase in Y, which corresponds to N-H bending vibration of ammonium cations.[30] These absorptions at 1657 cm^{-1} and 1550 cm^{-1} were not observed in neat PEA-$(COOH)_2$-8k and PEI. These results suggest that ionic hydrogen bonds were formed between carboxylic acids and amines by blending PEA-$(COOH)_2$-8k and PEI, which can serve as transient cross-links in forming supramolecular polymer networks. Note that peak intensity of the carboxylate anions reached maximum at around Y = 1, where n_{COOH} : n_{amine} = 1 : 10 (see Table 3-2). In another words, excess amounts of amines to carboxylic acids are required for ionization of the maximum molar amount of the carboxylic acids.

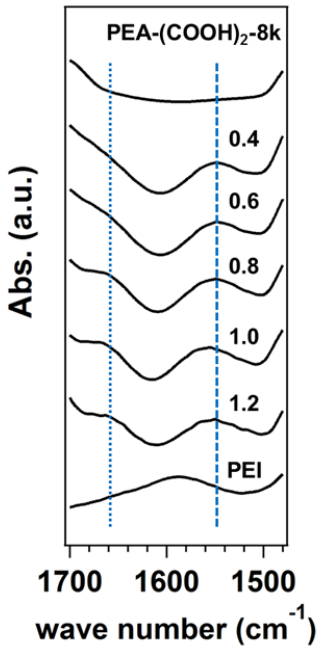

Figure 3-3. FT-IR spectra of neat PEA-$(COOH)_2$-8k, PEI and AI-8k-Y blend series. Values in the spectra represent *Y*. See reference #28, Figure 2.

Dynamic temperature ramp tests. Figures 3-4a through 3-4c express tanδ (= loss modulus *G"* / storage modulus *G'*) spectra obtained by dynamic temperature ramp tests (please also see the raw spectra of *G'* and *G"* as a function of temperature in Figures 3-5 through 3-7). In AI-8k series (Figure 3-4a), the liquid-like state with tanδ ≥ 1 was observed at higher temperatures, while the solid-like (gel-like) state with tanδ ≤ 1 was recognized at lower temperatures. The gradual transition between the liquid-like state and the solid-like one can be attributed to the dissociation or re-association of ionic hydrogen bonded cross-links between carboxylic acids on PEA-$(COOH)_2$ and amines on PEI. In this research, the temperature at tanδ = 1, i.e., *G'* = *G"*, was assigned as T_{cross}, which was used to evaluate the supramolecular network formation.[23,24,26] T_{cross} values for AI-8k series were plotted as a function of *Y* in Figure 3-4d. T_{cross} increased with an increase in *Y* at $Y \leq 1$, whereas it decreased at $Y \geq 1$, indicating that the

maximum T_{cross} was attained at $Y = 1$ in AI-8k series. Tanδ spectra of AI-14k and AI-26k were also represented in Figure 3-4b and 3-4c, where similar behavior to AI-8k-Y was observed. T_{cross} values of AI-14k-Y and AI-26k-Y were plotted against Y in Figure 3-4e and Figure 3-4f, respectively, and they are also summarized in Table 3-2. Note that thermoreversibility was confirmed by repeating the cooling and heating tests for AI-14k-0.6 as shown in Figure 3-8. The increase in T_{cross} toward the maximum with an increase in Y could be attributed to formation of effective cross-linking between PEA-$(COOH)_2$ and PEI,[24] while the decrease in T_{cross} beyond the maximum is probably due to lower cross-linking functionality on PEI molecules, originating from the presence of unused functional groups.[24] Schematic explanation is given in Figure 3-9.

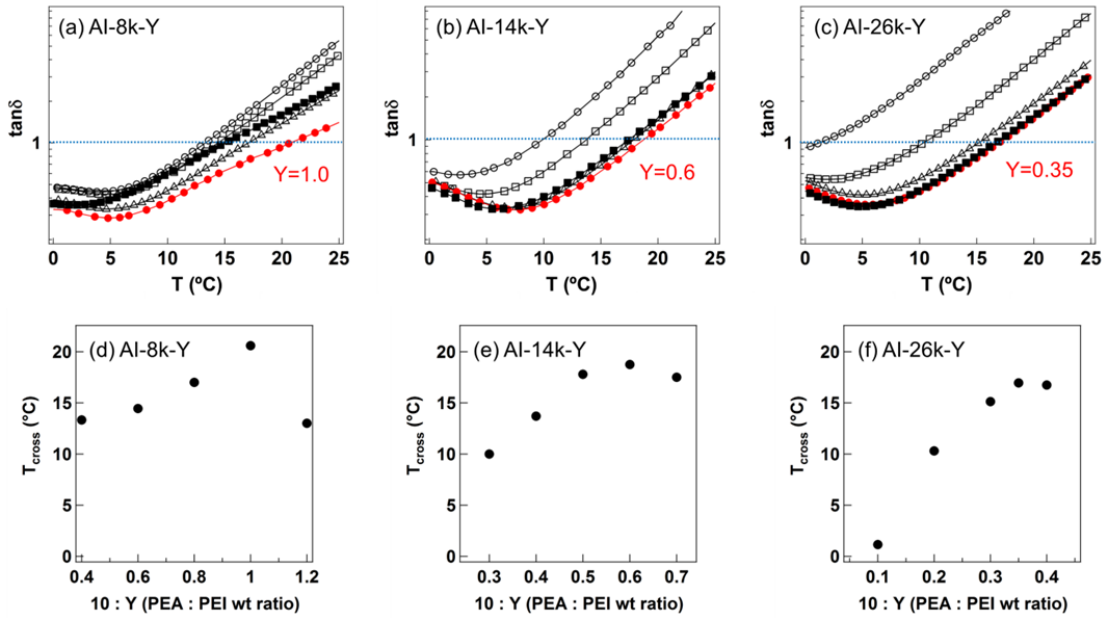

Figure 3-4. Tanδ spectra as a function of temperatures: (a) AI-8k-Y, where Y = 0.4(○), 0.6(□), 0.8(△), 1.0(●), and 1.2(■); (b) AI-14k-Y, where Y = 0.3(○), 0.4(□), 0.5(△), 0.6(●), and 0.7(■); (c) AI-26k-Y, where Y= 0.1(○), 0.2(□), 0.3(△) 0.35(●),and 0.4(■). Curves connecting data points are as guides for eyes, while blue dotted line represent tanδ = 1. T_{cross} of AI-8k-Y, AI-14k-Y, AI-26k-Y are also plotted as a function of Y in (d), (e), and (f), respectively. See reference #28, Figure 3.

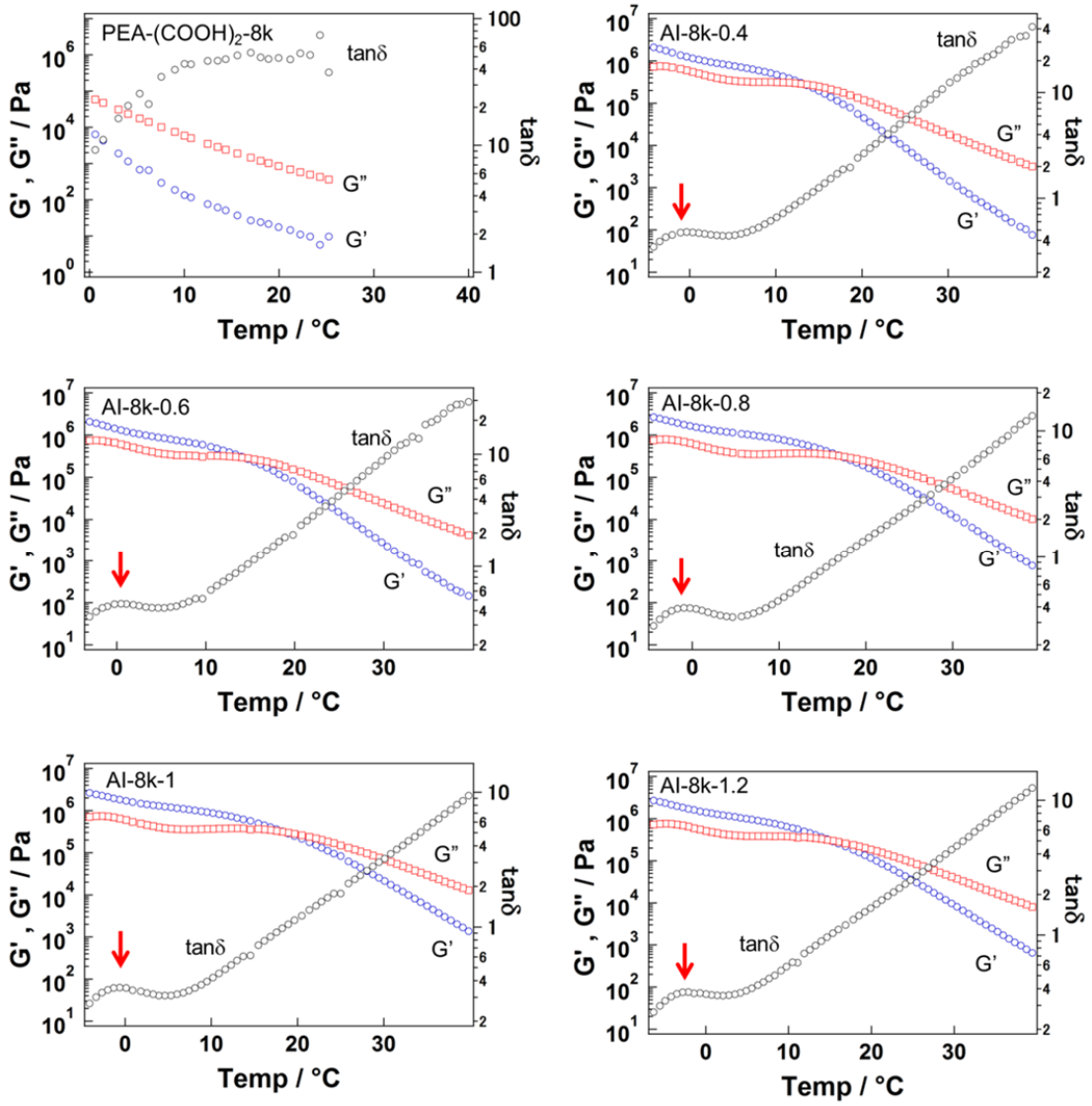

Figure 3-5. Storage moduli (*G'*, ○), loss moduli (*G"*,□), and loss tangent (tanδ, ○) of AI-8k-Yagainst temperatures. Red arrows represent α relaxation of the blends. See reference #28, Figure S8.

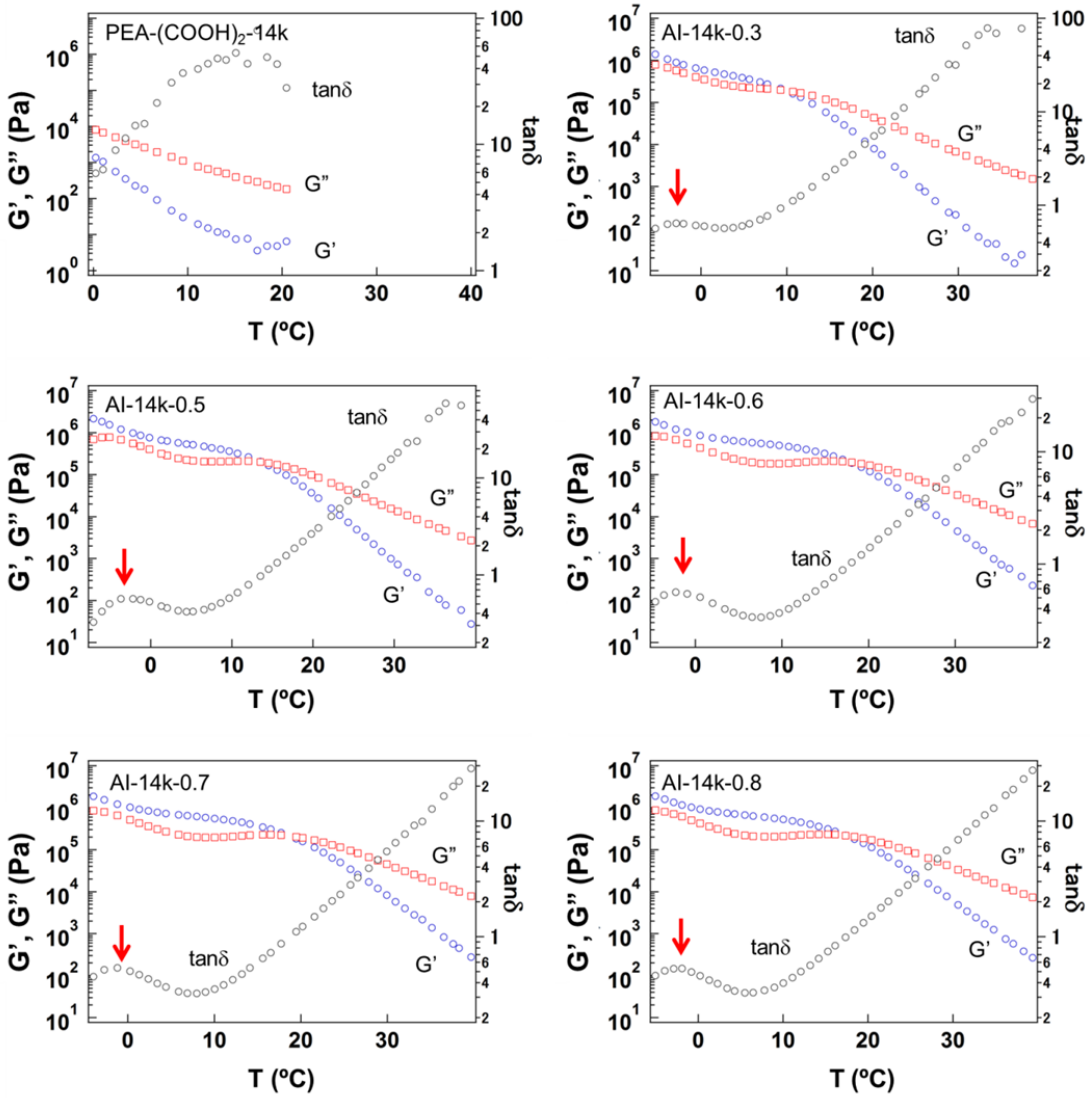

Figure 3-6. Storage moduli (*G'*, ○), loss moduli (*G"*,□), and loss tangent (tanδ, ○) of AI-14k-Yagainst temperatures. Red arrows represent α relaxation of the blends. See reference #28, Figure S9.

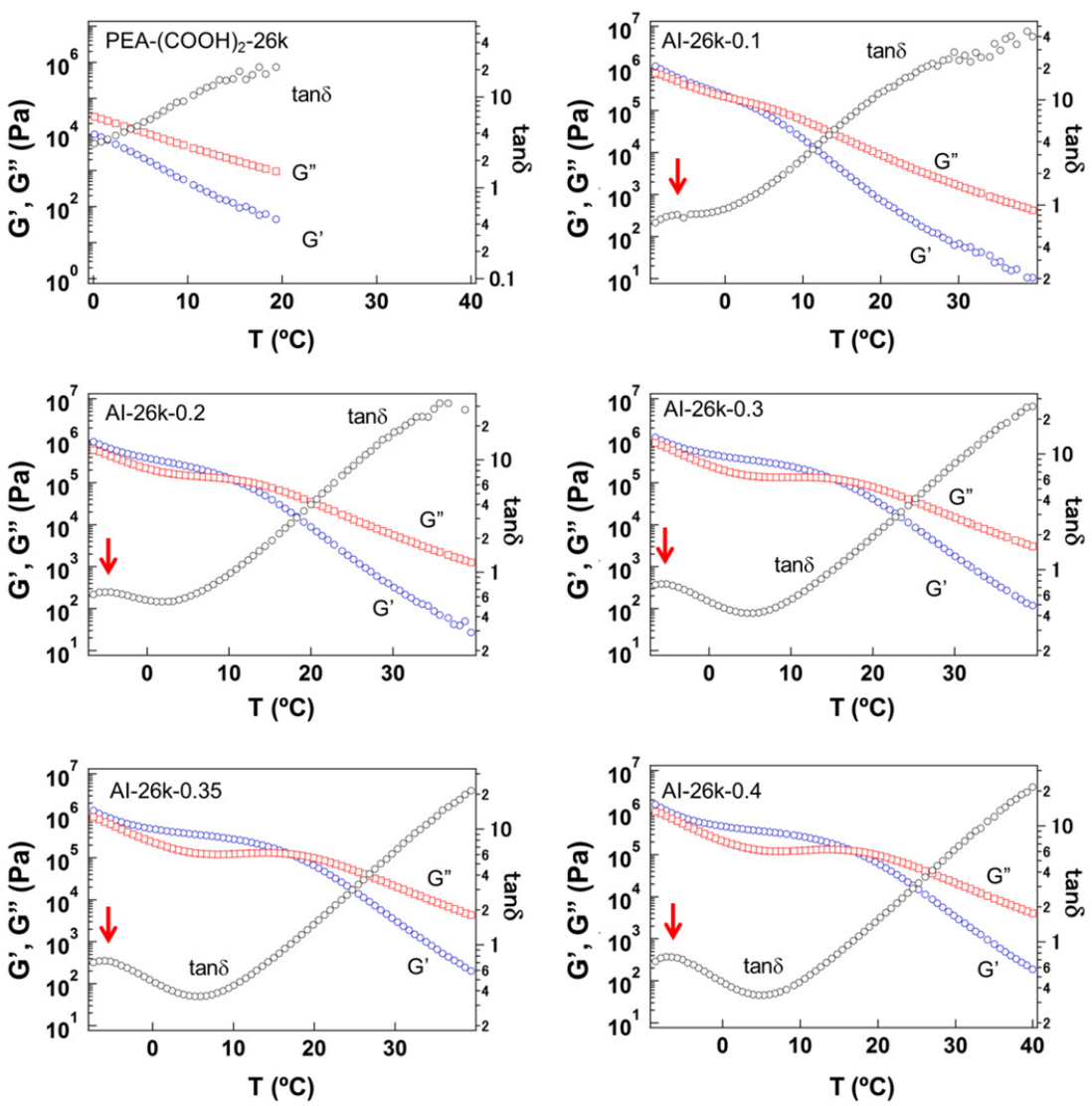

Figure 3-7. Storage moduli (*G'*, ○), loss moduli (*G"*,□), and loss tangent (tanδ, ○) of AI-26k-Yagainst temperatures. Red arrows represent α relaxation of the blends. See reference #28, Figure S10.

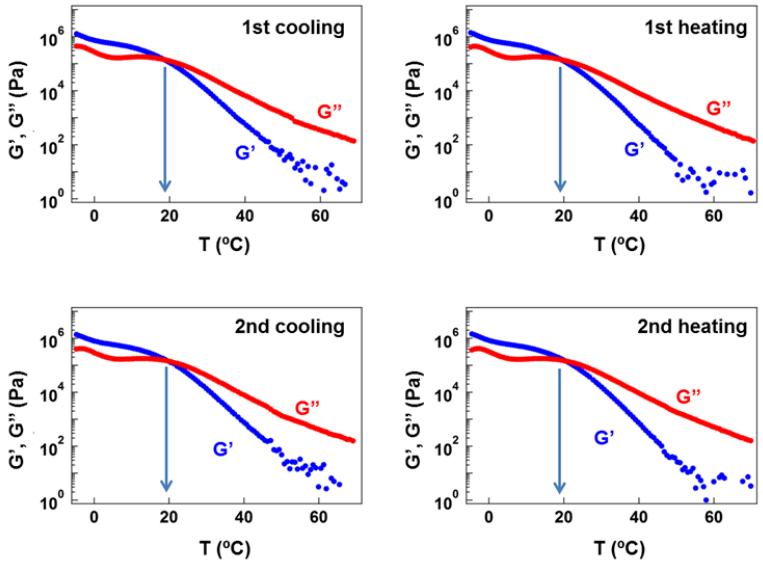

Figure 3-8. Storage modulus (*G'*, blue) and loss modulus (*G"*, red) of AI-14k-0.6 as a function of temperature on 1st cooling, 1st heating, 2nd cooling, and 2nd heating. Arrows represent T_{cross}. See reference #28, Figure S11.

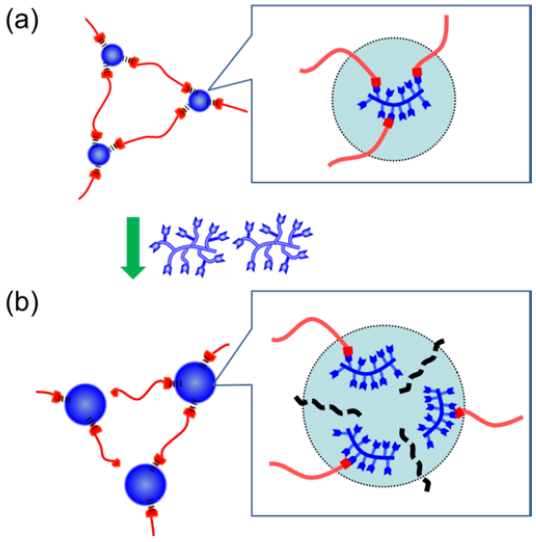

Figure 3-9. Schematic illustrations of a PEI cluster (a) at an optimized ratio (b) beyond the optimized ratio. A red chain, a blue chain, and a blue sphere represent PEA-$(COOH)_2$, PEI, and a PEI cluster, respectively. Dashed lines in the PEI cluster of (b) represent that each PEI chain does not work as an effective cross-linking to connect each network strand. See reference #28, Figure S12.

Dynamic frequency sweep tests. Since non-covalent bonded cross-links of supramolecular networks have finite lifetime, the networks also collapse after dissociation of the non-covalent bonded cross-links under strain. This means that supramolecular materials have time-dependency, and thus they are in viscoelastic liquid states. Note that typical behavior for viscoelastic liquid was observed in creep-recovery tests, where the strain was remaining after removal of applied stress (Figure 3-10). To understand the relaxation behavior depending on time, dynamic frequency sweeps were conducted for all samples at ten degree intervals from 70 °C to 0 °C. The master curves were constructed on the basis of time-temperature superposition (TTS) principle with the reference temperature (T_{ref}) of 0 °C. TTS worked well within the measured temperature range, meaning that the relaxation was governed by the same origin within the temperature range adopted.[27] The master curves of *G'* and *G"* for each blend series were shown in Figure 3-11a to 3-11f, where a_T denotes a shift factor ($a_T = \tau(T) / \tau(T_{ref})$), the ratio of relaxation time (τ) at an arbitrary temperature to that at a reference temperature.

In AI-8k-Y series, the plateau region was extended to lower frequencies with an increase in Y at $Y \leq 1$, while a narrower plateau was observed in $Y = 1.2$ than in $Y = 1$. Since the longest relaxation time (τ_1) should be proportional to the width of plateau region,[31] the above result suggests that τ_1 of supramolecular network depends on the blend ratio, and the maximum τ_1 was attained in $Y = 1$ for AI-8k-Y series. Similarly, the widest plateau was observed in $Y = 0.6$ and $Y = 0.35$ for AI-14k-Y and AI-26k-Y series, respectively, suggesting the maximum τ_1s were attained at these blend ratio.

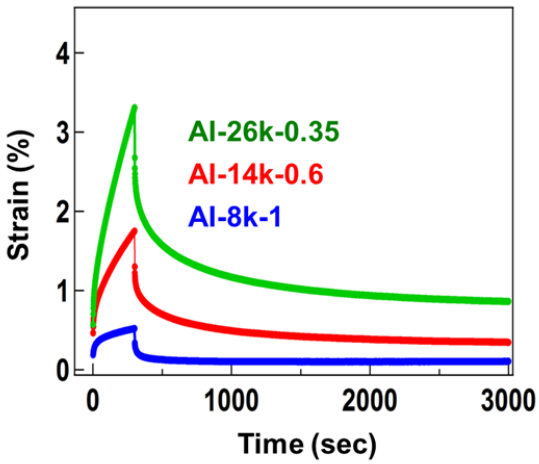

Figure 3-10. Creep-recovery curves for AI-8k-1 (blue), AI-14k-0.6 (blue), and AI-26k-0.35 (green).Creep-recovery behavior was investigated by applying a constant shear stress of 4000 Pa for 300 sec. After removal of the stress, sample recovery was measured for an additional period of 3000 sec. Remaining strain after 3000 sec was 0.11%, 0.35%, and 0.84% for AI-8k-1, AI-14k-0.6, and AI-26k-0.5, respectively. See reference #28, Figure S13.

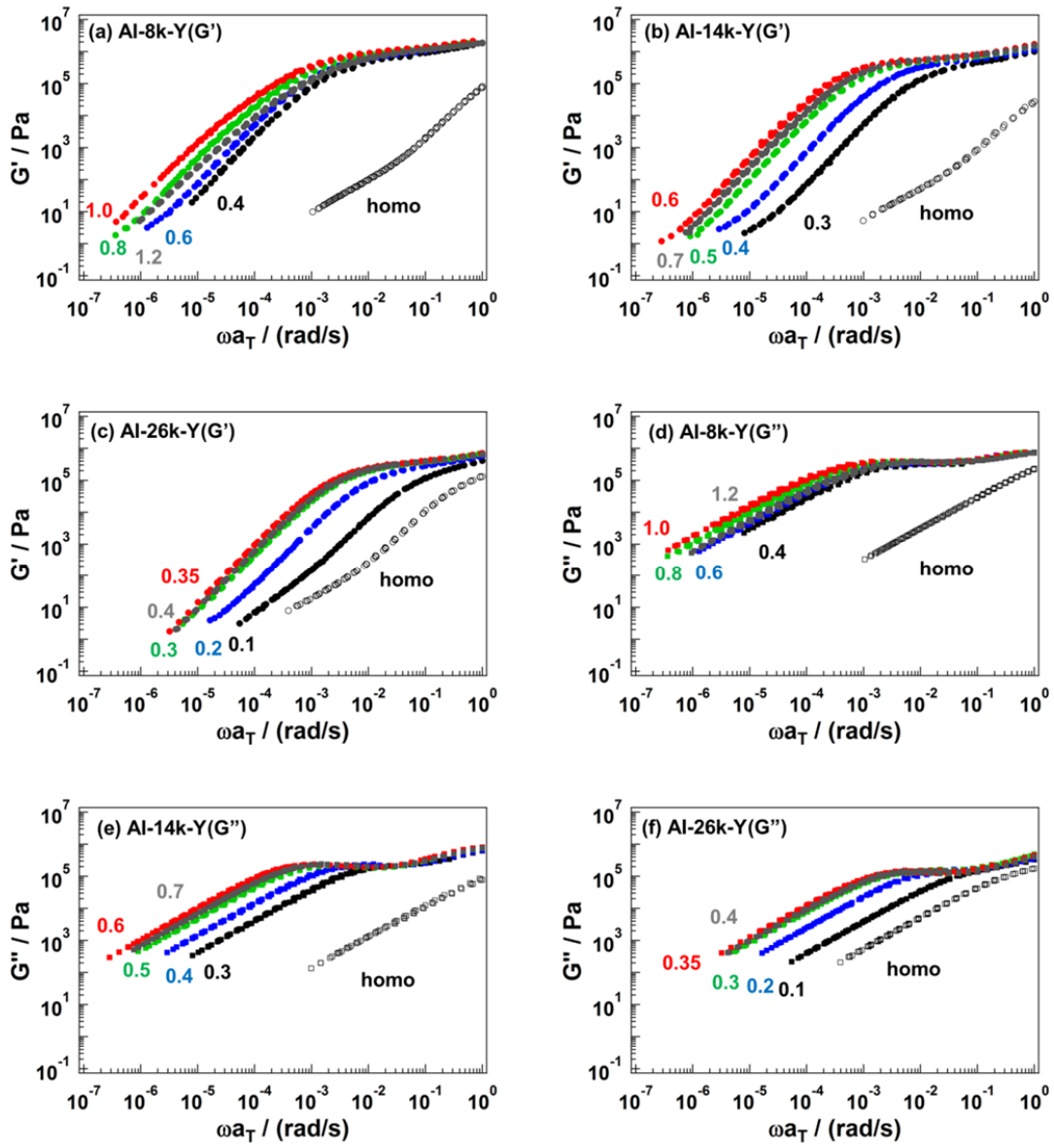

Figure 3-11. *G'* (a to c) and *G"* (d to f) master curves of AI-8k-Y, AI-14k-Y, and AI-26k-Y series with the reference temperature T_{ref} = 0 °C. The numerical values with various colors denote *Y*, corresponding to the data with the same color. See reference #28, Figure 4 and Figure S17.

Zero shear viscosity. It should also be noted that characteristic Newtonian liquid behavior ($G'' \sim \omega$) was observed in the terminal region of the master curves in Figure 3-12. In Figures 3-12a through 3-12c, dynamic shear viscosity (η') against frequencies at a T_{ref} of 0 °C are shown, where η' was calculated from the G'' divided by ωa_T. The η' showed constant value at low frequencies in all samples, and it corresponds to the zero shear viscosity (η_0). The η_0 values were plotted as a function of Y in Figures 3-12d through 3-12f. The maximum η_0 was attained at $Y = 1$ for AI-8k-Y, $Y = 0.6$ for AI-14k-Y, and $Y = 0.35$ for AI-26k-Y, suggesting that the largest aggregates via ionic hydrogen bonding could be formed at these blend ratios.

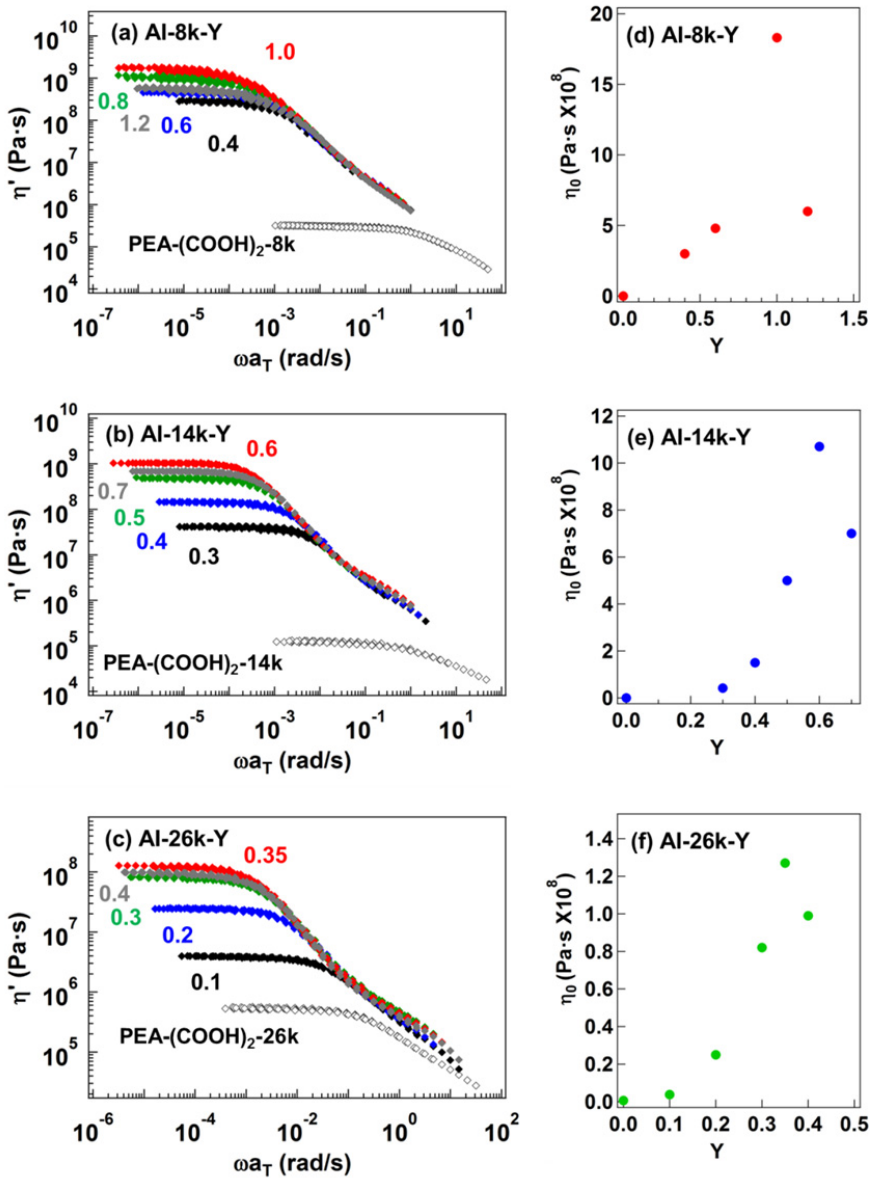

Figure 3-12. Dynamic shear viscosity as a function of ωa_T: (a) AI-8k-Y; (b) AI-14k-Y; (c) AI-26k-Y. The numerical values in graphs denote Y. Estimated zero shear viscosities at 0 °C of AI-8k-Y, AI-14k-Y, AI-26k-Y are also plotted in (d), (e), and (f), respectively, as a function of *Y*. See reference #28, Figure 6.

SAXS measurements. To investigate the self-assembled state at a nanometer scale, SAXS measurements were performed. Figure 3-13 compares the SAXS profiles of neat PEI and three blend series. The vertical axis expresses the intensities with a logarithmic scale, while the horizontal axis does the scattering vector q ($= 4\pi(\sin\theta)/\lambda$), where λ and 2θ denote the wavelength of X-rays and the scattering angle, respectively. There were no definite scattering peaks in the profiles of neat PEI and all three PEA-$(COOH)_2$ homopolymers. In contrast, a broad peak, which must be a correlation hole peak, appeared after blending, and the peak became evident with an increase in *Y*. An appearance of the peak could be attributed to the electron density fluctuation between PEA-$(COOH)_2$ and PEI with the length scale of several nanometers, and these self-assembled manners might be correlated with the formation of supramolecular polymer networks. Blend experiments at earlier stage already revealed that PEA chains and PEI chains reveal originally strong segregation (see Figure 3-2), and hence PEI could form self-assembled cross-linked clusters in the networks due to the strong segregation against PEA chains. Note that the q value at the peak top (q^*) was shifted to a lower q region with an increase in *Y* in the SAXS profile of each blend series. This is suggesting an increase in the correlation length of the electron fluctuation, which is probably because the cross-linked clusters of PEI were expanded gradually by incorporating the PEI added (schematic explanation is shown in Figure 3-9).

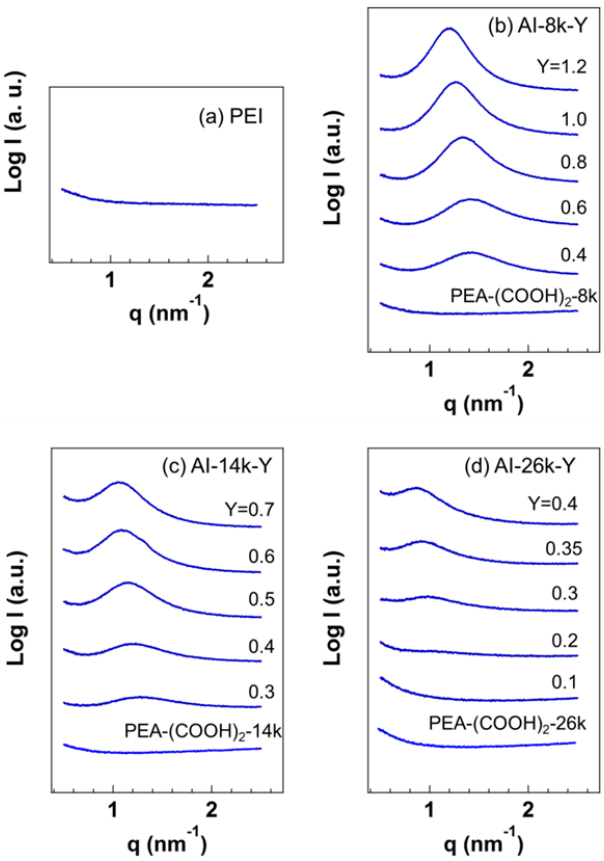

Figure 3-13. Scattering profiles of (a) PEI, (b) AI-8k-Y, (c) AI-14k-Y, and (d) AI-26k-Y obtained by SAXS measurements at 10 °C. See reference #28, Figure 7 and Figure S18.

Discussion

Stoichiometric Balance of Functional Groups on Formation of Optimized Supramolecular Networks. In the previous section concerning the dynamic temperature ramp tests, it was found that T_{cross} revealed the blend ratio dependence (Figure 3-4). The reversible transition between solid state and liquid one across T_{cross} can be correlated with the dissociation and re-association of ionic hydrogen bonded cross-links, which must be a thermally activated process. In addition, the flow activation energy (E_a) could be used as an indicator to assess stableness of supramolecular networks since the E_a represents the energy required for their relaxation, which is induced by the disassembly of the cross-links. The E_a can be estimated from a_T for constructing

master curves. It is known that the relation follow the Arrehenius-type equation as shown in eq (3-1) at a sufficiently higher temperature region than T_g of the component,[32,33]

$$a_T \approx \exp\left(\frac{E_a}{RT}\right) \qquad (3\text{-}1)$$

, where E_a, R, and T denote a flow activation energy, a gas constant, and an absolute temperature, respectively. Note that T_gs of samples were estimated on the basis of α relaxations observed in their tanδ spectra, which were all lower than 0 °C (see Figure 3-5 to 3-7). Then, E_as were evaluated from the slopes of the plots at a significantly higher temperature range than the T_gs of all samples, i.e., 40 °C ≤ T ≤ 70 °C (Figure 3-14). The E_a values obtained are summarized in Table 3-2, and they are also plotted as a function of Y for each blend series in Figure 3-15. The highest E_a was attained at Y = 1 for AI-8k-Y, Y = 0.6 for AI-14k-Y, and Y = 0.35 for AI-26k-Y, respectively, where the most stable supramolecular networks must be formed.

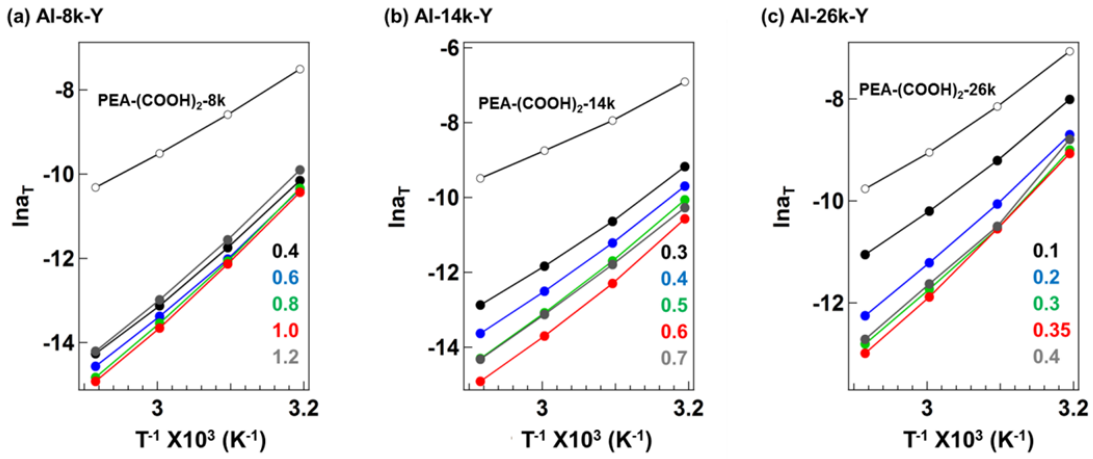

Figure 3-14. lna_T versus inverse temperature between 70 °C and 40 °C to estimate the flow activation energy E_a: (a) AI-8k-Y; (b) AI-14k-Y; (c) AI-26Y. The numerical values in graphs denote Y. See reference #28, Figure S20.

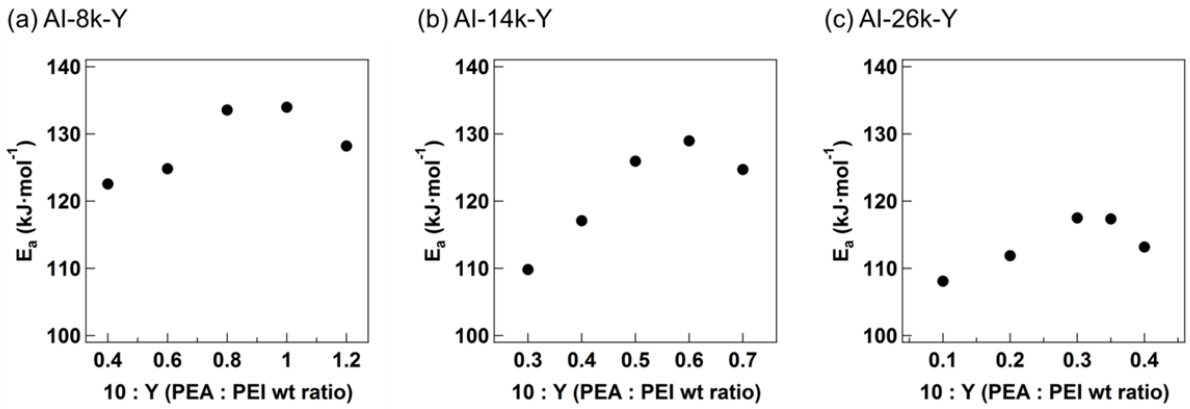

Figure 3-15. Flow Activation energy E_a of blends as a function of the blend weight ratio: (a) AI-8k-Y series; (b) AI-14k-Y series; (c) AI-26k-Y series. See reference #28, Figure 8.

To discuss the optimization of supramolecular network formation more deeply in terms of stoichiometry of functional groups, T_{cross} and E_a were plotted against mole ratio of amines on PEI to carboxylic acids on PEA-$(COOH)_2$ (amine / COOH) in the same figure (Figure 3-16). T_{cross} and E_a were changed depending on amine / COOH in the similar manner, however it is important to stress here that the maximum T_{cross} and E_a were attained at a certain amine / COOH (~ 10), irrelevant to molecular weight of PEA-$(COOH)_2$ (M_{PEA}). This result suggests that a key factor to optimize supramolecular networks is stoichiometric balance of functional groups for supramolecular cross-linking. Note that the best network was attained at high excess amount of amines. One probable reason is the steric hinderance; it was assumed that clusters formed by self-assembly of PEI serve as cross-linkers within the network in the previous section, where only a part of amines near the surface of clusters can be associated with the carboxylic acids. In the other words, the amines locating at the inner part of the clusters cannot form ionic hydrogen bonding with carboxylic acids on PEA-$(COOH)_2$. This might be the reason for the requirement of excessive molar amount of amine to form the optimized supramolecular networks.

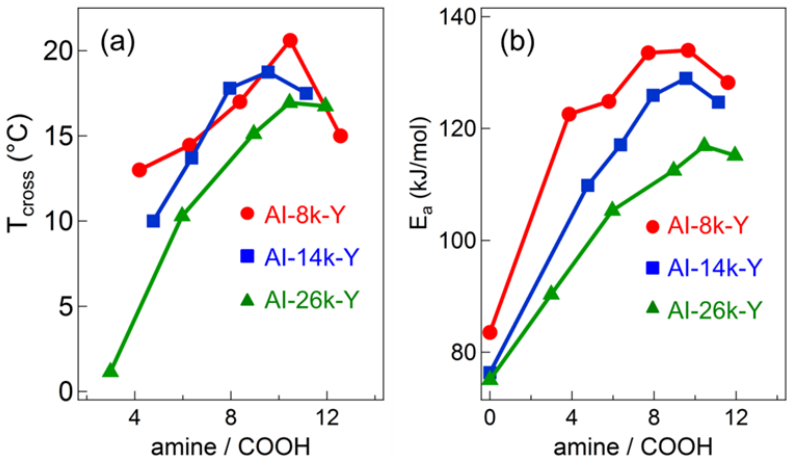

Figure 3-16. Plots of (a) T_{cross} and (b) E_a as a function of the mole ratio of the amine to the carboxylic acid (amine / COOH). Red circles, blue squares, and green triangles represent AI-8k-Y, AI-14k-Y, and AI-26k-Y, respectively. See reference #28, Figure 9.

Effects of the Molecular Weight of PEA-(COOH)$_2$ on Modulus of the Supramolecular Soft Materials at the Optimized Blend Ratio According to the classical rubber theory of affine network model, the plateau modulus (G_X) is known to be inverse proportional to the molecular weight between cross-links (M_x), as shown in eq (3-2).[34,35]

$$G_X = \frac{\rho RT}{M_X} \sim \frac{1}{M_x} \quad (3\text{-}2)$$

In the present molecular design, M_x could be dependent on M_{PEA} since PEA-(COOH)$_2$ serves as a network strand owing to the telechelic-type chemical structure. The G_X values obtained by dynamic temperature ramp tests were 1.2 MPa for AI-8k-1.0, 0.64 MPa for AI-14k-0.6, and 0.36 MPa for AI-26k-0.35, respectively, where they were estimated at the temperature with the minimal tanδ value in the plateau region. The G_X values are plotted against inverse M_{PEA} in Figure 3-17a, where the simple proportionality, i.e., $G_X \propto 1/M_{PEA}$, was observed. This result indicates that the length of network strands was systematically changed depending on M_{PEA}, which could be attributed to the relatively homogeneous network formation

induced by ionic hydrogen bonding between the functional groups.

In addition, G_X can also be related with the average mesh size (ξ_x) as shown in eq (2-3).[36,37]

$$G_X \sim \frac{1}{\xi_x^3} \quad (2\text{-}3)$$

The correlation length ξ, which is actually associated with ξ_x in the present system, can be estimated from q^* value, at which SAXS profiles give peak top ($\xi = 2\pi / q^*$).[38] The estimated ξ were 5.0 nm for AI-8k-1.0, 5.8 nm for AI-14k-0.6, and 6.9 nm for AI-26k-0.35, respectively, indicating that ξ increases with an increase in M_{PEA}, and this result is quite reasonable if the radius of gyration R_g of PEA molecules ($R_g \sim n^{1/2} \sim M^{1/2}$) is talking into account. G_Xs were plotted against inverse ξ^3, where the proportionality was also attained (Figure 3-17b), meaning that the mesh size in the present supramolecular network was mainly controlled by M_{PEA}. This analysis on the $G_X - M_{PEA}$ relationship suggests that the stiffness can be tuned by the molecular weight of telechelic-type network strands, indicating the strong advantage of the use of supramolecular associations in creating materials with relatively homogeneous networks.

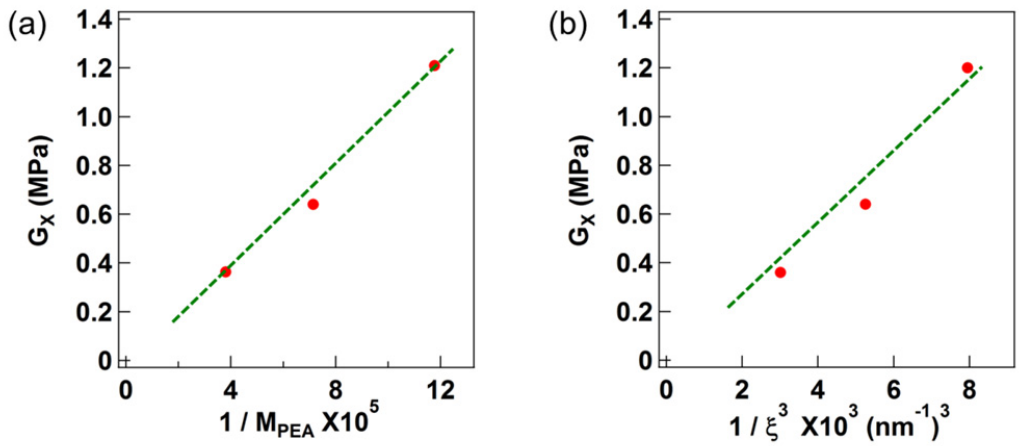

Figure 3-17. Plateau modulus G_X at the optimized blend ratioas a function of (a) $1/M_{PEA}$ and (b) $1/\xi^3$. Green dashed lines are drawn for a guide of eyes. See reference #28, Figure 10.

Chapter Summary

In this chapter, supramolecular soft materials were prepared by blending carboxy-terminated telechelic PEA-$(COOH)_2$ and PEI with multiple amines. Three kinds of PEA-$(COOH)_2$ having different molecular weights were synthesized and blended with PEI at various blend ratios to investigate the effects of the molecular weight and the blend ratio on the physical properties. It was confirmed by FT-IR measurements that ionic hydrogen bonds were formed between carboxylic acids on PEA-$(COOH)_2$ and amines on PEI. According to dynamic temperature ramp tests, reversible solid – liquid transition was observed, where T_{cross} at which $G' = G''$ was varied depending on the blend ratio. In addition, the flow activation energy E_a was also estimated assuming Arrhenius-type relational expression; $\ln a_T \propto \frac{E_a}{RT}$. The plots of T_{cross} and E_a against amine / COOH revealed that the highest T_{cross} and E_a were attained at amine / COOH ratio of around 10, irrelevant to M_{PEA}. These results indicate that stoichiometry between the functional groups must be a key factor to optimize supramolecular networks. At the optimized blend ratio, G_X was found to be inversely proportional to M_{PEA} due to the systematic change of average mesh size depending on M_{PEA}, suggesting the formation of relatively homogeneous supramolecular network.

References

[1] Sakai, T.; Matsunaga, T.; Yamamoto, Y.; Ito, C.; Yoshida, R.; Suzuki, S.; Sasaki, N.; Shibayama, M.; Chung, U.-i. *Macromolecules* **2008,** 41, 5379-5384.

[2] Okumura, Y.; Ito, K. *Adv. Mater.* **2001,** 13, 485-487.

[3] Gong, J. P.; Katsuyama, Y.; Kurokawa, T.; Osada, Y. *Adv. Mater.* **2003,** 15, 1155-1158.

[4] Flory, P. J. *J. Am. Chem. Soc.* **1941,** 63, 3083-3090.

[5] Hirschberg, J.; Beijer, F. H.; van Aert, H. A.; Magusin, P.; Sijbesma, R. P.; Meijer, E. W. *Macromolecules* **1999,** 32, 2696-2705.

[6] Burnworth, M.; Tang, L.; Kumpfer, J. R.; Duncan, A. J.; Beyer, F. L.; Fiore, G. L.; Rowan, S. J.; Weder, C. *Nature* **2011,** 472, 334-337.

[7] Weng, W.; Li, Z.; Jamieson, A. M.; Rowan, S. J. *Soft Matter* **2009,** 5, 4647-4657.

[8] Dong, S.; Luo, Y.; Yan, X.; Zheng, B.; Ding, X.; Yu, Y.; Ma, Z.; Zhao, Q.; Huang, F. *Angew. Chem., Int. Ed.* **2011,** 50, 1905-1909.

[9] Suzuki, T.; Shinkai, S.; Sada, K. *Adv. Mater.* **2006,** 18, 1043-1046.

[10] Yan, X.; Xu, D.; Chen, J.; Zhang, M.; Hu, B.; Yu, Y.; Huang, F. *Polym. Chem.* **2013,** 4, 3312-3322.

[11] Rossow, T.; Seiffert, S. *Polym. Chem.* **2014,** 5, 3018-3029.

[12] P. Cordier, F. Tournilhac, C. Soulie-Ziakovic and L. Leibler, *Nature* 2008, **451**, 977-980.

[13] Chino, K.; Ashiura, M. *Macromolecules* **2001,** 34, 9201-9204.

[14] Woodward, P. J.; Merino, D. H.; Greenland, B. W.; Hamley, I. W.; Light, Z.; Slark, A. T.; Hayes, W. *Macromolecules* **2010,** 43, 2512-2517.

[15] Yount, W. C.; Loveless, D. M.; Craig, S. L. *J. Am. Chem. Soc.* **2005,** 127, 14488-14496.

[16] Weng, W.; Beck, J. B.; Jamieson, A. M.; Rowan, S. J. *J. Am. Chem. Soc.* **2006,** 128, 11663-11672.

[17] Wojtecki, R. J.; Meador, M. A.; Rowan, S. J. *Nature Mater*. **2011**, 10, 14-27.

[18] Nair, K. P.; Breedveld, V.; Weck, M. *Macromolecules* **2011,** 44, 3346-3357.

[19] Ge, Z. S.; Hu, J. M.; Huang, F. H.; Liu, S. Y. *Angew. Chem., Int. Ed.* **2009,** 48, 1798-1802.

[20] Lewis, C. L.; Stewart, K.; Anthamatten, M. *Macromolecules* **2014,** 47, 729-740.

[21] Xu, D.; Craig, S. L. *Macromolecules* **2011,** 44, 5465-5472.

[22] Ali Aboudzadeh, M.; Eugenia Munoz, M.; Santamaria, A.; Jose Fernandez-Berridi, M.; Irusta, L.; Mecerreyes, D. *Macromolecules* **2012,** 45, 7599-7606.

[23] Noro, A.; Matsushita, Y.; Lodge, T. P. *Macromolecules* **2008**,41, 5839-5844.

[24] Noro, A.; Matsushita, Y.; Lodge, T. P. *Macromolecules* **2009**,42, 5802-5810.

[25] Matsushima, S.; Hayashi, M.; Yamagishi, H.; Noro, A.; Matsushita, Y. *Nihon Reoloji Gakk.* **2014**, 42, 135-141.

[26] Noro, A.; Matsushima, S.; He, X.; Hayashi, M.; Matsushita, Y. *Macromolecules* **2013**, 46, 8304-8310.

[27] Feldman, K. E.; Kade, M. J.; Meijer, E. W.; Hawker, C. J.; Kramer, E. J. *Macromolecules* **2009,** 42, 9072-9081.

[28] Hayashi, M.; Noro, A.; Matsushita, Y. *J. Polym. Sci., Part B: Polym. Phys.* **2014**, 52, 755-764.

[29] Noro, A. ; Hayashi, M.; Ohshika, A.; Matsushita, Y. *Soft Matter* **2011**, 7, 1167-1670

[30] Noro, A.; Ishihara, K.; Matsushita, Y. *Macromolecules* **2011,** 44, 6241-6244.

[31] Onogi, S.; Masuda, T.;Madua, T.; Kitagawa.K. *Macromolecules* **1970**, 3, 109-116.

[32] Li, J.; Lewis, C. L.; Chen, D. L.; Anthamatten, M. *Macromolecules* **2011,** 44, 5336-5343.

[33] Schneider, A. H.; Cantow, J. H.; Brekner, J. M. *Polym. Bull.* **1984**, 11, 383-390.

[34] Kuhn, W. *Kolloid-Zeitschrift* **1936,** 76, 258-271.

[35] Haraguchi, K.; Takehisa, T.; Fan, S. *Macromolecules* **2002,** 35, 10162-10171.

[36] van de Manakker, F.; Vermonden, T.; el Morabit, N.; van Nostrum, C. F.; Hennink, W. E. *Langmuir* **2008,** 24, 12559-12567.

[37] Zhang, Y.; Yang, Z. M.; Yuan, F.; Gu, H. W.; Gao, P.; Xu, B. *J. Am. Chem. Soc.* **2004,** 126, 15028-15029.

[38] Cortese, J.; Soulie-Ziakovic, C.; Cloitre, M.; Tence-Girault, S.; Leibler, L. *J. Am. Chem. Soc.* **2011,** 133, 19672-19675.

Chapter 4

Preparation and Mechanical Property Enhancement of ABA-triblock Copolymer-based Elastomers by Incorporating Transient Cross-links into the Soft Middle Block

Abstract: In this chapter, a new strategy was proposed to enhance mechanical properties of ABA triblock copolymer-based elastomers by incorporating hydrogen bonds into the soft middle block. An ABA triblock-type copolymer, poly(4-vinylpyridine)-*b*-[(poly(butyl acrylate)-*co*-polyacrylamide]-*b*-poly(4-vinylpyridine) (P-Ba-P), was designed and synthesized via RAFT polymerization. In this molecular design, the glassy poly(4-vinylpyridine) end blocks form pseudo cross-link domains due to segregation and phase separation from the soft middle block, whereas self-complementary hydrogen bonds must be formed between acrylamide units on the soft middle block, serving as transient and weak cross-links. According to tensile tests, the Young's modulus, elongation at break, maximum stress, and toughness were 1.9 MPa, 200%, 2.6 MPa, and 2.8 MJ/m^3, respectively, and all values obtained were significantly larger than a control sample, poly(4-vinylpyridine)-*b*-(poly(butyl acrylate)-*b*-poly(4-vinylpyridine) (P-B-P). Among them, it should be stressed on the fact that the toughness of P-Ba-P (2.8 MJ/m^3) was approximately 140 times larger than that of P-B-P (0.02 MJ/m^3). The enhancement in mechanical properties in P-Ba-P is attributed to the dynamic nature of hydrogen bonds between acrylamide groups on the middle block, which works to prevent local stress concentration in the network during elongation.

Introduction Elastomers are representative soft materials, showing unique mechanical properties,[1-3] such as stretchability and damping property, which are attributed to the 3D network structures composed of cross-linked polymers. In conventional elastomers, such as rubbers, the cross-linkings are realized via covalent bonds with semi-permanent life time.[4,5] Thus, in general, elastomers present difficulty in material processing and lack of recyclability.

To overcome these problems, thermoplastic elastomers (TPEs) have been widely used in our daily lives.[6-8] In typical TPEs, ABA-type block copolymers, such as polystyrene-*b*-polybutadiene-*b*-polystyrene (SBS) and polystyrene-*b*-polyisoprene-*b*-polystyrene (SIS),[9-11] are used as the components, where a glassy polymer with a T_g higher than room temperature and a melt polymer with a T_g lower than room temperature are adopted as the A and B blocks, respectively. Since TPEs can melt at higher temperatures than T_g of the glassy A end block, there are several advantages in good processability or recyclability unlike conventional elastomers which contain cross-linking via covalent bonds. Moreover, as for TPEs from block copolymers, the glassy A block are segregated from the B middle block, resulting in forming pseudo cross-link domains, where the B block serve as matrix strand bridging the A block domains in the network.

Recently, studies on soft materials including ABA triblock copolymers have been paid attention, mainly because the bridge-type conformation of B chains can directly enhance the macroscopic physical properties of the materials.[12-14] Although there are a lot of efforts on the physical property control of soft materials by decorating or modifying A end blocks,[15-18] there are few reports attaining mechanical property control by modifying the soft B middle block instead. If transient and weak cross-links are incorporated into the soft middle blocks without losing the softness, such cross-links would improve the stiffness due to an increase in the cross-link density. Furthermore, the transient cross-links can be repeatedly dissociated and re-associated during

application of stress, which can prevent local stress concentration in the network. In another words, incorporating transient cross-links[19] into the soft middle block is expected to enhance the mechanical properties of elastomers.

In this chapter, a new molecular design was proposed to eanhnce mechanical properties of an ABA triblock copolymer by incorporating transient cross-links into the soft B middle block.[20] An ABA triblock copolymer with a random sequence in the B middle block, that is, poly(4-vinylpyridine)-*b*-[poly(butyl acrylate)-*co*-polyacrylamide]-*b*-poly(4-vinylpyridine) (P-Ba-P, Figure 4-1), was designed and synthesized via reversible addition-fragmentation chain transfer (RAFT) polymerization. Poly(4-vinylpyridine) end blocks with a T_g higher than room temperature (> 100 °C) forms pseudo cross-link domains due to the segregation and phase separation from the soft middle block. According to this design, the middle block with a low T_g can serve as strands in the network, where self-complementary hydrogen bonds between the acrylamide units[21,22] behave as transient cross-links. For control experiments, a random copolymer, poly(butyl acrylate)-*co*-polyacrylamide (Ba), and another triblock copolymer, poly(4-vinylpyridine)-*b*-poly(butyl acrylate)-*b*-poly(4-vinylpyridine) (P-B-P), were also prepared. Physical properties of these materials were investigated by dynamic mechanical measurements and tensile tests together with morphological investigations.

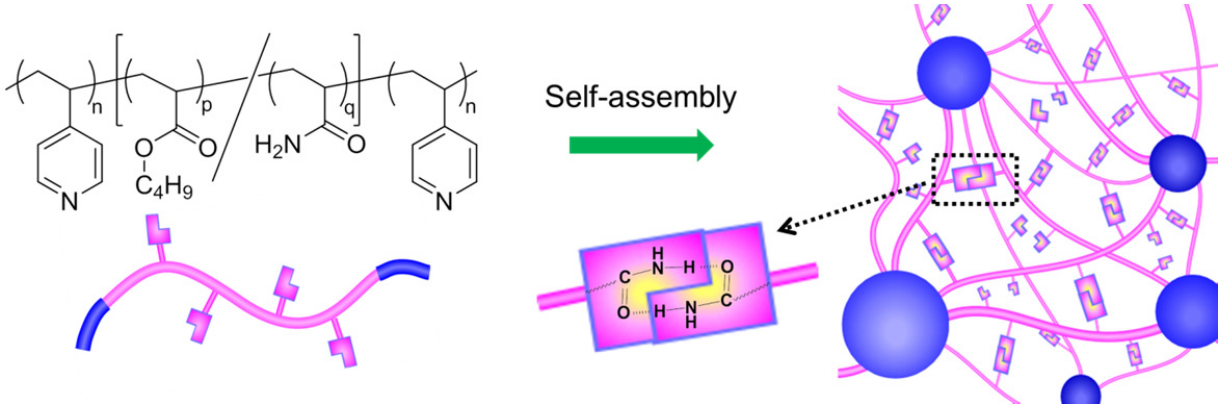

Figure 4-1. Simplified chemical structure of P-Ba-P (left top) and schematic illustration of P-Ba-P chain (left bottom) and network structure. The P block assemblies are illustrated as blue spheres in the schematic representation of the network structure (right), where the Ba middle block and acrylamide units are drawn as pink lines and pink "L-type" blocks, respectively. See reference #20, Figure 1.

Characteristics and their codes of polymers synthesized.

Table 4-1. Molecular characteristics of polymers

Sample code	N_P[a]	N_B[a]	N_a[a]	f_a[b]	M_{middle}[c]	M_{total}[c]	PDI[d]	T_g/°C
B	-	194	-	-	-	25,000	1.05	-50[e]
Ba	-	195	30	0.13	-	27,000	1.10	-26[e]
P-B-P	48	196	-		25,000	30,000	1.22	-45[e], 115[f]
P-Ba-P	48	178	30	0.15	25,000	30,000	1.17	-23[e], 106[f]

[a]Average number of monomeric units of 4-vinylpyridine (N_P), butyl acrylate (N_B), and acrylamide (N_a) in a polymer chain determined by ^{1}H-NMR. [b]Mole fraction of acrylamide units in a random copolymer chain, which was calculated from $N_a/(N_B+N_a)$. [c]Number average molecular weight of the middle block (M_{middle}) and the triblock copolymer (M_{total}), which was calculated from the number of monomeric units and the mass of each monomeric unit. [d]Polydispersity indices measured by SEC. [e]Glass transition temperatures determined by DSC. [f]Glass transition temperatures determined by rheological measurements.

RESULTS

Sample appearance. Figure 4-2 presents appearances of the samples. B and Ba were viscous materials at room temperature,[23] while P-B-P and P-Ba-P were self-standing and elastic ones, where the yellow color of samples originates from the RAFT agent residue in the polymers. These results are clearly showing that glassy end blocks play an important role to generate elasticity of these materials.

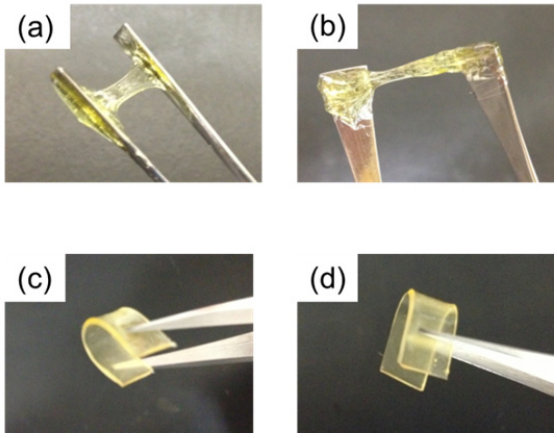

Figure 4-2. Photos of macroscopic appearance of (a) B, (b) Ba, (c) P-B-P, and (d) P-Ba-P. See reference #20, Figure 2.

Molecular characterization of polymers. Firstly, FT-IR measurements were performed to confirm the hydrogen bonds between acrylamide units (Figure 4-3a). In the spectra of Ba and P-Ba-P at the wavenumber range from 3300 cm^{-1} to 3600 cm^{-1}, two absorption peaks were observed at 3350 cm^{-1} (dashed line) and at 3450 cm^{-1} (dotted line), and these were assigned to hydrogen bonded N-H and free N-H stretching vibration modes, respectively.[24,25] Therefore, it was found that not all but a part of acrylamide units were in the associated state. In addition, the interaction between P block and acrylamide was evaluated by the spectra at the wave number region around 1000 cm^{-1} (Figure 4-3b). According to the literature,[26,27] the absorption associated with hydrogen bonded pyridine rings should appear at approximately 1005 cm^{-1}, however, there

are no distinctive peaks at this wave number, and only an absorption peak for free pyridine rings was observed at 993 cm^{-1} instead. These facts indicate that hydrogen bonds were not formed between P and acrylamide.

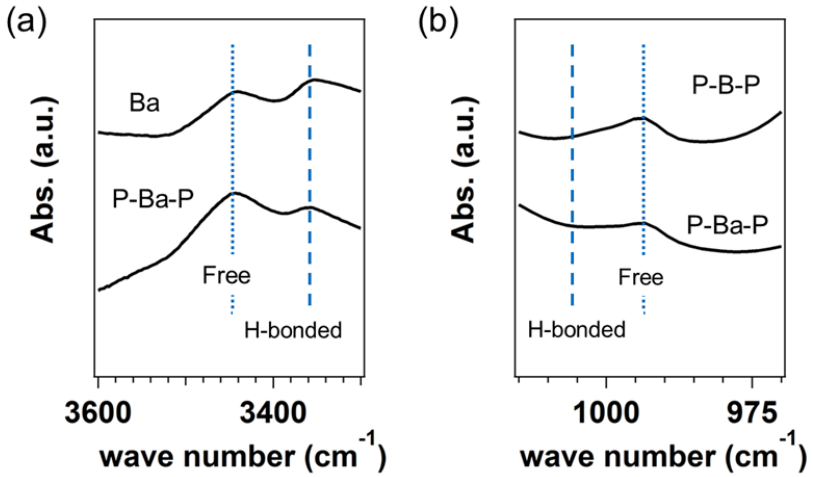

Figure 4-3. (a) FT-IR spectra of Ba and P-Ba-P within a wave number range from 3300 to 3600 cm^{-1}, where a dashed line at 3350 cm^{-1} and a dotted line at 3450 cm^{-1} correspond to the absorption bands of hydrogen bonded N-H and free N-H stretching vibration modes, respectively. (b) FT-IR spectra of P-B-P and P-Ba-P within a wave number range from 970 to 1010 cm^{-1}, where a dotted and a dashed line represent the wave numbers corresponding to the absorption bands of free and hydrogen bonded pyridine rings, respectively. See reference #20, Figure 3.

DSC measurements were conducted to investigate the T_g of the polymers, and the DSC thermograms are shown in Figure 4-4a. One endothermic peak each was observed in the thermograms of B and Ba at -50 °C and -26 °C, respectively, which can be assigned to their T_gs. The T_g of Ba was significantly higher than that of B, which is due to the incorporation of acrylamide units. Similarly, one endothermic peak each was also observed in the thermograms at -45 °C for P-B-P and at -23 °C for P-Ba-P, which were assigned to their T_gs. Since the observed T_gs in P-B-P and P-Ba-P were close enough to the T_gs of B and Ba, respectively, the T_gs observed

in P-B-P and P-Ba-P thermograms are attributed to the segmental motion of each middle block. The T_g values are summarized in Table 4-1. On the other hand, the T_gs of P blocks were observed neither in P-B-P nor P-Ba-P. This is probably because the fraction of P end block (~ 10%) in each chain is too small to detect endothermic heat from glass transition of P.[26] Therefore, the T_g of P block was estimated using α relaxation observed in the tanδ spectrum of dynamic temperature ramp tests. In the tanδ spectra of P-B-P and P-Ba-P (Figure 4-4b), two α relaxations were evidently observed in both P-B-P and P-Ba-P, where α relaxations at lower and higher temperatures are conceived to be originated from segmental motion of each middle block and P end block, respectively; thus, the higher temperatures at around 100 °C were assigned to the T_g of P block (Table 4-1).

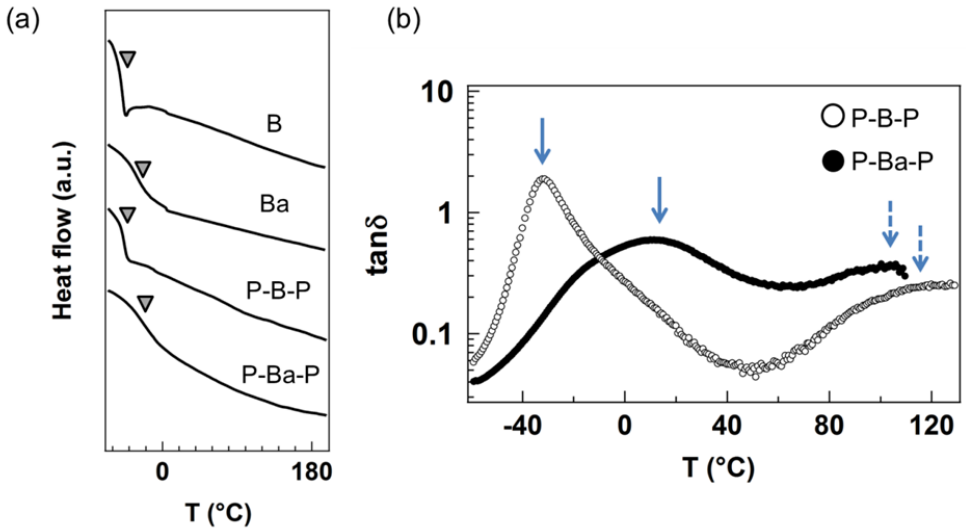

Figure 4-4. (a) DSC thermograms for the polymers, where the arrows indicate T_gs. (b) Tanδ spectra obtained by dynamic temperature ramp tests for P-B-P (open symbols) and P-Ba-P (filled symbols), where the solid and dashed arrows indicate α relaxations originating from each middle block and P end block, respectively. See reference #20, Figure 3 and Figure S10.

Figure 4-5a compares the scattering profiles obtained by SAXS measurements. The vertical axis represents the intensities with a logarithmic scale, while the horizontal axis is the scattering vector q (= $4\pi(\sin\theta)/\lambda$), where 2θ and λ are the scattering angle and the wavelength of X-rays, respectively. Distinctive scattering peaks were not observed in B and Ba, meaning that there were no electron density fluctuations at a nanometer scale in these two polymers. This also suggests that acrylamide units in Ba do not form large aggregates, indicating that they are randomly distributed throughout the chain. In contrast to these results, scattering peaks were observed in P-Ba-P and P-B-P. This indicates nanophase separated structure, where spherical structures could presumably be formed according to the volume fraction of the P block.[28] Unfortunately, structure specification was not clear for P-Ba-P by TEM observation (see Figure 4-5b), while the TEM observations were not conducted for P-B-P because it was too soft to prepare ultrathin sections by microtoming. It should be noted that scattering intensities in the P-B-P profile were larger than those in the P-Ba-P profile, which is partially because the electron density difference between the middle block and the end block became small by incorporating acrylamide units into the middle block of P-Ba-P. Note that higher order peaks were observed in P-B-P unlike in P-Ba-P, reflecting the difference in segregation strength between components. To evaluate the segregation strength difference, blends of P/B and P/Ba were prepared (Figure 4-6). It was found by the simple blend experiments that macrophase separation was easier to occur in P/B than in P/Ba, meaning that the segregation strength between P and B is stronger than that between P and Ba. These results imply that incorporation of acrylamide units into the middle block causes lowering of the effective interaction parameter ($\chi_{\text{effective}}$).

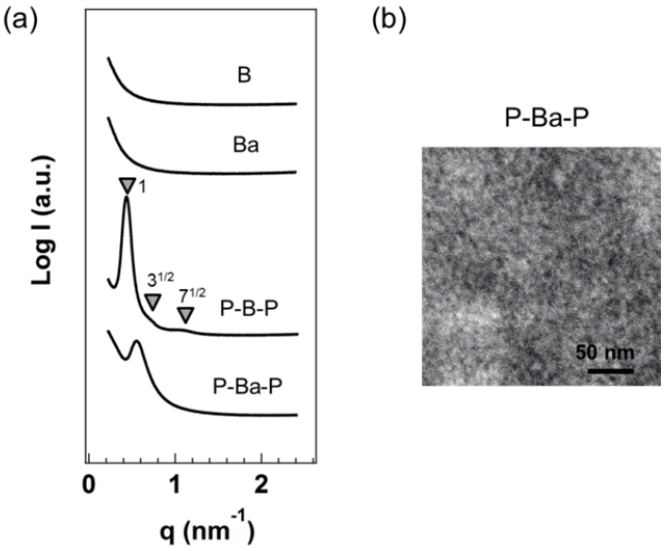

Figure 4-5. (a) Small-angle X-ray scattering profiles for the four polymers. Arrows with numbers in P-B-P profiles represent relative *q* positions at peaks. (b) A TEM image of P-Ba-P. The darker area and the brighter area can be assigned to the P block assemblies and the middle block matrix, respectively. The scale bar represents 50 nm. See reference #20, Figure 3 and Figure S11.

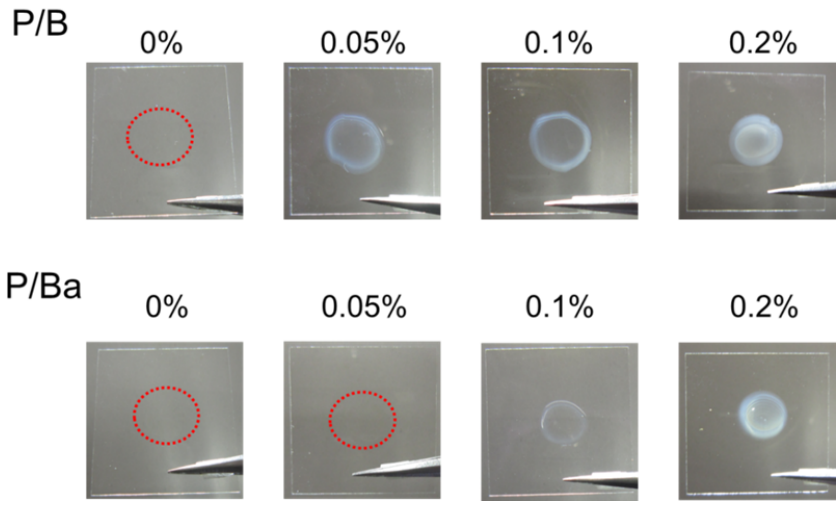

Figure 4-6. Macroscopic appearance of the blends of P/B (top), and the blends of P/Ba (bottom), where the numbers represent the P weight concentration in the blends. Red circles show the sample position (transparent). The blends were prepared by drop casting procedures on glass plates and they were annealed at 120 °C for 24 hours. See reference #20, Figure S12.

Viscoelastic properties. The viscoelastic properties dependent on temperatures of B and Ba are firstly compared in Figure 4-7a. In the spectrum of B, the storage moduli *G'* are larger than the loss moduli *G"* covering the whole measurement temperature rage. Although *G'* are slightly larger than *G"* at lower temperatures than 10 °C in the spectrum of Ba, distinctive rubbery plateau is not observed. Both B and Ba are in the flow region with *G"* >> *G'* at higher temperatures than -20 °C and 20 °C, respectively. Secondly, the dynamic temperature ramp spectra for P-B-P and P-Ba-P are shown in Figure 4-7b. P-B-P and P-Ba-P were in the glassy state with $E' > 10^9$ Pa at the temperature range from -60 °C to -40 °C and from -60 °C to -20 °C, respectively. At higher temperatures, the glass – rubber transitions can be observed, where the transitions are due to each middle block. Note that the temperature range for the transition of P-Ba-P (-20 °C ~ 20 °C) is broader than that of P-B-P (-40 °C ~ -20 °C), which could be attributed to hydrogen bonds on the middle block. In contrast to B and Ba, the rubbery regions are observed at the temperature range from -20 °C to 90 °C for P-B-P and from 20 °C to 90 °C for P-Ba-P. *E'* of P-B-P in the rubbery region remained almost constant while *E'* of P-Ba-P decreased with an increase in temperatures. According to FT-IR measurements for P-Ba-P with changing temperature, the fraction of hydrogen bonded acrylamide units decreased with an increase in temperatures (Figure 4-8). Therefore, the decrease in *E'* of P-Ba-P in the rubbery region should be due to dissociation of hydrogen bonded cross-links on the middle block with an increase in temperatures, causing a decrease in the cross-link density. The plateau moduli (E_P) were estimated at the temperatures with the minimal tanδ values in the rubbery region, and E_P values determined were 0.6 MPa for P-B-P and 1.6 MPa for P-Ba-P. Since E_P is known to proportional to the average cross-link density ν ($E_P \sim \nu k_B T$),[29-31] where k_B and T is the Boltzmann constant and the absolute temperature, respectively, these results indicate that P-Ba-P possesses a higher cross-link density. This is owing to the formation of hydrogen bonds on the

middle block of P-Ba-P (more detailed discussion will be given in the discussion section). The *E'* kept dropping in P-B-P and P-Ba-P at around 100 °C, where the disassembly of pseudo cross-link domains composed of P block might proceed because the temperature was close to the T_g of P block. It should be noted that the drop in *E'* was more gradual for P-B-P than for P-Ba-P.

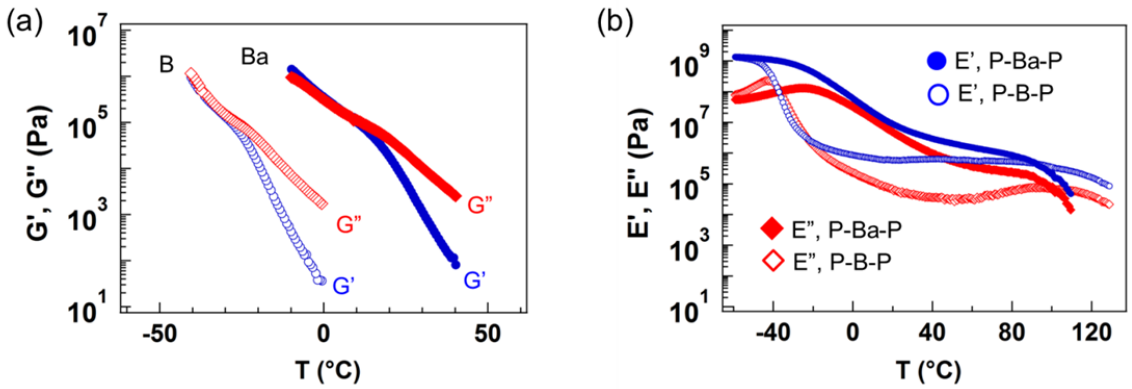

Figure 4-7. Rheological curves of storage moduli (*G'* or *E'*) and loss moduli (*G"* or *E"*) acquired by dynamic temperature ramp tests for B and Ba (a), and for P-B-P and P-Ba-P (b). See reference #20, Figure 4.

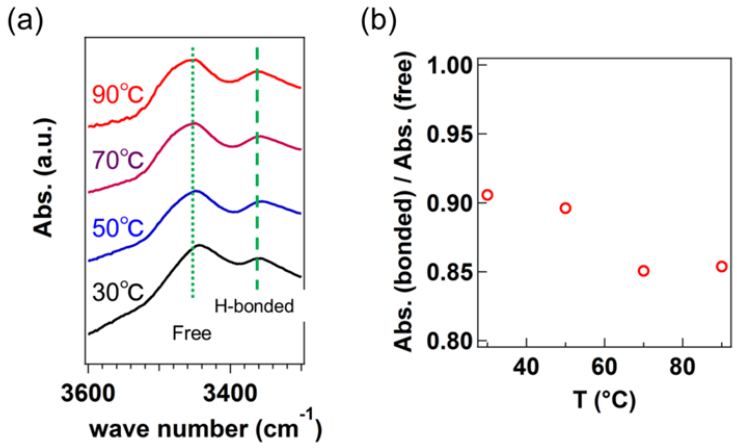

Figure 4-8. (a) FT-IR spectra of P-Ba-P at various temperatures within a wave number range from 3300 to 3600 cm^{-1}, where a dashed line at 3350 cm^{-1} and a dotted line at 3450 cm^{-1} correspond to the absorption bands of hydrogen bonded N-H and free N-H stretching vibration modes, respectively. (b) The plots of relative ratio of N-H stretching vibration mode absorbance for hydrogen bonded amide groups to that for free amide groups as a function of temperatures. See reference #20, Figure S13.

The viscoelastic properties dependent on frequencies were also investigated. Figure 4-9a represents the master curves of B and Ba following the time-temperature (TTS) principle with the reference temperature (T_{ref}) of 30 °C. TTS worked well for both B and Ba, indicating that the origin of the relaxation is the same within the temperature range adopted. It is obvious that Ba possesses a slower relaxation than B, which is due to incorporation of acrylamide units. Note that the typical power laws at the terminal region, $G' \sim \omega^2$ and $G'' \sim \omega$, were observed in the low frequency regions of B and Ba,.

Since the molecular weight of the present homopolymer B is lower than the entanglement molecular weight of poly(butyl acrylate),[32] the relaxation behavior can be described by the Rouse model as written in eq (4-1) and (4-2) for G' and G'', respectively,[33]

$$G'(\omega) = \frac{\rho RT}{M} \sum_{p=1}^{N} \frac{\tau_p{}^2 \omega^2}{1 + \tau_p{}^2 \omega^2} \qquad (4\text{-}1)$$

$$G''(\omega) = \frac{\rho RT}{M} \sum_{p=1}^{N} \frac{\tau_p \omega}{1 + \tau_p{}^2 \omega^2} \qquad (4\text{-}2)$$

, where ρ, R, and M represent the polymer density, the gas constant, and the molecular weight. The term τ_p in eq (4-1) and (4-2) represents the relaxation time of the pth mode which has the relationship with the Rouse relaxation time, τ_R as $\tau_R = \tau_p p^2$. Fitting curves following the Rouse model is represented in Figure 4-9a, where the τ_R ($\cong 0.0004$ sec) was estimated from the crossover frequency (ω_{cross}) of the extended lines of G' and G'' in the terminal region, i.e., $\tau_R = 1/\omega_{cross}$.

In the similar manner, the relaxation for Ba was treated by the Rouse-like model for associated polymers, i.e., the sticky Rouse model,[34-37] because the molecular weight of Ba is also lower than M_e of poly(butyl acrylate) and the acrylamide hydrogen bonds can serve as active stickers in the chain. Fitting curves were created according to eq (4-3) and (4-4),[37,38]

$$G'(\omega) = \frac{k_B T \nu_s}{n_s} \frac{(\omega\tau_R)^2}{\sqrt{\left[1+(\omega\tau_R)^2\right]\left[\sqrt{1+(\omega\tau_R)^2}+1\right]}} \qquad (4\text{-}3)$$

$$G''(\omega) = \frac{k_B T \nu_s}{n_s} \omega\tau_R \sqrt{\frac{\sqrt{1+(\omega\tau_R)^2}+1}{1+(\omega\tau_R)^2}} \qquad (4\text{-}4)$$

, where ν_s and n_s represent the network strand density, and the number of active stickers per chain, respectively. The fitting curves with τ_R = 0.2 sec (dashed line in Figure 4-9a), which was estimated by $\tau_R = 1/\omega_{cross}$, described well the experimental Ba spectra at n_s = 8. From this result, the average number of active hydrogen bonds was found to be around 8 in a chain, which is nearly 30% of acrylamide units in Ba ($N_a \sim 30$). In addition, the effective bond life time (τ_b) can be estimated by the related expression between τ_R and n_s ($\tau_R = \tau_b(n_s)^2$),[37,39] and the obtained τ_b was 3 msec.

Furthermore, the effects of hydrogen bonds on the flow activation energy (E_a) were also investigated. The relationship between a_T and inverse temperatures is known to follow the Arrehenius-type equation as in eq (4-5) at significantly higher temperatures than T_g of the polymers.[40,41]

$$a_T \approx \exp\left(\frac{E_a}{RT}\right) \qquad (4\text{-}5)$$

$$\ln a_T = A + \frac{E_a}{R} \cdot \frac{1}{T} \qquad (4\text{-}6)$$

The eq (4-6) is simply the logarithmic form of eq (4-5), where A is a constant. As shown in Figure 4-9b, linear relationships between $\ln a_T$ and $1/T$ can be attained at a higher temperature range, i.e. $0.0033 < 1/T < 0.0037$ for B and $0.003 < 1/T < 0.0033$ for Ba. Note that the temperature range for the linear relationship is much higher than the T_gs of B (-45 °C) or Ba (-23 °C). Slopes of the straight lines in Figure 4-9b correspond to E_a/R in eq (4-6), which then gives the E_a. The estimated E_a of Ba (110 kJ/mol) is higher than B (77 kJ/mol), suggesting that

the incorporation of hydrogen bonds retarded the flow of Ba chains.

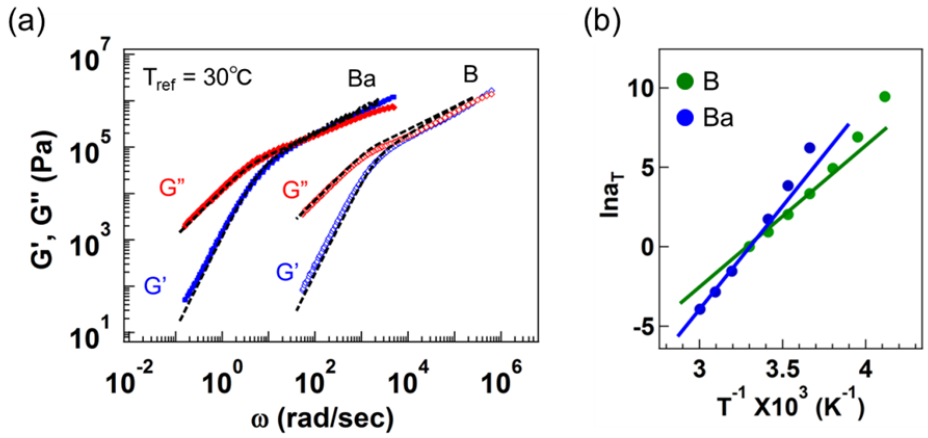

Figure 4-9. (a) Master curves of B and Ba with the reference temperature of 30 °C. The dashed lines represent the fitting curves with the Rouse model for B and the sticky Rouse model for Ba, respectively. (b) Plots of lna_T as a function of the inverse temperatures, where the straight lines were used to estimate E_a. See reference #20, Figure 5 and Figure S14.

Dynamic frequency sweep tests were also conducted for P-B-P and P-Ba-P. Figure 4-10 compares the *E'* spectra at 60 °C, 90 °C, and 100 °C, where the temperatures correspond to the rubbery plateau region (60 °C) and rubbery flow region (90 °C and 100 °C), respectively. In the spectra at 60 °C, *E'* of P-Ba-P were always larger than those of P-B-P in the whole frequency range due to higher cross-link density originating from the hydrogen bonds on the Ba middle block. Similar to the dynamic temperature ramp spectra, *E'* of P-B-P remained constant while those of P-Ba-P were decreasing with a lowering of frequencies, where the decrease in *E'* of P-Ba-P could be due to the decrease of network density caused by dissociation in acrylamide hydrogen bonds with a lowering of frequencies. On the other hand, *E'* of P-B-P were larger than those of P-Ba-P in lower frequencies than 2.5 Hz at 90 °C, and *E'* of P-B-P was larger than that of P-Ba-P in the whole frequencies at 100 °C. These results are similar to those observed in dynamic temperature ramp spectra at the corresponding temperatures (Figure 4-7b).

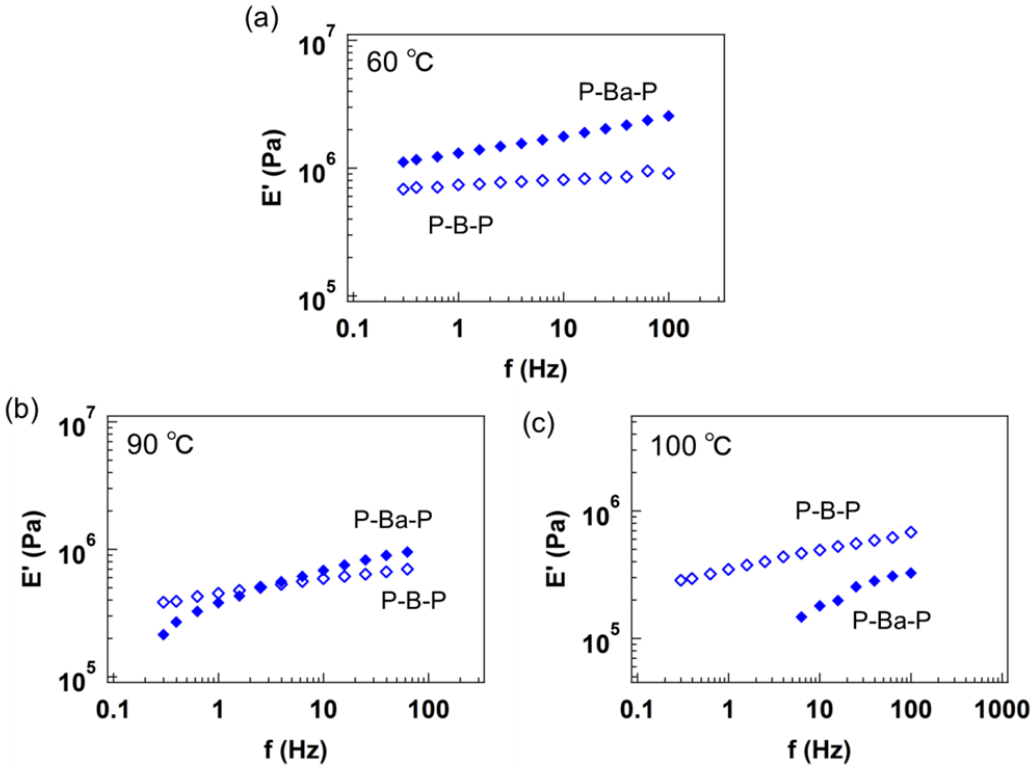

Figure 4-10. The frequency dependence of *E'* for P-B-P and P-Ba-P at (a) 60 °C, (b) 90 °C, and (c) 100 °C, where the open and filled symbols represent *E'* spectra of P-B-P and P-Ba-P, respectively. See reference #20, Figure 5 and Figure S17.

Tensile properties. Elongation characteristics were investigated by tensile tests, and the stress-strain (S-S) curves are shown in Figure 4-11. Table 4-2 summarizes the elongation properties, including the elongation at break ε_b, maximum tensile stress σ_{max}, Young's modulus E_Y, and mechanical toughness S, where E_Y and S were estimated from the slopes of S-S curves within a 10% strain and the area covered under S-S curves, respectively. Obviously from Figure 4-11 and Table 4-2, P-Ba-P shows much longer ε_b and larger σ_{max} than P-B-P, while E_Y is nearly the same as E_P estimated by dynamic viscoelastic measurements. The most notable feature here is the toughness; S of P-Ba-P (2.8 MJ/m^3) is approximately 140 times larger than that of P-B-P

(0.02 MJ/m^3). It should be stressed that difference in chemical structure between P-Ba-P and P-B-P is not so large, that is, merely 15% acrylamide units is incorporated into the middle block of P-Ba-P. Therefore, it can be simply assumed that the mechanical property enhancement attained in P-Ba-P could be attributed to the formation of acrylamide hydrogen bonds on the middle block, where the hydrogen bonds can repeat dissociation and re-association at a short time scale under stress application. The dynamic behavior of hydrogen bonds on the middle block could work to prevent local stress concentration, and hence energy dissipation could be induced by rupturing the hydrogen bonds, which can provide the mechanical property enhancement in P-Ba-P. It is also important to mention that the dissociation and re-association occurs at a length scale (~ the length between acrylamide units ~ several nm) shorter than the typical length scale for activating the break/failure of materials (~ length scale between cross-link domains ~ several ten nm).[10] The effects of the fractions of acrylamide unit in the middle block on the elongation properties was also investigated as shown in Figure 4-12. More detailed discussion will be given in the discussion section.

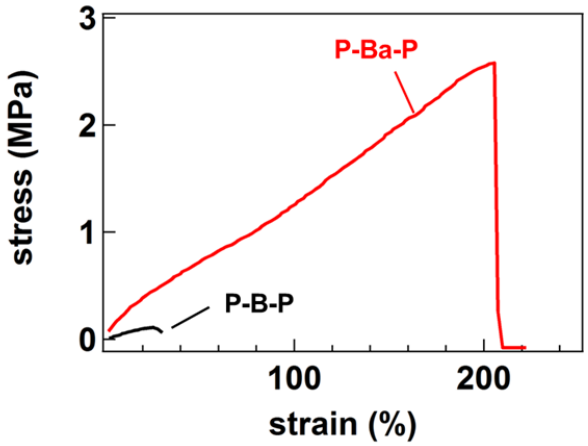

Figure 4-11. Stress-strain curves of P-Ba-P and P-B-P obtained by tensile tests. See reference #20, Figure 6.

Table 4-2. Mechanical characteristics of the triblock copolymers and blends

Sample	E_P[a] (MPa)	ε_b[b] (%)	σ_{max}[c] (MPa)	E_Y[d] (MPa)	S[e] (MJ/m^3)
P-B-P	0.62	25	0.11	0.60	0.020
P-Ba-P	1.6	201	2.6	1.9	2.8

[a]Rubbery plateau modulus determined at the temperature with a minimum tanδ value. [b]Elongation at break. [c]The maximum tensile stress. [d]Young's modulus estimated from the slope of S-S curves within a 10% strain. [e]Mechanical toughness estimated from the area under S-S curves.

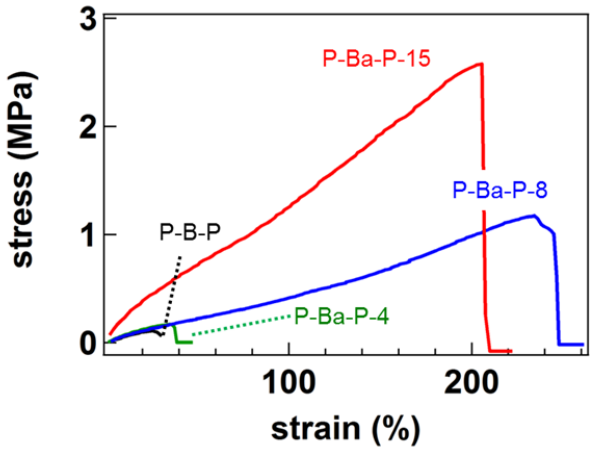

Figure 4-12. S-S curves obtained by tensile tests for various P-Ba-P with different acrylamide unit fraction (f_a), where the S-S- curve for P-B-P is also shown for comparison. The number of X in P-Ba-P-X represents f_a. Detailed molecular characteristics for various P-Ba-P polymers are summarized in Table 2-4. The tests were performed with an elongation rate of 10 mm/min. See reference #20, Figure S19.

Discussion

Plateau modulus of the ABA triblock copolymer-based elastomers.

The plateau moduli (E_P) estimated by the rheological measurements were 0.62 MPa for P-B-P and 1.6 MPa for P-Ba-P (see Table 4-2). These values can be conceived to include the contribution from glassy P blocks. For typical ABA triblock copolymer-based elastomers containing spherical, glassy A domains, the modulus is enhanced by the glassy domains as fillers

in the elastic matrix and the contribution to the modulus from the filler is known to be expressed by eq (4-7),[14,42]

$$E = E_{elas} F_{filler} \text{ with } \; F_{filler} = 1 + 2.5 v_g + 14.1 v_g^{\,2} \qquad (4\text{-}7)$$

, where E_{elas} denotes the modulus of the elastic matrix and F_{filler} represents the filler-enhancement factor actually associated with the volume fraction of the fillers (v_g).

For P-B-P, the volume fraction of P block is approximately 0.2, i.e., $v_g \sim 0.2$, which gives $F_{filler} \cong 2$, and hence E_{elas} of P-B-P is estimated to be approximately 0.3 by using the E_P (0.62 MPa). This E_{elas} value is to be compared with the theoretical rubbery modulus E_{rub} estimated from the classical rubber theory,[33]

$$E_{rub} = \frac{\rho}{M}(3RT) \qquad (4\text{-}8)$$

, where M represents the molecular weight between cross-links. For ABA triblock copolymer-based elastomers having no entanglement in the matrix phase, M is replaced with the molecular weight of the middle B block. By using $\rho \sim 1.09$ g/cm^3, $M \sim 25{,}000$ g/mol, and $T \sim 323$ K, E_{rub} of P-B-P was estimated to be ~ 0.35 MPa, which is close to the E_{elas} ($\cong 0.3$ MPa).

Since P-Ba-P has a similar v_g (~ 0.2) to P-B-P, F_{filler} for P-Ba-P is also determined to be, $F_{filler} \cong 2$. Therefore, E_{elas} of P-Ba-P was estimated to be 0.8 MPa from the E_P value (1.6 MPa), while the E_{rub} estimated by eq (4-8) is 0.35 MPa. It should be noted here that E_{elas} is obviously larger than E_{rub} for P-Ba-P. This difference suggests that some of acrylamide hydrogen bonds in P-Ba-P serve as cross-links and contributed to E_{elas}, where the E_{elas} / E_{rub} ratio can be a measure of the increase in the cross-link density by incorporating hydrogen bonds. Since E_{elas} / E_{rub} was estimated to be 2 for P-Ba-P, approximately one hydrogen bond per Ba middle block appears to serve as an extra cross-link to enhance E_{elas}, considering the modulus is proportional to the inverse of molecular weight between cross-links ($E \sim 1 / M_x$).

Dynamics of the ABA triblock copolymer bearing hydrogen bonds on the middle block

Figure 4-13b shows the master curve of P-B-P (filled red circles) created following TTS principle with the reference temperature T_{ref} = 30 °C, where the raw data were acquired at the temperature range from -30 °C to 30 °C. Within this temperature range, the B middle block is in the melt state and the P end block is in the glassy state according to the T_g values summarized in Table 4-1. Since the relaxation originating from segmental motion of P block can be negligible at well below T_g of P block (~ 100 °C), the relaxation of P-B-P observed in Figure 4-13b is predominantly attributed to the relaxation of B middle block. In fact, the superposition with tanδ spectra of P-B-P held well (Figure 4-13a), indicating that the relaxation is governed by the single mechanism.

For this case, it can be expected that the E' data of P-B-P is also contributed from the $E'_{P\text{-}B\text{-}P,eq}$, which is mainly determined by the molecular weight of B middle block and the volume fraction, and the Rouse relaxation modulus of B block ($E'_{B,Rouse}$). The value of $E'_{P\text{-}B\text{-}P,eq}$ was determined at the lower frequency in Figure 4-13b and represented as a dashed black line. $E'_{B,Rouse}$ can be estimated from the G' data of B homopolymer having the same molecular weight. The G' data of B homopolmer was multiplied by a factor of 3, which is associated with the conversion from the shear condition to the tensile condition ($E = 3G$),[33] and further multiplied by the filler-enhancement factor 2 ($F_{filler} \sim 2$) examined in the previous section to estimate $E'_{B,Rouse}$ for the summation. The data of $E'_{B,Rouse}$ is plotted as a function of f (= $\omega/2\pi$) in Figure 4-13b (unfilled black circles). The sum spectrum of $E'_{P\text{-}B\text{-}P,eq}$ and $E'_{B,Rouse}$ represented by unfilled green circles is pretty close to the E' data of P-B-P (filled red circles), suggesting the validity of the simple expectation.

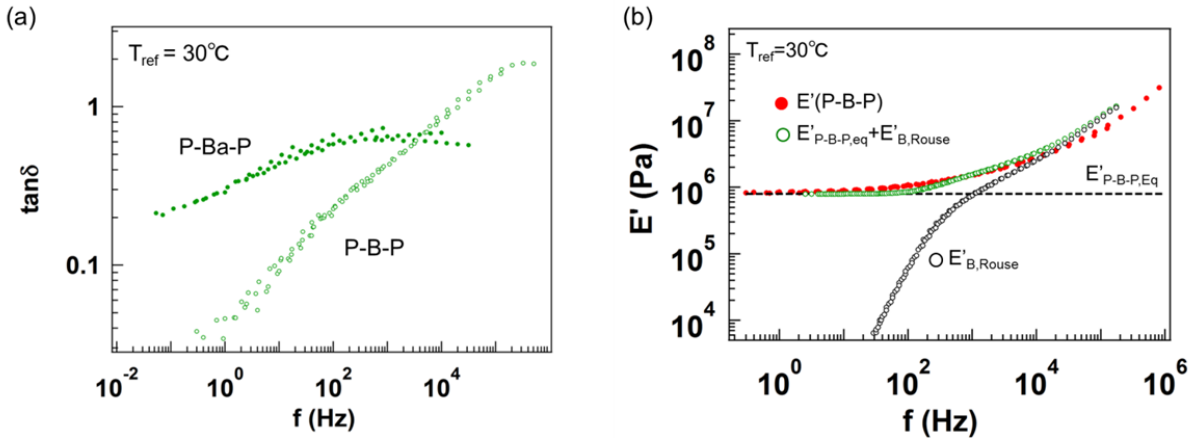

Figure 4-13. (a) Tanδ master curves of P-B-P and P-Ba-P with the reference temperature T_{ref} = 30 °C. The raw data for the superposition were acquired at the temperature range from -30 °C to 30 °C for P-B-P and 0 °C to 40 °C for P-Ba-P. (b) Comparison of the *E'* data of P-B-P (filled red circles) with the sum spectrum (unfilled green circles) of $E'_{P\text{-}B\text{-}P,eq}$ (dashed black line) and $E'_{B,Rouse}$ (unfilled black circles). The range of *E'* smaller than 10^4 was omitted for clarity. See reference #20, Figure S25 and Figure 9.

In the similar manner, an attempt was made to compare the *E'* data of P-Ba-P with a sum of equilibrium *E'* of P-Ba-P ($E'_{P\text{-}Ba\text{-}P,eq}$) and sticky Rouse relaxation modulus of Ba middle block ($E'_{Ba,s\text{-}Rouse}$). For this comparison, the superposed spectrum of P-Ba-P cannot be used because the superposition with TTS principle could not be applied to P-Ba-P data, which was found by the deviation of tanδ master curve shown in Figure 4-13a. Therefore, the analyses for P-Ba-P data was conducted with the raw spectra at each temperature.

Here, the analysis for P-Ba-P at 10 °C is presented as an example. By the similar way to the treatment for the analyses for P-B-P data, *G'* data of Ba homopolymer was multiplied by 6 to estimate the storage Young's modulus, $E'_{P\text{-}Ba\text{-}P,s\text{-}Rouse}$, which is expected for the sticky Rouse relaxation of the Ba middle block of P-Ba-P subjected to the filler effect (characterized by $F_{filler} \cong 2$). Furthermore, the $E'_{Ba,s\text{-}Rouse}$ spectrum was extended to the higher frequency region with the assumption that the sticky Rouse model expressed with eq (4-3) holds up to the actual frequency region of the raw data of Ba, and the resulting fitting curve is shown as dashed orange curve. A

sum of this expected sticky Rouse relaxation modulus of Ba (the dashed orange curve) and the equilibrium modulus of P-Ba-P $E'_{\text{P-Ba-P,eq}}$ (1.6 MPa determined as the plateau modulus in Table 4-2; horizontal black dashed line) is shown as a solid black curve in Figure 4-14. Obviously, the sum underestimated the E' data of P-Ba-P (filled red circles), which is different from the analytical results for P-B-P. Therefore, the present expectation for the sticky Rouse modulus, $E'_{\text{Ba,s-Rouse}}$ without frequency shift does not describe the actual behavior of Ba middle block in P-Ba-P.

For further examination of relaxation behavior of Ba middle block, it is formative to examine the sticky Rouse modulus $E'_{\text{Ba,s-Rouse}}$ with a frequency shift, i.e., $E'_{\text{Ba,s-Rouse}}(f) = 3F_{\text{filler}}G'_{\text{homo-Ba}}(\lambda f)$, where λ represents the difference of relaxation rates of Ba homopolymer and Ba middle block in P-Ba-P. By comparing $E'_{\text{Ba,s-Rouse}}$ spectrum with E' data of P-Ba-P, λ was determined to be 13. $E'_{\text{Ba,s-Rouse}}(f)$ with λ =13 and the sum of $E'_{\text{P-Ba-P,eq}}$ and $E'_{\text{Ba,s-Rouse}}(f) = 3F_{\text{filler}}G'_{\text{homo-Ba}}(13f)$ are shown as a dashed blue curve and a solid green curve, respectively, where the sum is satisfactorily close to the E' data of P-Ba-P (filled red circles). This result suggests that the E' data of P-Ba-P can be described as a simple sum of the equilibrium modulus and the sticky Rouse modulus, the latter is accompanied with the retardation by the factor of λ = 13 as compared to the Ba homopolymer. Figure 4-14a, 4-14c, and 4-14d also represents comparisons of the E' data of P-Ba-P with a sum of $E'_{\text{P-Ba-P,eq}}$ and $E'_{\text{Ba,s-Rouse}}(f)$ (= $3F_{\text{filler}}G'_{\text{homo-Ba}}(\lambda f)$) at 0 °C, 20 °C, and 30 °C, respectively. Note that the value of λ for describing the E' data of P-Ba-P by the sum was 10 at 0 °C, 30 at 20 °C, and 60 at 30 °C; the data are pointing out that necessary λ was increased with an increase in temperatures.

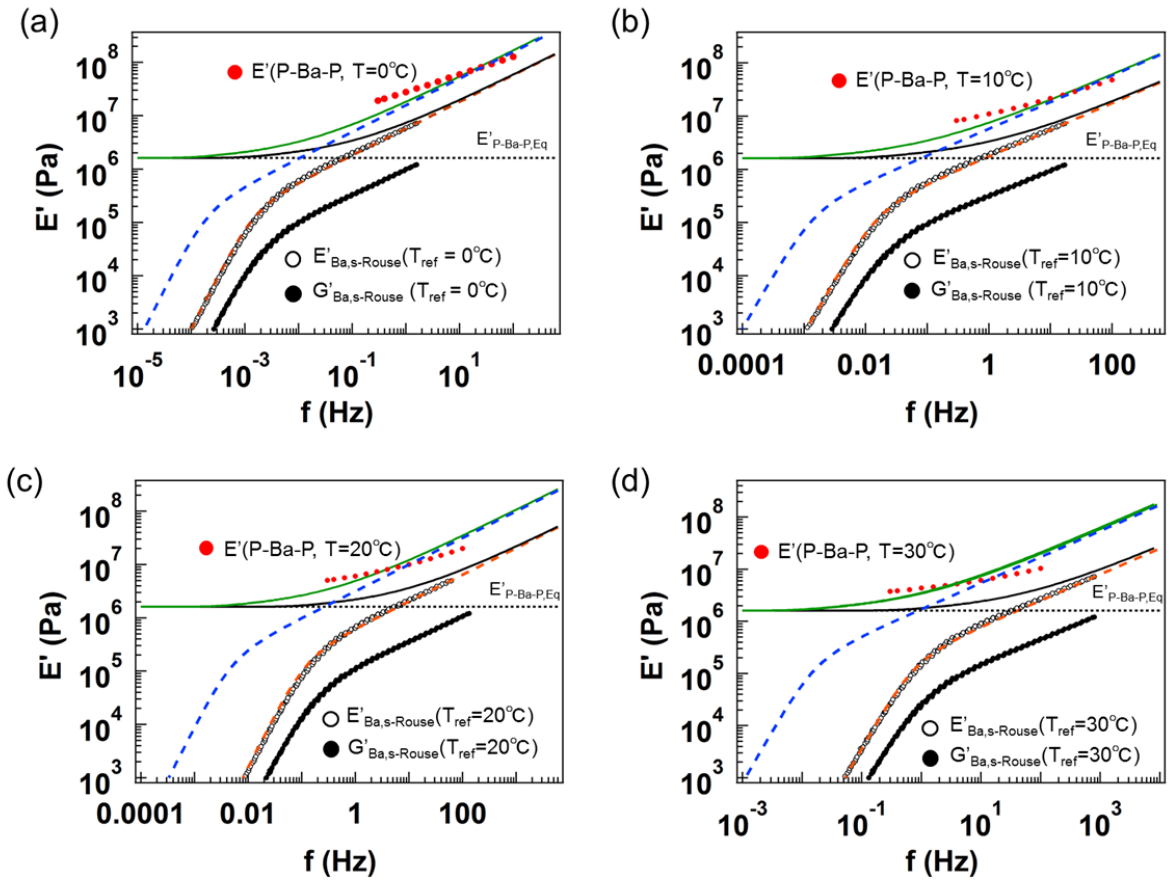

Figure 4-14. Comparison of the E' data of P-Ba-P (filled red circles) with the sum (solid black curve) of the equilibrium modulus $E'_{\text{P-Ba-P,eq}}$ (black dashed line) and the sticky Rouse modulus $E'_{\text{Ba,s-Rouse}}(f)$ (unfilled black circles; fit with eq (4-3) as shown with the dashed orange curve by using corresponding τ_R (see Figure 4-15), the latter being evaluated from G' data of B homopolymer without an extra shift in the frequency. Solid green curve indicates the sum but with $E'_{\text{Ba,s-Rouse}}(f)$ (= $3F_{\text{filler}}G'_{\text{homo-Ba}}(\lambda f)$) shown as dashed blue curve. See reference #20, Figure 10 and Figure S27.

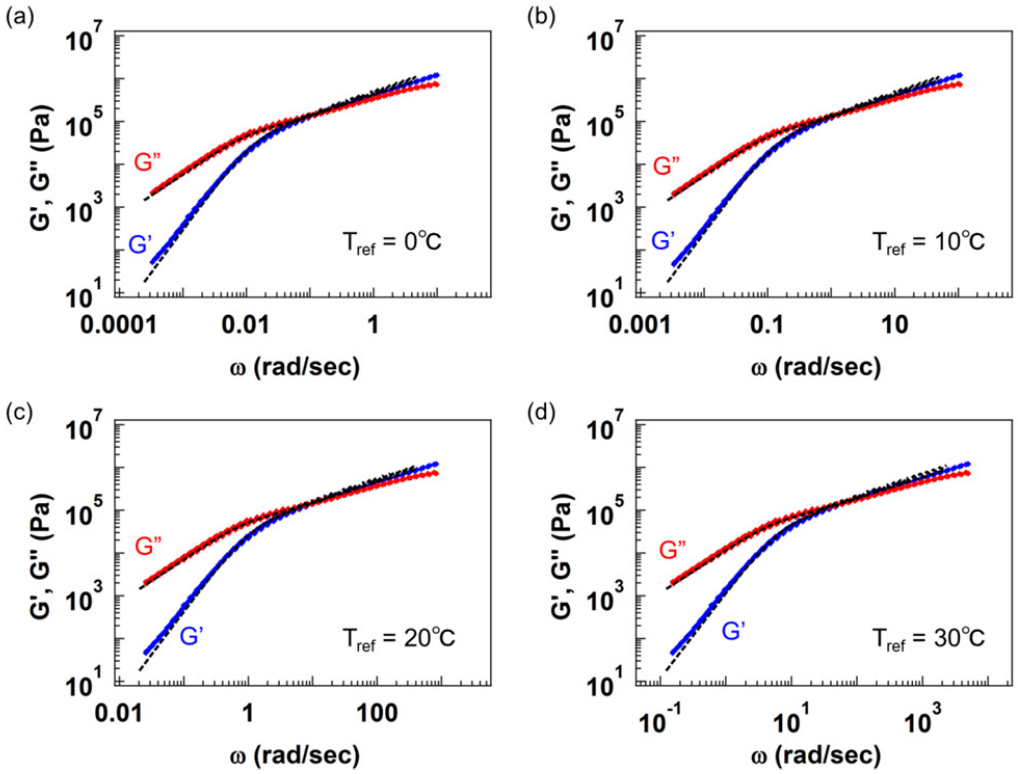

Figure 4-15. Comparison of the experimental spectra of Ba and the calculated spectra on the basis of the sticky Rouse model at (a) 0 °C, (b) 10 °C, (c) 20 °C, and (d) 30 °C. *G'* and *G"* were plotted with blue and red symbols, respectively, while dashed lines represent the fitting curves estimated by eq (4-3) and (4-4). The calculated spectra, instead of the experimental spectra, were used for the summation with $E'_{\text{P-Ba-P,eq}}$. The validity of τ_R values for fitting with eq (4-3) and (4-4) was confirmed as shown above, where τ_R was 0.2 sec at 30 °C, 1.5 sec at 20 °C, 11 sec at 10 °C, and 120 sec at 0 °C. See reference #20, Figure S26.

The retardation observed in the present analysis for P-Ba-P could have resulted from several structural/molecular mechanisms, while no similar retardation was observed for the analyses of P-B-P data. It should be again noted that the sticky Rouse relaxation model with correlated dissociation/association of hydrogen bonds was successfully applied to the analysis of Ba homopolymer without extra constrain at the chain ends (see Figure 4-9a). To the contrary, however, for the Ba middle block with chain ends being rigidly anchored by domains of glassy P blocks, an extra correlation of dissociation/association of the hydrogen bonds emerged, since

many Ba middle block chains are bridging the P block domains and the hydrogen bonds on those Ba block tend to be re-associated with the original partner more frequently than the hydrogen bonds on the end-free Ba homopolymer. This could naturally result in the “retarded” sticky Rouse relaxation for the Ba block compared to the Ba homopolymer without changing much in the relaxation mode distribution. In addition, the increase in λ with an increase in temperatures can be explained by the assumption that the correlation of dissociation/association of the hydrogen bonds is accelerated by temperatures, promoting the retardation.

Above analysis suggests that the hydrogen bonds serve as dynamic stickers on the elastic strands of Ba in P-Ba-P. The dynamic behavior of the hydrogen bonds can be understood not only in the linear viscoelastic regime but also in the non-linear elongational state under large tensile stress. This must be the key issue for the mechanical property enhancement attained in P-Ba-P.

Chapter Summary

In this chapter, a new strategy was proposed and described to enhance the mechanical properties of ABA triblock copolymer-based elastomers by incorporating hydrogen bonds into the soft middle block. A triblock-type block copolymer, P-Ba-P, was synthesized via RAFT polymerization. In a self-assembled state, the P end blocks formed glassy cross-link domains, and transient cross-links of hydrogen bonds were formed between acrylamide units on the Ba soft middle block. Comparison of plateau modulus between P-Ba-P and a control sample, P-B-P, revealed that P-Ba-P attained approximately three times higher modulus than P-B-P due to an increase in the cross-link density originating from the hydrogen bonds on the middle block. According to tensile tests, P-Ba-P showed greater elongation properties. Among them, the toughness of P-Ba-P (2.8 MJ/m^3) was nearly 140 times larger than that of P-B-P (0.2 MJ/m^3). The origin of the mechanical property enhancement was also discussed in terms of viscoelastic behaviors of the triblock copolymers, where it has been found that the hydrogen bonds on the elastic strand of Ba in P-Ba-P serve as dynamic stickers. Such dynamic behavior of the hydrogen bonds can also influence the chain extension behavior under elongation, which works to prevent local stress concentration during elongation. This is the key issue for the mechanical property enhancement attained in P-Ba-P.

References

[1] Lendlein, A.; Langer, R. *Science* **2002,** 296, 1673-1676.

[2] Davis, D. A.; Hamilton, A.; Yang, J.; Cremar, L. D.; Van Gough, D.; Potisek, S. L.; Ong, M. T.; Braun, P. V.; Martinez, T. J.; White, S. R.; Moore, J. S.; Sottos, N. R. *Nature* **2009,** 459, 68-72.

[3] Kupfer, J.; Finkelmann, H. *Makromole. Chem. Rapid Commun.* **1991,** 12, 717-726.

[4] Wang, M. *J. Rubber Chem. Technol.* **1999**, 72, 430-448.

[5] Arroyo, M.; Lopez-Manchado, M. A.; Herrero, B. *Polymer* **2003,** 44, 2447-2453.

[6] Bailey, J. T.; Bishop, E. T.; Hendrick.Wr; Holden, G.; Legge, N. R. *Rubber Age* **1966,** 98, 69.

[7] Holden, G.; Bishop, E. T.; Legge, N. R. *J. Polym. Sci., Part C: Polym. Symp.* **1969,** 37.

[8] Koerner, H.; Price, G.; Pearce, N. A.; Alexander, M.; Vaia, R. A. *Nature Mater.* **2004,** 3, 115-120.

[9] Goosen, M. F. A.; Sefton, M. V. *J. Biomed. Mater. Res.* **1979,** 13, 347-364.

[10] Takano, A.; Kamaya, I.; Takahashi, Y.; Matsushita, Y. *Macromolecules* **2005,** 38, 9718-9723.

[11] Matsumiya, Y.; Watanabe, H.; Takano, A.; Takahashi, Y. *Macromolecules* **2013,** 46, 2681-2695.

[12] Honeker, C. C.; Thomas, E. L. *Chem. Mater.* **1996,** 8, 1702-1714.

[13] Watanabe, H.; Kuwahara, S.; Kotaka, T. *J. Rheol.* **1984**, 28, 393-409.

[14] Yamaguchi, D.; Cloitre, M.; Panine, P.; Leibler, L. *Macromolecules* **2005**, 38, 7798-7806.

[15] Noro, A.; Matsushita, Y.; Lodge, T. P. *Macromolecules* **2008**, 41, 5839-5844.

[16] Noro, A.; Matsushita, Y.; Lodge, T. P. *Macromolecules* **2009**, 42, 5802-5810.

[17] Lei, Y.; Lodge, T. P. *Soft Matter* **2012**, 8, 2110-2120.

[18] Noro, A.; Matsushima, S.; He, X.; Hayashi, M.; Matsushita, Y. *Macromolecules* **2013**, 46, 8304-8310.

[19] Hayashi, M.; Noro, A.; Matsushita, Y. *J. Polym. Sci., Part B: Polym. Phys.* **2014**, 52, 755-764.

[20] Hayashi, M.; Matsushima, S.; Noro, A.; Matsushita, Y. *Macromolecules,* in press.

[21] Aakeroy, C. B.; Beatty, A. M.; Helfrich, B. A. *J. Am. Chem. Soc.* **2002,** 124, 14425-14432.

[22] Dakovic, M.; Popovic, Z. *Mineral. Petrol.* **2013,** 107, 341-348.

[23] Yamauchi, K.; Lizotte, J. R.; Long, T. E. *Macromolecules* **2003,** 36, 1083-1088.

[24] *Spectrometric identification of organic compounds 4th ed.* Silverstein, R. M.; Bassler, G. C.; Morrill, T. C. WILEY, **1981**.

[25] Chen, Y.; Wu, W.; Himmel, T.; Wagner, M. H. *Macromol. Mater. Eng.* **2013**, 298, 876-887.

[26] Noro, A.; Higuchi, K.; Sageshima, Y.; Matsushita, Y. *Macromolecules* **2012**, 45, 8013-8020.

[27] Ruokolainen, J.; Saariaho, M.; Ikkala, O.; ten Brinke, G.; Thomas, E. L.; Torkkeli, M.; Serimaa, R. *Macromolecules* **1999,** 32, 1152-1158.

[28] Matsen, M. W.; Thompson, R. B. *J. Chem. Phys.* **1999,** 111, 7139-7146.

[29] Flory, P. J.; Rehner, J. *J. Chem. Phys.* **1943**, 11, 512-520.

[30] He, Y.; Boswell, P. G.; Buhlmann, P.; Lodge, T. P. *J. Phys. Chem. B* **2007,** 111, 4645-4652.

[31] Li, J.; Lewis, C. L.; Chen, D. L.; Anthamatten, M. *Macromolecules* **2011**, 44, 5336-5343.

[32] Yamazaki, H.; Takeda, M.; Kohno, Y.; Ando, H.; Urayama, K.; Takigawa, T. *Macromolecules* **2011**, 44, 8829-8834.

[33] *Polymer Chemistry 2nd ed*. Himenz, P. C.; Lodge, T. P. CRC Press, **2007**.

[34] Semenov, A. N.; Rubinstein, M. *Macromolecules* **1998**, 31, 1373-1385.

[35] Yamazaki, H.; Takeda, M.; Kohno, Y.; Ando, H.; Urayama, K.; Takigawa, T. *Macromolecules* **2011**, 44, 8829-8834.

[36] Rubinstein, M.; Semenov, A. N. *Macromolecules* **1998**, 31, 1386-1397.

[37] Tanaka, F.; Edwards, S. F. *Macromolecules* **1992,** 25, 1516-1523.

[38] Feldman, K. E.; Kade, M. J.; Meijer, E. W.; Hawker, C. J.; Kramer, E. J. *Macromolecules* **2009**, 42, 9072-9081.

[39] *Polymer Physics*. Rubinstein, M.; Colby, R. OXFORD UNIVERSITY PRESS, **2003**.

[40] Spruijt, E.; Stuart, M. A. C.; van der Gucht, J. *Macromolecules* **2013,** 46, 1633-1641.

[41] Schneider, A. H.; Cantow, J. H.; Brekner, J. M. *Polym. Bull.* **1984**, 11, 383-390.

[42] Mucha, M. *Macromol. Chem. Phys.* **1997**, 198, 471-484.

[43] Wang, M. J. *Rubber Chem. Technol.* **1999**, 72, 430−448.

Chapter 5

Mechanical Properties and Morphological investigation of Supramolecular Elastomers Cross-linked via Metal-ligand Coordination and Hydrogen Bonding

Abstract: In the previous chapter, the mechanical property enhancement of ABA triblock copolymer-based elastomers by incorporating hydrogen bonds into the soft middle block was introduced and argued. The polymer used there was poly(4-vinylpyridine)-*b*-[(poly(butyl acrylate)-*co*-polyacrylamide]-*b*-poly(4-vinylpyridine) (P-Ba-P). In this chapter, further enhancement in mechanical properties of ABA triblock copolymer-based elastomers is reported, where P chains in phase separated spherical domains were cross-linked via metal-ligand coordination by blending metal salts, $ZnCl_2$, to P-Ba-P, coupled with hydrogen bonding on the middle block. The physical properties were investigated by morphological investigations and mechanical property measurements. By comparing the tensile test results between P-Ba-P/$ZnCl_2$ and neat P-Ba-P, it has been found that the material toughness was further increased by a factor of 2 due to metal-ligand coordination formed in P domains selectively.

Introduction Incorporation of non-covalent bonded cross-links into soft materials to enhance their properties have recently been paid attention.[1-7] Such materials are regarded as supramolecular soft material,[3] including functional polymers,[8,9] polymer gels,[10,11] or rubbers,[12-14] and they acquire stimuli-responsiveness owing to the weak association strength in the cross-links.

There are several reports on the network materials with "high" strength by purposely incorporating "weak" noncovalent bonding into the networks. Gong et al. have reported double network hydrogels with extremely high mechanical strength, where the weaker network is formed by ionic association between polyelectrolytes, whereas the stronger one with covalent bonds is composed of flexible neutral polymers.[15,16] In their system, preferential dissociation of the weaker network under stress can dissipate the applied stress, so that the weaker interaction plays a role of "sacrificial" bond.[17,18] Kushner et al. have reported a biomimetic design of a twofold cross-link composed of 2-ureido-4-[1H]-pyrimidone (Upy) and cyclic alkyl chains bridged across the Upy structures, which attained the enhancement of tensile strength energy dissipation capability by unfolding Upy association.[19-21] In the most of the molecular designs with multiple cross-links, however, covalent bonds were necessarily chosen as the stronger cross-links, and hence there are only few reports on preparation of high toughness network materials with the combination of multiple noncovalent bonds, though it is anticipated that there are useful advantages of noncovalent bonded soft materials, such as stimuli-responsiveness or self-healing ability.

Here in this chapter, a novel idea of creating supramolecular elastomers cross-linked via dual non-covalent bondings, i.e., metal-ligand coordination and hydrogen bonding, is proposed and executed for aiming to produce tough supramolecular network materials.[22] A triblock-type copolymer poly(4-vinylpyridine)-*b*-[(poly(butylacrylate)-*co*-polyacrylamide]-*b*-

poly(4-vinylpyridine) (P-Ba-P) was used following the previous chapter, it being blended with zinc chloride $ZnCl_2$. In this molecular design, metal-to-ligand coordination is formed between a nitrogen atom in the poly(4-vinylpyridine) end blocks and $ZnCl_2$, whereas self-complementally hydrogen bonding is simultaneously formed between two acrylamide units on the middle block. The effects brought by simultaneous cross-linkings with hydrogen bonds and coordination bonds on the physical properties were investigated by morphological observations and mechanical measurements.

Polymers and blends. The polymer samples used in this work are the ones prepared in the chapter 2 and used in the chapter 4, i.e., P-Ba-P and P-B-P, the latter being adopted as a control sample (see the characteristics in Table 4-1). The blends P-Ba-P or P-B-P and $ZnCl_2$ were coded as P-Ba-P/$ZnCl_2$ or P-B-P/$ZnCl_2$, respectively (the method for blend preparation was described in the chapter 2).

Results and Discussion

Sample appearance. As a result of blending $ZnCl_2$ to the triblock copolymers, transparent and elastic films were obtained as shown in Figure 5-1a and 5-1b. On the other hand, the blend of Ba and $ZnCl_2$ was turbid and sticky (Figure 5-1c), indicating that any attractive interactions were not generated between acrylamide or butyl acrylate moiety and $ZnCl_2$. These results strongly suggest that $ZnCl_2$ preferentially forms coordination bonds with nitrogen atoms on P block.

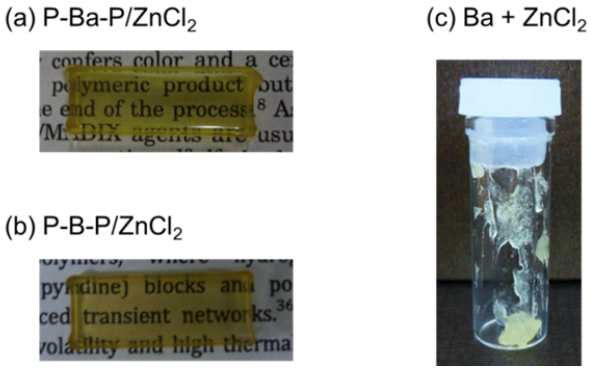

Figure 5-1. Macroscopic appearance of (a) P-Ba-P/$ZnCl_2$, (b) P-B-P/$ZnCl_2$, and (c) Ba/$ZnCl_2$. See reference #22, Figure S20 and Figure S21.

Molecular Characterization of the blends.

To confirm the coordination between 4-vinylpyridine group and $ZnCl_2$, FT-IR measurements were conducted. In the spectra of neat P-B-P and P-Ba-P (Figure 5-2a), only a

peak corresponding to a C-N vibration mode of free pyridine ring was observed at 1597 cm^{-1}.[23] After blending $ZnCl_2$, another peak originating from coordination bonded pyridine ring was newly observed at 1618 cm^{-1} in P-B-P/$ZnCl_2$ and P-Ba-P/$ZnCl_2$, suggesting the coordination bond formation in the P blocks.[23] In addition, an absorption associated with hydrogen bonded amide units was observed at 3350 cm^{-1} in P-Ba-P/$ZnCl_2$ as well as in the neat P-Ba-P (Figure 5-2b).[24,25] It should be also noted that the relative intensity ratio of absorption for hydrogen bonded amide units to that for free amide units was much larger in P-Ba-P/$ZnCl_2$ than in P-Ba-P, indicating that the fraction of the associated acrylamide moiety is higher for the former. This could be related to the morphological change by blending $ZnCl_2$, which will be examined in later section.

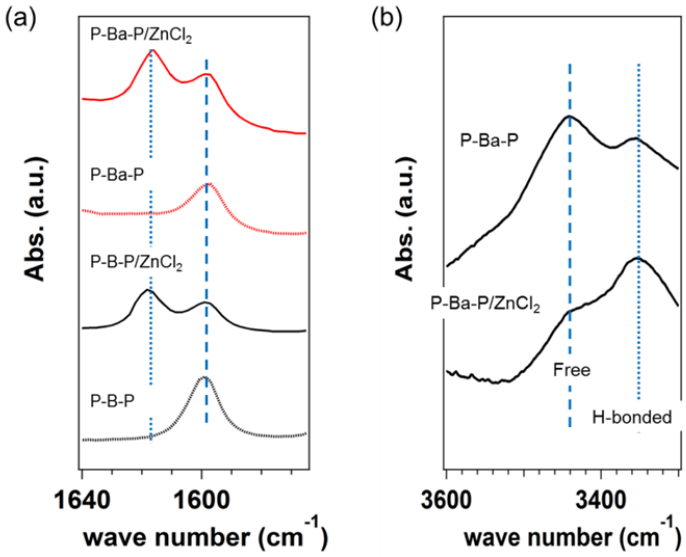

Figure 5-2. (a) FT-IR spectra of the neat polymers and the blends in a wave number range from 1560 to 1640 cm^{-1}, where a dashed line at 1597 cm^{-1} and a dotted line at 1618 cm^{-1} represent C-N vibration modes of free and coordination bonded pyridine groups, respectively. (b) FT-IR spectra of Ba and P-Ba-P within a wave number range from 3300 to 3600 cm^{-1}, where a dashed line at 3350 cm^{-1} and a dotted line at 3450 cm^{-1} correspond to the absorption bands of hydrogen bonded N-H and free N-H stretching vibration modes, respectively. See reference #22, Figure 7.

The T_g change after blending $ZnCl_2$ was also evaluated. Figure 5-3a represents DSC thermograms of P-B-P/$ZnCl_2$ and P-Ba-P/$ZnCl_2$, where the thermograms of neat P-B-P and P-Ba-P are also shown for comparison. It was already found in the previous chapter that the endothermic heat changes associated with the T_g of middle block were observed in P-B-P and P-Ba-P, while T_g of P blocks were evaluated by α relaxations observed in tanδ spectra of dynamic temperature ramp tests instead. The endothermic heat changes of P-B-P/$ZnCl_2$ and P-Ba-P/$ZnCl_2$ were observed at the almost same temperatures as those of P-B-P and P-Ba-P, respectively, indicating that blending $ZnCl_2$ to the copolymers did not affect T_gs of the middle blocks. To the contrary, however, α relaxations from P block chains in the blends were not observed in their tanδ spectra unlike the neat triblock copolymers (Figure 5-3b). This can be attributed to the increase in T_gs due to the constrained segmental motions of the P blocks by the coordination.[23,26] Thus it has been revealed by this investigation on T_gs that the coordination bonds were selectively formed in the P end blocks.

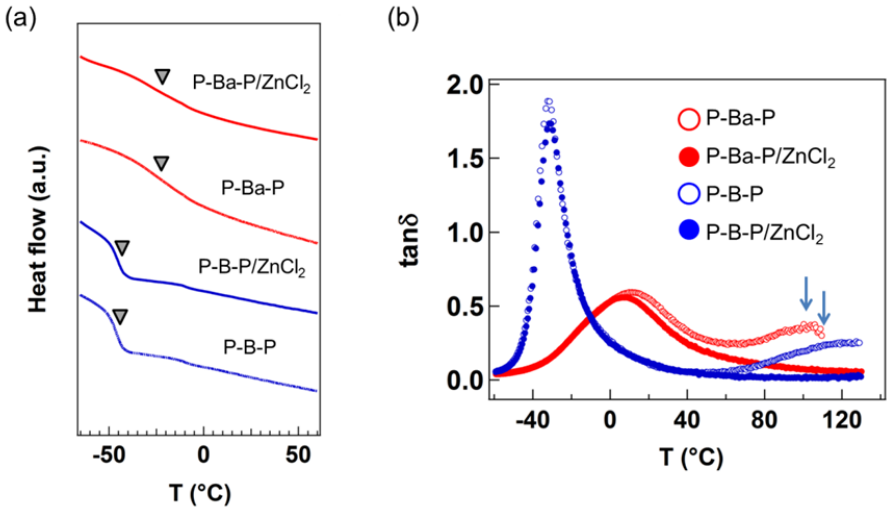

Figure 5-3. (a) DSC thermograms of P-B-P/$ZnCl_2$ and P-Ba-P/$ZnCl_2$, where the themograms of neat triblock copolymers are also shown for comparison. (b) Tanδ spectra of the neat triblock copolymers and the blends, where the arrows represent α relaxation originating from P block of P-B-P and P-Ba-P, respectively. See reference #22, Figure S10 and Figure S22.

The change in degree of nanophase separation after blending $ZnCl_2$ was investigated by SAXS and TEM. Figure 5-4a represents SAXS profiles of the blends as well as the neat triblock copolymers. It is apparent that the scattering intensities increased after blending, which is mainly due to the increase in electron density difference between the middle block and the end block induced by selective coordination of $ZnCl_2$ into the P blocks. In addition, higher order peaks were observed in P-Ba-P/$ZnCl_2$ in contrast to neat P-Ba-P, reflecting the formation of higher-contrast nanophase separation by blending $ZnCl_2$. In fact, clearer nanophase-separated structure with spherical domains composed of P blocks and $ZnCl_2$ was observed in TEM observations in P-Ba-P/$ZnCl_2$ unlike P-Ba-P (Figure 5-4b). Improvement in contrast of nanophase separation after blending $ZnCl_2$ can possibly be attributed to the increase in effective interaction parameter between the end block and the middle block by the selective incorporation of $ZnCl_2$ into the P end blocks.[27,28]

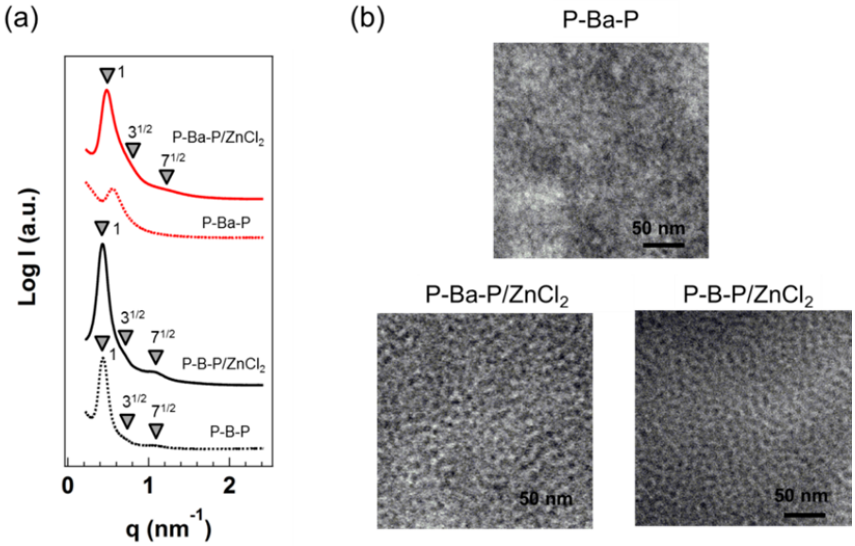

Figure 5-4. (a) SAXS profiles of P-Ba-P/$ZnCl_2$ and P-B-P/ $ZnCl_2$, where the profiles of neat triblock copolymers are also shown for comparison. Arrows with numbers represent relative *q* positions at peaks. (b) TEM images of P-Ba-P/$ZnCl_2$ and P-B-P/$ZnCl_2$. The darker area and the brighter area can be assigned to the

assemblies of P/$ZnCl_2$ and the middle block matrix, respectively. The scale bar represents 50 nm. See reference #22, Figure 7 and Figure S11.

Effects of the coordination in the P domains on the mechanical properties. The effects of the coordination in the P domains on the viscoelastic properties were investigated by rheological measurements. The *E'* spectra for two blends, i.e., P-Ba-P/$ZnCl_2$ and P-B-P/$ZnCl_2$, as a function of temperature are shown in Figure 5-5 with the spectra of neat triblock copolymers, where the plateau moduli (E_P) have found to be increased after blending $ZnCl_2$, especially for P-Ba-P. The E_P values are summarized in Table 5-1. According to the morphological investigations as shown in Figure 5-4, nanophase-separated structures with higher contrast and orders were formed in the blends than in the neat polymers. Thus, the increase in plateau modulus for blends can be attributed to the decrease of dangling chains.[29,30] The moduli in the plateau region of P-Ba-P/$ZnCl_2$ and P-B-P/$ZnCl_2$ were nearly kept constant, and the drops in *E'* were not observed at high temperatures (~ 130 °C) unlike the cases of the neat triblock copolymers. This is due to the increase in the T_g of P blocks by forming the selective coordination as supported by tanδ spectra in Figure 5-3b, where α relaxations of P blocks were not observed even at high temperatures.

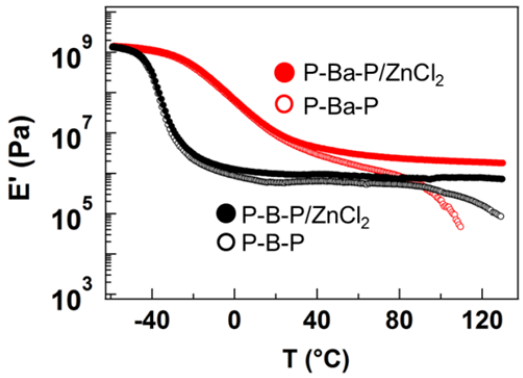

Figure 5-5. The *E*' spectra of P-Ba-P/$ZnCl_2$ and P-B-P/$ZnCl_2$ obtained by dynamic temperature ramp tests. The spectra of P-Ba-P and P-B-P are also shown for comparison. See reference #22, Figure 8.

Table 5-1. Mechanical Characteristics of the Triblock Copolymers and Blends

Sample	E_P[a] (MPa)	ε_b[b] (%)	σ_{max}[c] (MPa)	E_Y[d] (MPa)	S[e] (MJ/m^3)
P-B-P	0.62	25	0.11	0.60	0.020
P-Ba-P	1.6	201	2.6	1.9	2.8
P-B-P/$ZnCl_2$	0.91	60	0.41	0.94	0.15
P-Ba-P /$ZnCl_2$	6.0	165	6.8	6.4	6.3

[a]Rubbery plateau modulus determined at the temperature with a minimum tanδ value. [b]Elongation at break. [c]The maximum tensile stress. [d]Young's modulus estimated from the slope of S-S curves within a 10% strain. [e]Mechanical toughness estimated from the area under S-S curves.

Tensile tests were performed for the blends, and the stress-strain (S-S) curves are shown in Figure 5-6 together with the results for neat P-B-P and P-Ba-P. The elongation properties are also summarized in Table 5-1. The Young's moduli (E_Y) for both blends were found to be increased after blending $ZnCl_2$, which may be due to the decrease in the fractions of dangling chains as explained for the increase in E_P. The elongation at break (ε_b) of P-Ba-P/$ZnCl_2$ (165%) was smaller than that of P-Ba-P (201%). Two reasons can be conceived. 1) Larger stress was applied to the blends than the neat copolymer at the same level of elongation due to the larger E_Y. 2) The ability of stress dissipation in the cross-link domains of P could be lowered by the rigid cross-links because of the coordination in the P block domains. Nevertheless, blending $ZnCl_2$ to P-Ba-P provided further increase in toughness; S of P-Ba-P/$ZnCl_2$ (6.3 MJ/m^3) is more than double compared to neat P-Ba-P (2.8 MJ/m^3). By comparing S for P-B-P (0.2 MJ/m^3) and for P-Ba-P/$ZnCl_2$, the increase in the toughness was found to be approximately by a factor of 300 by incorporating hydrogen bonds coupled with forming coordination bond. This successful result is

owing to the simultaneous use of metal-ligand coordination bonds and hydrogen bonds.

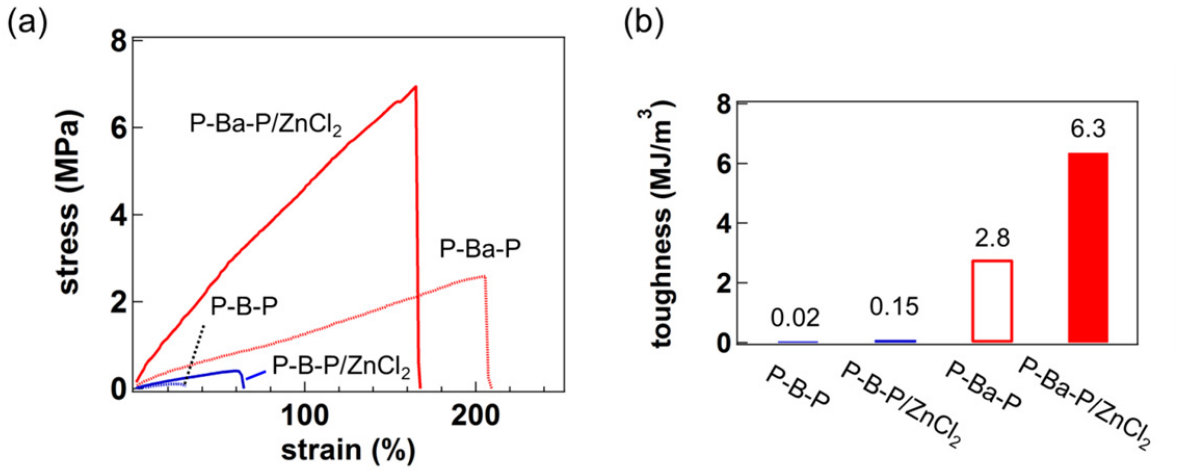

Figure 5-6. (a) Stress-Strain curves obtained by tensile tests for the blends, where the curves for the neat polymers are also shown for comparison. (b) The *S* values estimated from the area under S-S curves. See reference #22, Figure S23.

Chapter Summary

In this chapter, further mechanical property enhancement of ABA triblock copolymer-based elastomers having dual cross-linking via coordination and hydrogen bonds was reported. After blending $ZnCl_2$ to P-Ba-P, the coordination selectively occurred between pyridine units and $ZnCl_2$, while self-complementary hydrogen bonds were simultaneously formed between acrylamide units on the middle block. According to the morphological investigation by SAXS and TEM, high contrast nanophase-separated structure was formed after blending $ZnCl_2$, which caused the increase in plateau modulus as well as Young's modulus. By the comparison of tensile test results between neat P-Ba-P and P-Ba-P/$ZnCl_2$, it was found that the materials toughness was further increased by a factor of 2. This could be attributed to the metal-ligand coordination formed in the P end blocks, which can cause the formation of nanophase-separated structure with high contrast, probably induced by an increase in segregation strength between the end block and the middle block.

References

[1] Noro, A.; Hayashi, M.; Ohshika, A.; Matsushita, Y. *Soft Matter* **2011**, 7, 1667-1670.

[2] Noro, A.; Hayashi, M.; Matsushita, Y. *Soft Matter* **2012**, 8, 6416-6429.

[3] Hayashi, M.; Noro, A.; Matsushita, Y. *J. Polym. Sci., Part B: Polym. Phys.* **2014**, 52, 755-764.

[4] Noro, A.; Matsushima, S.; He, X.; Hayashi, M.; Matsushita, Y. *Macromolecules* **2013**, 46, 8304-8310.

[5] Matsushima, S.; Hayashi, M.; Yamagishi, H.; Noro, A.; Matsushita, Y. *Nihon Reoloji Gakk.* **2014**, 42, 135-141.

[6] Noro, A.; Matsushita, Y.; Lodge, T. P. *Macromolecules* **2009**, 42, 5802-5810.

[7] Noro, A.; Matsushita, Y.; Lodge, T. P. *Macromolecules* **2008**, 41, 5839-5844.

[8] Nair, K. P.; Breedveld, V.; Weck, M. *Macromolecules* **2008,** 41, 3429-3438.

[9] Seiffert, S.; Sprakel, J. *Chem. Soc. Rev.* **2012,** 41, 909-930.

[10] Yan, X.; Xu, D.; Chen, J.; Zhang, M.; Hu, B.; Yu, Y.; Huang, F. *Polym. Chem.,* **2013,** 4, 3312-3322.

[11] Weng, W.; Fang, X.; Zhang, H.; Peng, H.; Lin, Y.; Chen, Y. *Eur. Polym. J.* **2013,** 49, 4062-4071.

[12] Zhang, A.; Yang, L.; Lin, Y.; Yan, L.; Lu, H.; Wang, L. *J. Appl. Polym. Sci.* **2013,** 129, 2435-2442.

[13] Montarnal, D.; Cordier, P.; Soulie-Ziakovic, C.; Tournilhac, F.; Leibler, L. *J. Polym. Sci., Part A: Polym. Chem.* **2008,** 46, 7925-7936.

[14] Cordier, P.; Tournilhac, F.; Soulie-Ziakovic, C.; Leibler, L. *Nature* 2008, **451**, 977-980.

[15] Gong, J. P.; Katsuyama, Y.; Kurokawa, T.; Osada, Y. *Adv. Mater.* **2003,** 15, 1155-1158.

[16] Na, Y. H.; Kurokawa, T.; Katsuyama, Y.; Tsukeshiba, H.; Gong, J. P.; Osada, Y.; Okabe, S.; Karino, T.; Shibayama, M. *Macromolecules* **2004**, 37, 5370-5374.

[17] Ducrot, E.; Chen, Y. L.; Bulters, M.; Sijbesma, R. P.; Creton, C. *Science* **2014**, 344, 186-189.

[18] Haque, M. A.; Kurokawa, T.; Gong, J. P. *Polymer* **2012**, 53, 1805−1822

[19] Hofmeier, H.; Hoogenboom, R.; Wouters, M. E. L.; Schubert, U. S. *J. Am. Chem. Soc.* **2005**, 127, 2913-2921.

[20] Hofmeier, H.; Schubert, U. S. *Chem. Commun.* **2005,** 19, 2423-2432.

[21] Mansfeld, U.; Winter, A.; Hager, M. D.; Hoogenboom, R.; Guenther, W.; Schubert, U. S., *Polym. Chem.* **2013,** 4, 113-123.

[22] Hayashi, M.; Matsushima, S.; Noro, A.; Matsushita, Y. *Macromolecules,* in press.

[23] Sageshima, Y.; Noro, A.; Matsushita, Y. *J. Polym. Sci., Part B: Polym. Phys.* **2014**, 52, 377-386.

[24] *Spectrometric identification of organic compounds 4th ed.* Silverstein, R. M.; Bassler, G. C.; Morrill, T. C. WILEY, **1981**.

[25] Chen, Y.; Wu, W.; Himmel, T.; Wagner, M. H. *Macromol. Mater. Eng.* **2013**, 298, 876-887.

[26] Noro, A.; Sageshima, Y.; Arai, S.; Matsushita, Y. *Macromolecules* **2010**, 43, 5358-5364.

[27] Lee, D. H.; Kim, H. Y.; Kim, J. K.; Huh, J.; Ryu, D. Y. *Macromolecules* **2006,** 39, 2027-2030.

[28] Lee, D. H.; Han, S. H.; Joo, W.; Kim, J. K.; Huh, J. *Macromolecules* **2008,** 41, 2577-2583.

[29] Yamaguchi, D.; Cloitre, M.; Panine, P.; Leibler, L. *Macromolecules* **2005**, 38, 7798-7806.

[30] Takano, A.; Kamaya, I.; Takahashi, Y.; Matsushita, Y. *Macromolecules* **2005,** 38, 9718-9723.

Chapter 6

Summary

In this thesis, two types of supramolecular soft materials, one with noncovalent bonded cross-links on the chain ends of telechelic-type polymer, and the other with the middle block possessing self-complementary hydrogen bonding moiety in an ABA triblock copolymer, were designed and prepared. The effects of the noncovalent cross-links on their rheological and mechanical properties were studied.

In the chapter 1, general introduction for soft materials, particularly for supramolecular soft materials was given.

In the chapter 2, the synthetic procedures and the characterization of the component polymers were described. In addition, the experimental conditions and the analytical methods for the rheological measurements and others were explained.

In the chapter 3, the supramolecular soft materials were prepared by blending two liquid polymers, that is, carboxy-terminated telechelic poly(ethyl acrylate) (PEA-$(COOH)_2$) and polyethyleneimine (PEI) with multiple amines. Ionic hydrogen bonds were formed between carboxylic acids on PEA-$(COOH)_2$ and amines on PEI by blending them, which generated the supramolecular networks. The effects of the molecular weight of PEA-$(COOH)_2$ and the blend ratio on the viscoelastic properties were investigated by focusing on T_{cross}, the temperature at which *G'* and *G"* cross each other, and the flow activation energy (E_a). It has been found that the stoichiometry between functional groups is a key issue to optimize the supramolecular networks. Moreover, systematic change in the plateau modulus (G_X) was achieved simply by changing the

molecular weight of PEA-$(COOH)_2$.

In the chapter 4, an ABA triblock copolymer based-elastomer with transient cross-links of hydrogen bonds on the soft middle block, that is, poly(4-vinylpyridine)-*b*-[(poly(butyl acrylate)-*co*-polyacrylamide]-*b*-poly(4-vinylpyridine) (P-Ba-P) was prepared. The mechanical property enhancement induced by incorporation of the hydrogen bonds into the soft middle block was demonstrated by dynamic mechanical measurements and tensile tests. In addition, the effects of the middle block hydrogen bonds on the viscoelastic properties of the triblock copolymer were discussed and explained using the idea of the sticky Rouse-type relaxation of the Ba middle block.

In the chapter 5, supramolecular elastomers cross-linked via metal-ligand coordination coupled with hydrogen bonds were prepared by blending $ZnCl_2$ to P-Ba-P. Morphological investigations by SAXS measurements and TEM observations revealed that clearer nanophase separation was formed due to an increase in segregation strength between the middle block and the end block after blending $ZnCl_2$, which led to further enhancement of mechanical properties, i.e., plateau modulus and the mechanical toughness, in comparison with those for neat P-Ba-P.

List of publication

1. "Simple Preparation of Supramolecular Polymer Gels via Hydrogen Bonding by Blending Two Liquid Polymers" Atsushi, Noro; **Mikihiro, Hayashi**; Akihisa, Ohshika; Yushu, Matsushita, *Soft matter*, **2011**, 7, 1667-1670.

2. "Viscoelastic Properties of Supramolecular Soft Materials with Transient Polymer Network" **Mikihiro, Hayashi**; Atsushi, Noro; Yushu, Matsushita. *Journal of Polymer Science Part B: Polymer Physics*, **2014**, 52, 755-764.

3. “Mechanical Property Enhancement of ABA Block Copolymer-Based Elastomers by Incorporating Transient Cross-Links into Soft Middle Block” **Mikihiro, Hayashi**; Satoru, Matsushima; Atsushi, Noro; Yushu, Matsushita, *Macromolecules*, in press.

Further Publication

1. "Design and Properties of Supramolecular Polymer Gels" Atsushi, Noro; **Mikihiro, Hayashi**; Yushu, Matsushita, *Soft matter*, **2012**, 8, 6416-6429.

2. "Thermoreversible Supramolecular Polymer Gels via Metal-Ligand Coordination in an Ionic Liquid" Atsushi, Noro; Satoru, Matsushima; Xudong, He; **Mikihiro, Hayashi**; Yushu, Matsushita, *Macromolecules*, **2013**, 46, 8304-8310.

3. "Preparation and Viscoelasticity of Hydrogen Bonded Supramolecular Ion Gels Composed of ABA Triblock Copolymer and C Homopolymer in an Ionic Liquid" Satoru, Matsushima; **Mikihiro, Hayashi**; Hajime, Yamagishi; Atsushi, Noro; Yushu, Matsushita. *NIHON REOROJI GAKKAISHI*, **2014**, 52, 135-141.

Acknowledgment

This thesis was thoroughly conducted by the author during the Ph.D curse in Department of Applied Chemistry, Graduate School of Engineering, Nagoya University.

The author greatly thanks Prof. Yushu Matsushita for his fruitful help and suggestions on the thesis, as well as his tolerant mind to give the author a lot of valuable opportunities, including several research visits to abroad. The author thanks Prof. Masami Kamigaito, Prof. Hiroyuki Asanuma, and Associate Prof. Atsushi Takano for their kind suggestions for this thesis. The author thanks assistant Prof. Atsushi Noro for his longtime help and suggestions for accomplishing the thesis.

This thesis was also supported by researchers in other research laboratories. The author profoundly thanks Prof. Hiroshi Watanabe for his tremendous help on the rheological data analysis. The author also thanks professors and researchers in the Society of Rheology, Japan for their beneficial suggestions and discussions on this thesis. The authors thank Mr. Aikawa, Mrs. Maeda at TA Instruments, Japan for their help in performing rheological measurements and DSC measurements. The authors also thank Mr. T. Hikage at High Intensity X-ray Diffraction Laboratory in Nagoya University for his help in measuring X-ray scattering.

This thesis was financially supported by the Program for Leading Graduate Schools at Nagoya University entitled “Integrative Graduate Education and Research Program in Green Natural Sciences,” and by JSPS Research Fellowships for Young Scientists (No. 13J02357). The author thanks the above support.

The author would also love to thank Prof. Ludwik Leibler (ESPCI, France), Prof. François Tournilhac (ESPCI, France), and Prof. Xinyuan Zhu (Shanghai Jiao Tong University, China) for their acceptance of the author’s research visits and for their giving the author meaningful opportunities.